HAWC Observations of the Spectrum, Composition and Anisotropy of Cosmic Rays Below the Knee

Juan Carlos Díaz Vélez

on behalf of the HAWC Collaboration

15 Oct. 2024

SuGAR 2024

Madison, WI

SuGAR MADISON 2024

SEARCHING FOR THE SOURCES OF GALACTIC COSMIC RAYS

OCTOBER 14-17

Image: tecreview.tec.mx

The HAWC Observatory

Pico de Orizaba (Citlaltépetl)
5636m

Sierra Negra
4640m

Alfonso Serrano Large
Millimeter Telescope

HAWC Site
4100m

The HAWC Observatory

HAWC
High Altitude Water Cherenkov
Gamma-Ray Observatory

Mapping the Northern Sky in High-Energy Gamma Rays

HAWC Observatory

HAWC operates day and night, providing a large field of view for the observation of the highest energy gamma rays.

Pico de Orizaba
(5,626 m)

HAWC is located at 4,100 m above sea level, covering an area of 20,000 m^2.

150 m

Water Cherenkov tank

HAWC comprises an array of 300 tanks that record the particles created in gamma-ray and cosmic-ray showers.

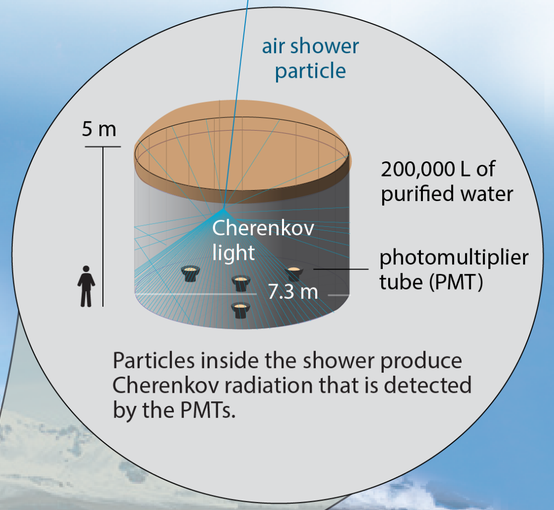

Particles inside the shower produce Cherenkov radiation that is detected by the PMTs.

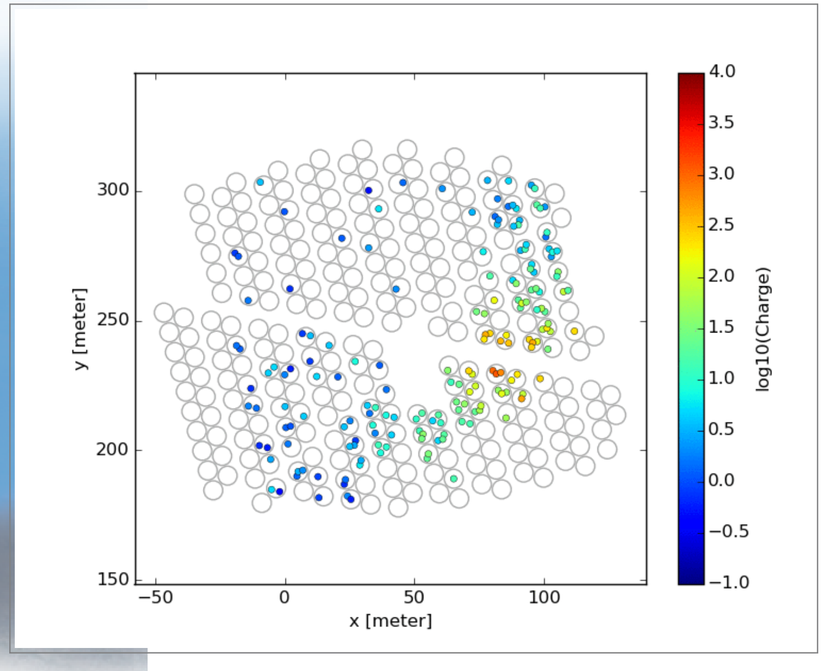

Gamma rays vs cosmic rays

HAWC selects gamma rays from among a much more abundant background of cosmic rays.

gamma-ray shower

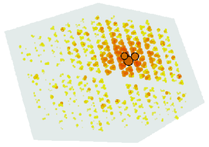

"hot" spots concentrate around the core

cosmic-ray shower

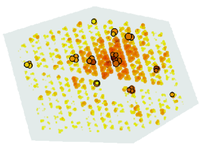

"hot" spots are more dispersed

The HAWC Observatory

HAWC
High Altitude Water Cherenkov
Gamma-Ray Observatory

Mapping the Northern Sky in High-Energy Gamma Rays

HAWC Observatory

HAWC operates day and night, providing a large field of view for the observation of the highest energy gamma rays.

Pico de Orizaba
(5,626 m)

HAWC is located at 4,100 m above sea level, covering an area of 20,000 m^2.

150 m

Water Cherenkov tank

HAWC comprises an array of 300 tanks that record the particles created in gamma-ray and cosmic-ray showers.

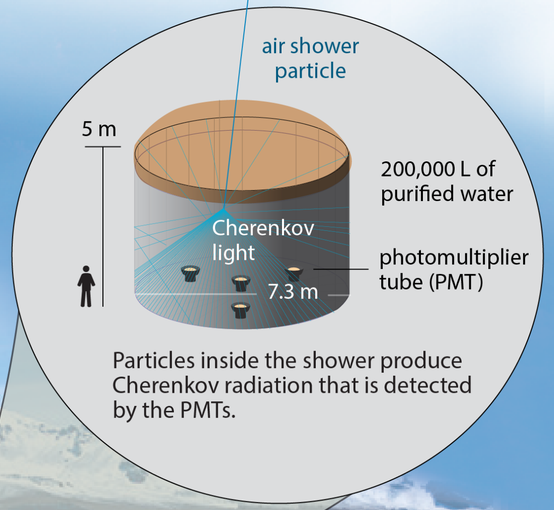

Particles inside the shower produce Cherenkov radiation that is detected by the PMTs.

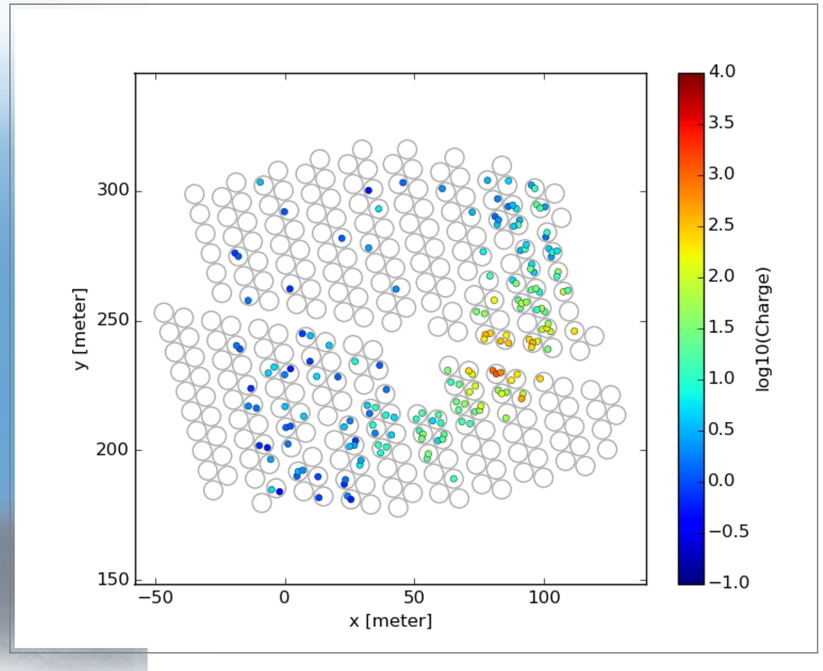

Gamma rays vs cosmic rays

HAWC selects gamma rays from among a much more abundant background of cosmic rays.

gamma-ray shower

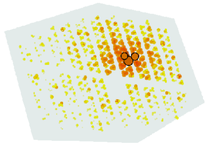

"hot" spots concentrate around the core

cosmic-ray shower

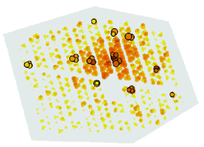

"hot" spots are more dispersed

The HAWC γ-ray observatory

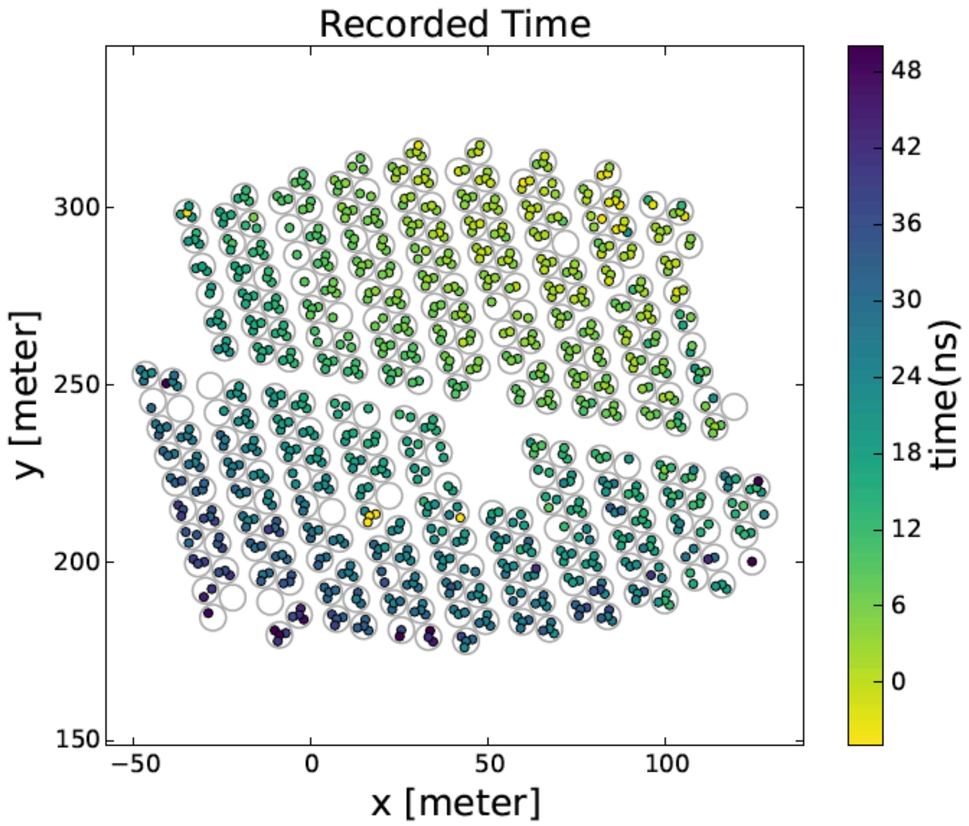

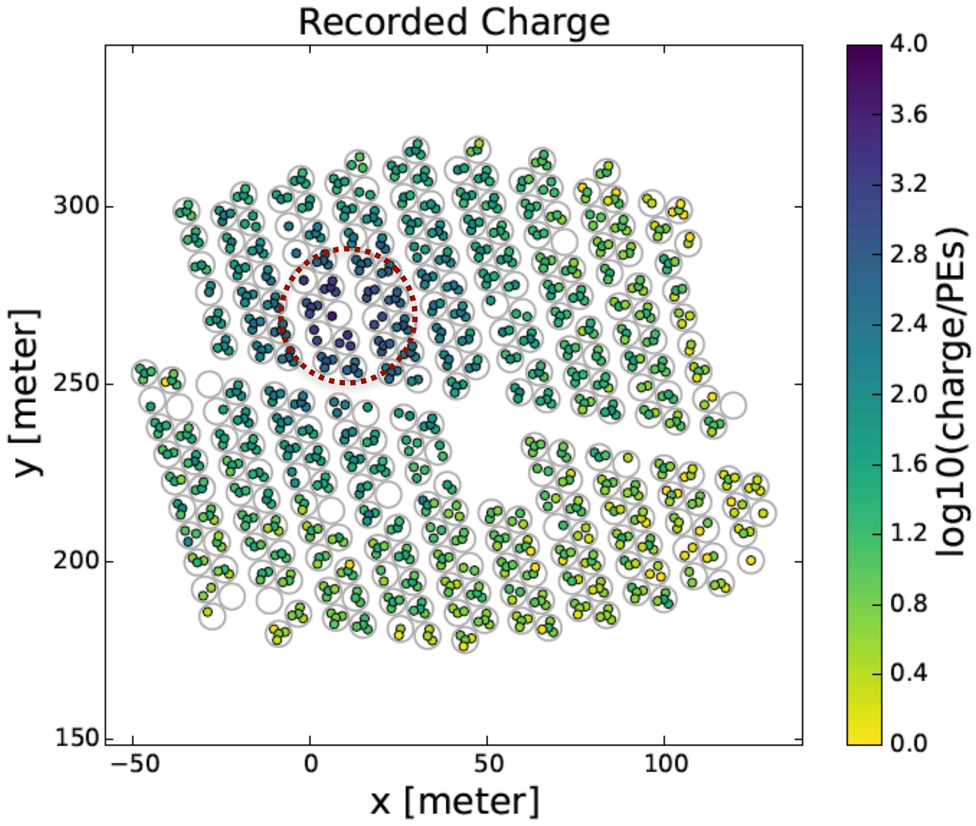

- From hit times at PMTs, deposited charged, number of PMT's with signal:
  - Core location, (X_c, Y_c)
  - Arrival direction, θ
  - Fraction of hit PMT's, f_{hit}
  - Lateral charge profile, Qeff(r)
  - **...**

[HAWC Coll., ApJ 843 (2017) 39]

Energy Spectrum

The Cosmic-Ray Energy Spectrum

- **Spectral characteristics** from acceleration and propagation mechanism effects
- **Mass composition** reveals information about local source environment and of cosmic ray propagation in the Galaxy.
- In general, it is thought that cosmic rays with energies **below PeV are of galactic origin** and that their acceleration and transport in the Galaxy occur through diffusive processes driven by B-fields.
- Energies up to PeV assumed from 1st order Fermi acceleration in shocked plasmas of SNRs with propagation through scattering on random fluctuations in the ISMF.
- CR of **extra-galactic** origin above 10^9 GeV

https://web.physics.utah.edu/~whanlon/spectrum.html

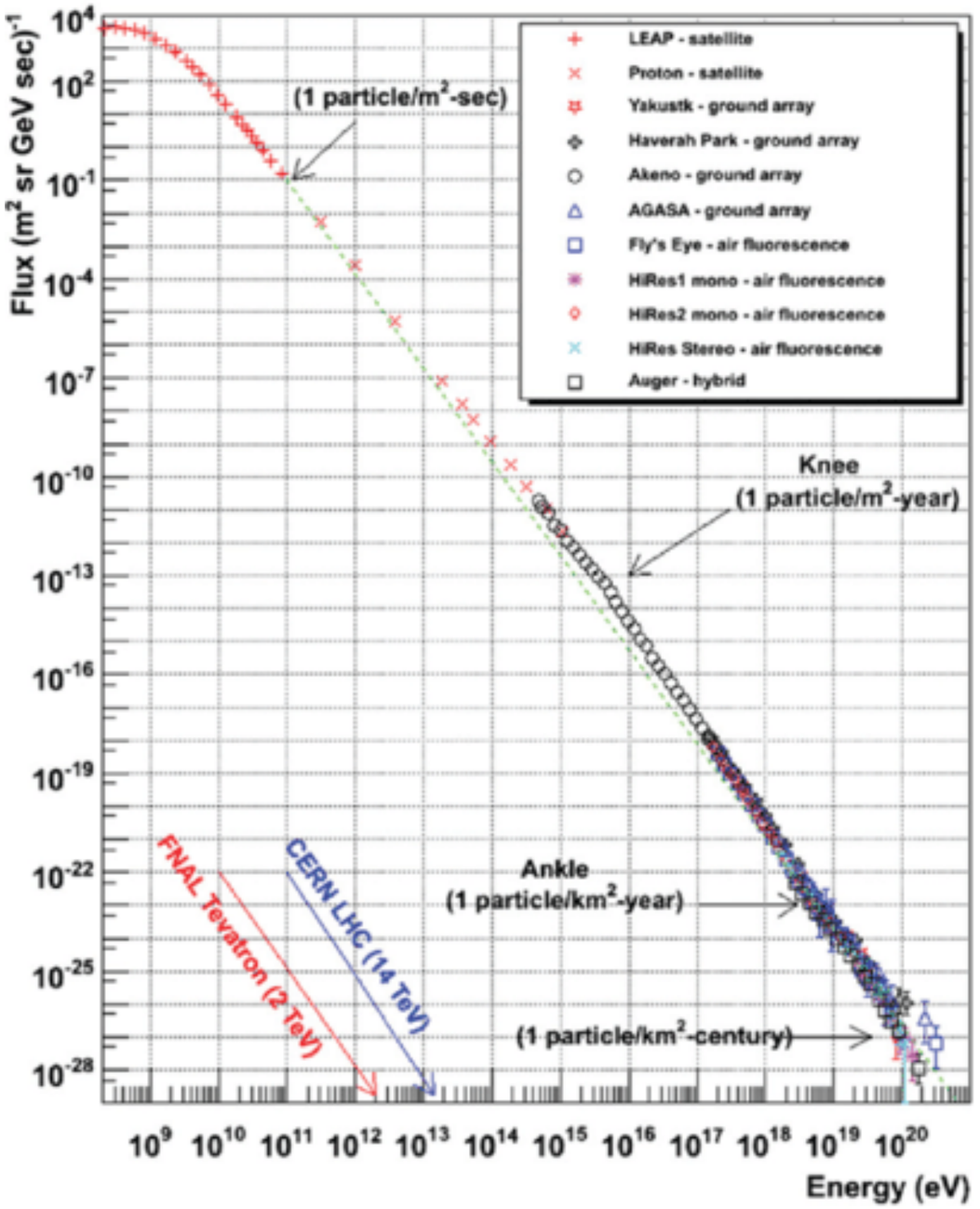

The Cosmic-Ray Energy Spectrum

https://web.physics.utah.edu/~whanlon/spectrum.html

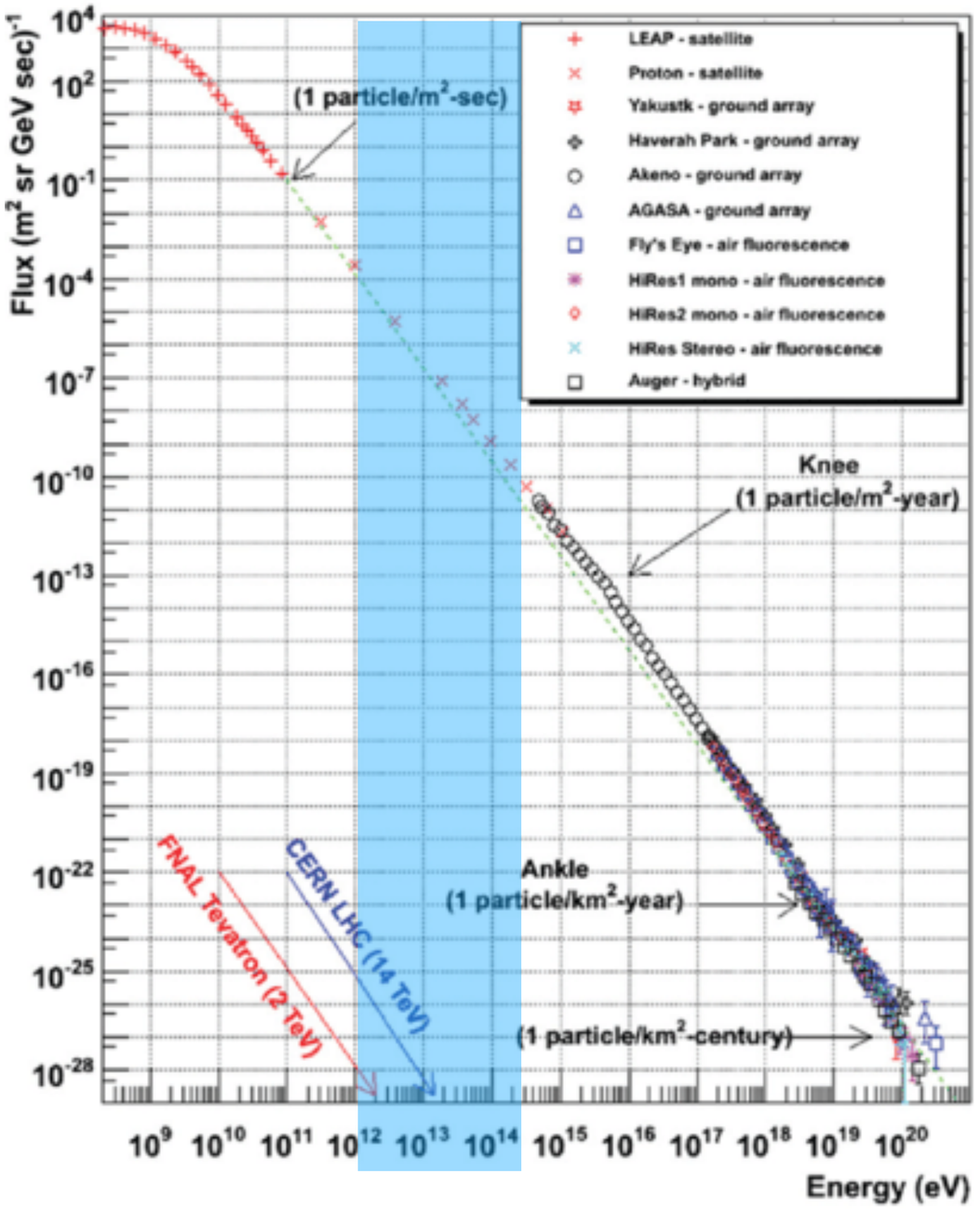

- Previously: little data in 10 TeV - 100 TeV region
  - Recent **direct** measurements have been extended to **higher energies**
  - **Ground-based** experiments to **lower energies**
  - Overlap allows for cross-calibration

All-particle cosmic ray energy spectrum

A measurement of the all-particle energy spectrum of cosmic rays from 10^{13} to 10^{15} eV using HAWC

Alfaro, R. et al. Astroparticle Physics (in preparation)

Bayesian Unfolding

G. D'Agostini, Nucl. Inst. Meth. Phys. Res., **362** (1995).

The number of events observed in time T, within the solid angle Ω, and with reconstructed energy E_{reco}, $N(E_{reco})$ is related to the true energy distribution $N(E)$ by

$$N(E_{\rm reco}) = \frac{1}{\Omega}\int A_{\rm eff}(E, E_{\rm reco})N(E)dE,$$

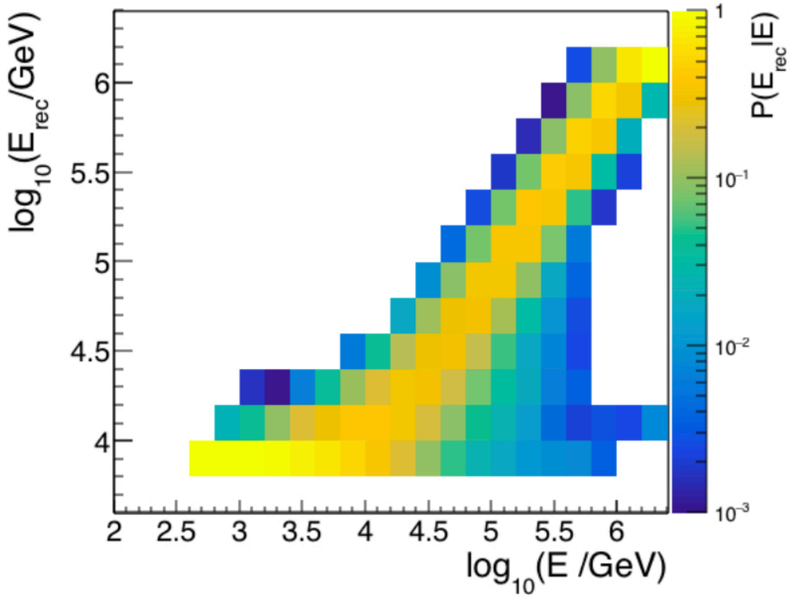

Response matrix $P(E_{rec}|E)$ calculated from MC simulations and our nominal cosmic-ray composition model using QGSJET-II-04.

with

$$A_{\rm eff}(E, E_{\rm reco}) = A_{\rm thrown}P(E_{\rm reco}|E),$$

and the probability of a shower with reconstructed energy E_{reco} to have been produced by a primary particle with energy E is given by

$$P(E_i|E_{{\rm rec},j}) = \frac{P(E_{{\rm rec},j}|E_i)P(E_i)}{\sum_{l=1}^{n_t} P(E_{{\rm rec},j}|E_l)P(E_l)},$$

so the unfolded energy distribution is given by convolving the unfolding matrix with the reconstructed energy distribution iteratively via

$$N(E_i) = \sum_{i=1}^{n_r} P(E_i|E_{{\rm rec},j})N(E_{{\rm rec},j}).$$

All-particle cosmic ray energy spectrum

A measurement of the all-particle energy spectrum of cosmic rays from 10^{13} to 10^{15} eV using HAWC
Alfaro, R. et al. Astroparticle Physics (in preparation)

From the unfolded energy distribution, we reconstruct the all-particle energy spectrum via

$$\Phi(E) = \frac{N(E)}{\Delta E\, \Delta t\, A_{\rm eff}(E)\, \Delta\Omega} \qquad A_{\rm eff}(E) = A_{\rm thrown}\epsilon(E)$$

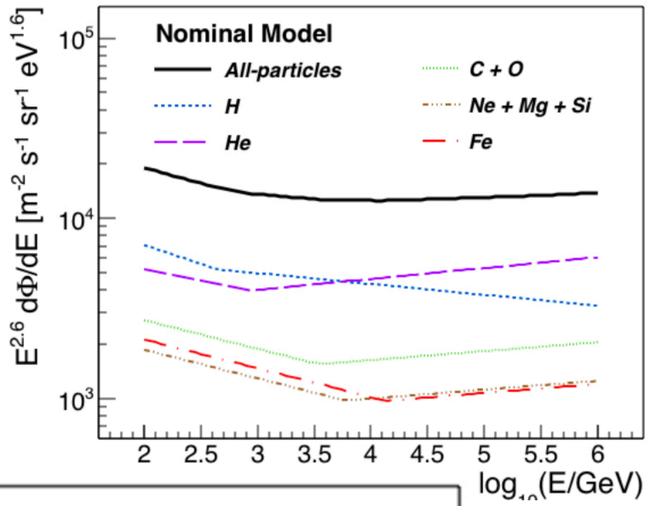

- Φ(E): Energy Spectrum: Intensity as a function of Energy
- N(E): Number of events in energy bin with mean energy (4.7x10^{10} total EAS events)
- ΔE: width of energy bin with mean energy E
- Δt: exposure time = 1.67 × 10^8 s (5.3 years)
- ΔΩ: solid angle = 1.14 sr
- $A_{\rm eff}$(E): Effective Area

The effective area is estimated from MC simulations using QGSJET-II-04 and the mixed component of our nominal composition model which is based on fits to CREAM I-II, PAMELA and AMS-2 data using broken power-law formulas.

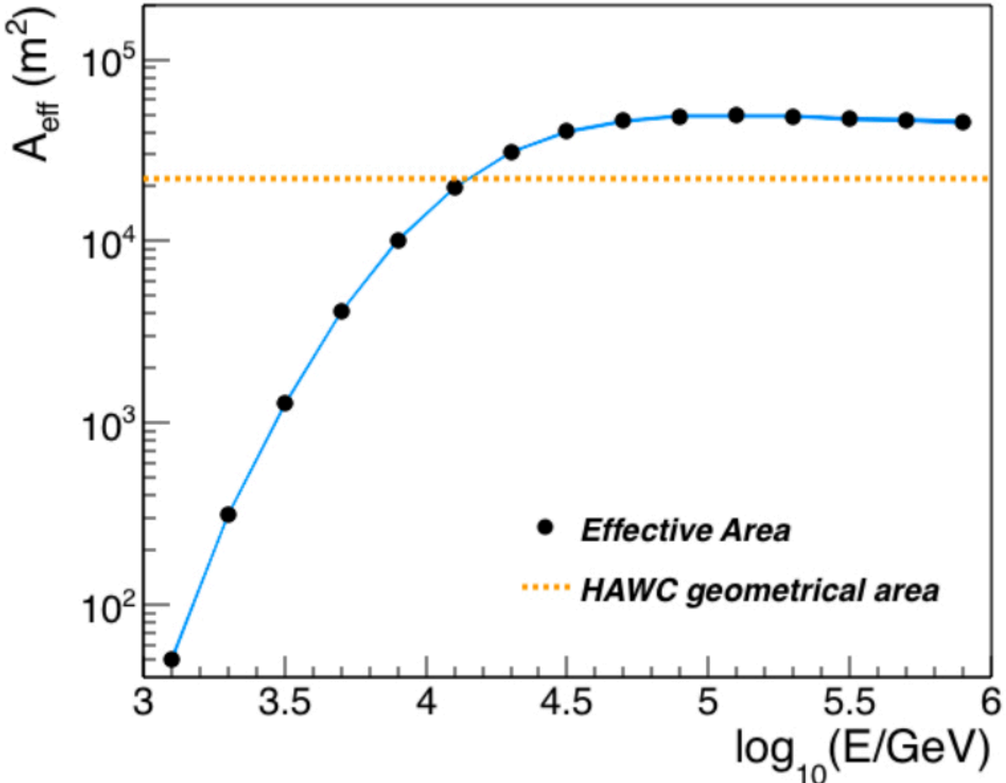

All-particle cosmic ray energy spectrum

A measurement of the all-particle energy spectrum of cosmic rays from 10^{13} to 10^{15} eV using HAWC

Alfaro, R. et al. Astroparticle Physics (in preparation)

- Extended the energy range up to 1 PeV where CRs can be studied with direct and indirect experiments.
- Updated Monte Carlo(MC) simulations (QGSJET-II-04)
- Include the systematic effects from modeling of PMTs.
- Increased statistics, livetime equivalent to 5.3 years and larger FoV.
- Updated the smoothing algorithm in unfolding method to reduce systematic uncertainty from regularization procedure.

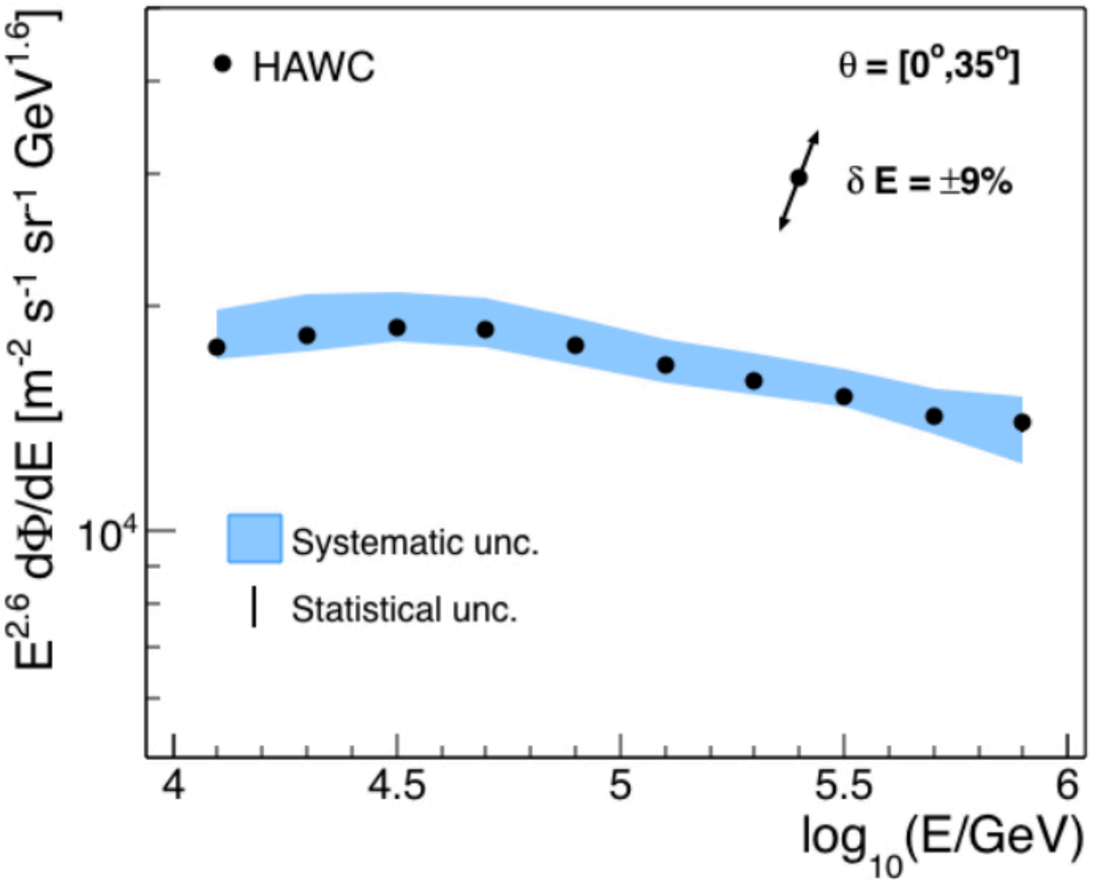

The all-particle energy spectrum is shown with its corresponding systematic and statistical errors. Vertical error bars represent statistical uncertainties though error bars are smaller than the marker size. The error band represents the total systematic uncertainties. The uncertainty in the energy spectrum induced by a systematic error in the energy scale equal to δE = ±9%

All-particle cosmic ray energy spectrum

A measurement of the all-particle energy spectrum of cosmic rays from 10^{13} to 10^{15} eV using HAWC

Alfaro, R. et al. Astroparticle Physics (in preparation)

All-particle spectrum consistent with a broken power law

$$\Phi(E) = \Phi_0 E^{\gamma_1} \left[1 + \left(\frac{E}{E_0}\right)^{\epsilon}\right]^{(\gamma_2-\gamma_1)/\epsilon}$$

with an index of

$$\gamma_1 = -2.52 \pm 0.01 \text{ (stat.)} \ {}^{+0.09}_{-0.05} \text{(sys.)}$$

with a break at

$$E_0 = 38.7^{+2.5}_{-2.3} \text{ (stat)} {}^{+16.1}_{-16.6} \text{ (syst) TeV},$$

followed by an index of

$$\gamma_2 = -2.71 \pm 0.01 \text{(stat.)} \ {}^{0.02}_{-0.04} \text{(sys.)}$$

The broken power-law model is preferred by the data over a single power-law with a statistical significance > 5σ but decreases to 2.6σ after accounting for systematic uncertainties.

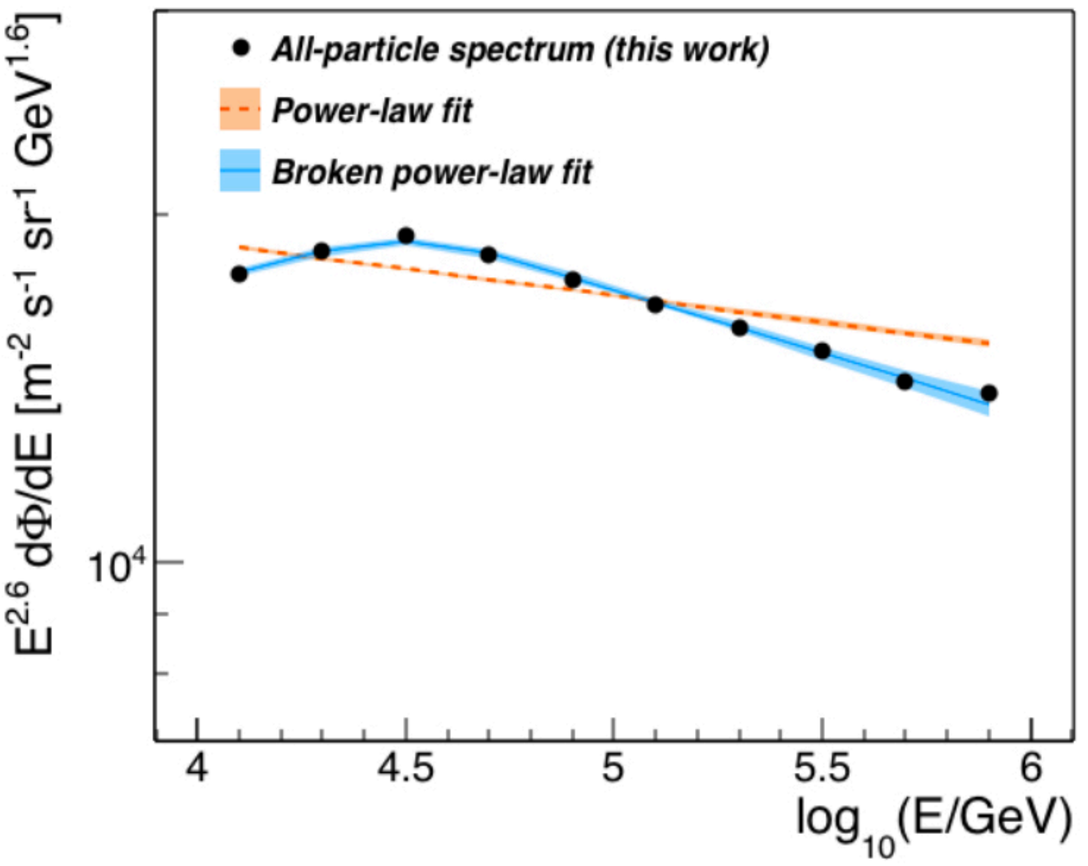

All-particle cosmic ray energy spectrum

A measurement of the all-particle energy spectrum of cosmic rays from 10^{13} to 10^{15} eV using HAWC

Alfaro, R. et al. Astroparticle Physics (in preparation)

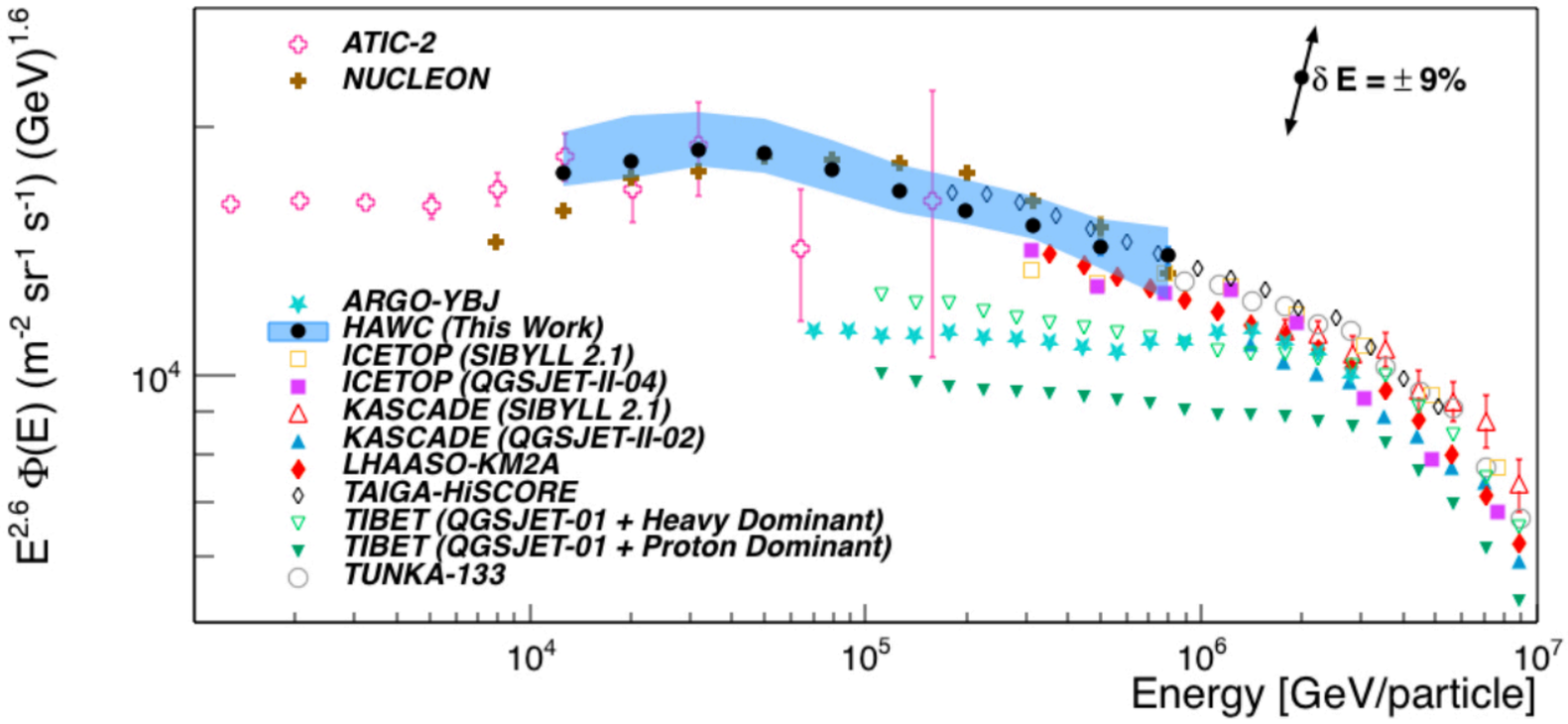

- Result agrees with direct data from ATIC-2 at low energies, and with LHAASO-KM2A, TAIGA-HiScore and TUNKA-133 at high energies, and is in good agreement (within total uncertainties) with NUCLEON.
- CR intensity observed by HAWC is larger than the measurements from the ICETOP, ARGO-YBJ, and TIBET-III EAS arrays.
- Differences may be ascribed to the energy estimation method employed by each collaboration. This may be investigated in more detail in the near future as more high-precision data from other new direct and indirect experiments.

Mass Composition

HAWC H+He Energy Spectrum

Cosmic ray spectrum of protons plus helium nuclei between 6 and 158 TeV from HAWC data
HAWC Collaboration: A. Albert et al. 2022, PRD **105** (2022), 063021

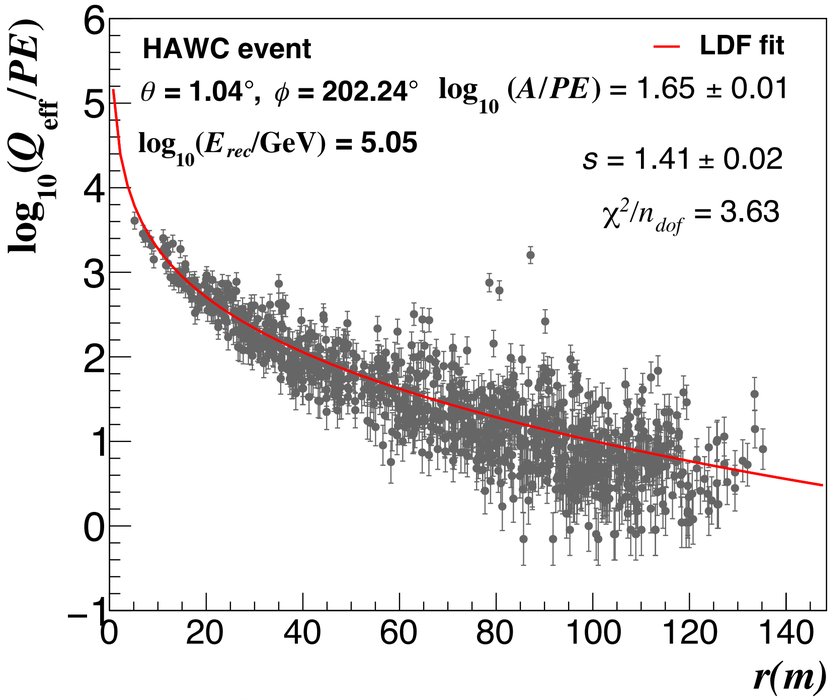

[HAWC Collab., PRD 105 (2022)]

Lateral age parameter (*s*)

- Obtained event-by-event
- Fit of Qeff(r) with a NKG-like function:

$$f_{ch}(r) = A \cdot (r/r_0)^{s-3} \cdot (1 + r/r_0)^{s-4.5}$$

with r_0 = 124.21 m.

A, ***s*** are free parameters

[HAWC Collab., APJ 881 (2017); J.A. Morales Soto et al., PoS(ICRC2019 359 (2019)]

Select a sample enriched with light nuclei

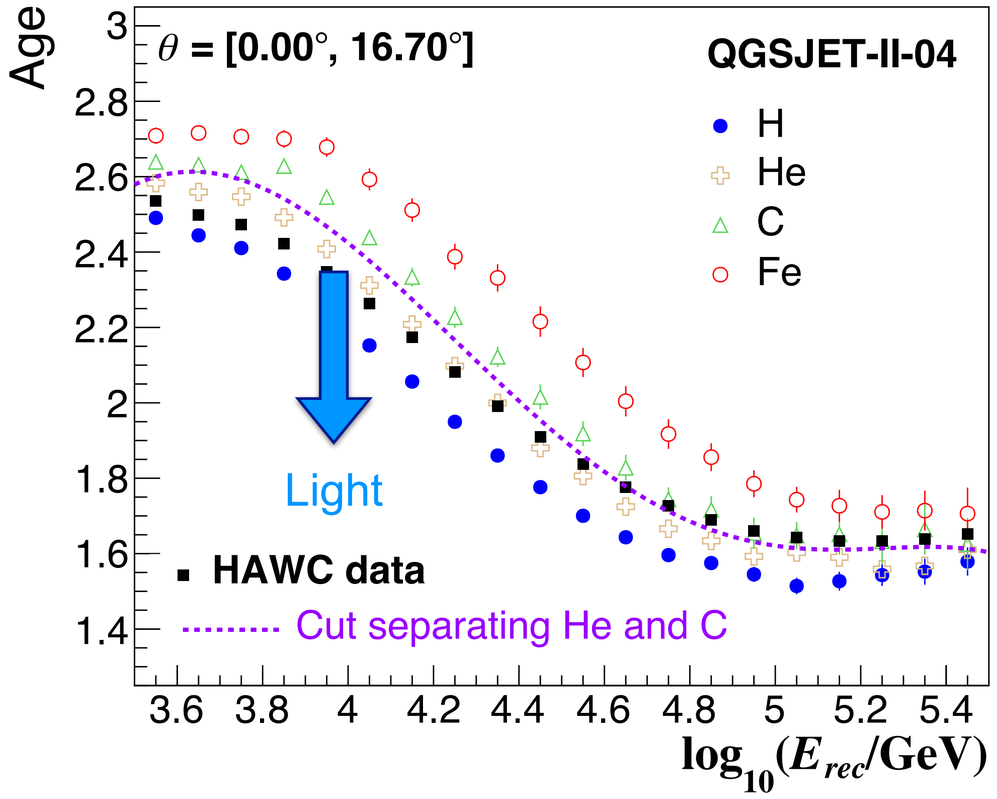

- Age parameter is sensitive to composition
- Select a subsample using a cut on the age
  - Subsample must have a large relative abundance of H and He.

HAWC H+He Energy Spectrum

Build raw energy spectrum of subsample: $N_{raw}(E_{rec})$

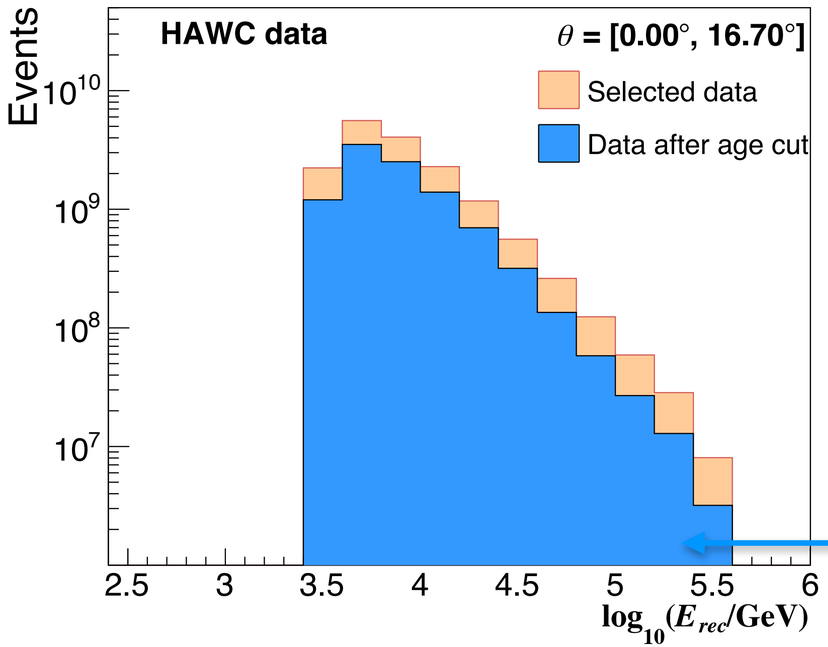

- Experimental data used for analysis:

  HAWC-300

  Δt_{eff} = 3.74 years (94% livetime)

  (June/11/15-June/03/19)

  $\Delta\,\Omega$ = 0.27 sr

Total events	: 2.9 x 10^{12} EAS
+ selection cuts	: 1.6 x 10^{10} EAS
+ age cut	: 9.9 x 10^{9} EAS

Correct $N_{raw}(E_{rec})$ for migration effects

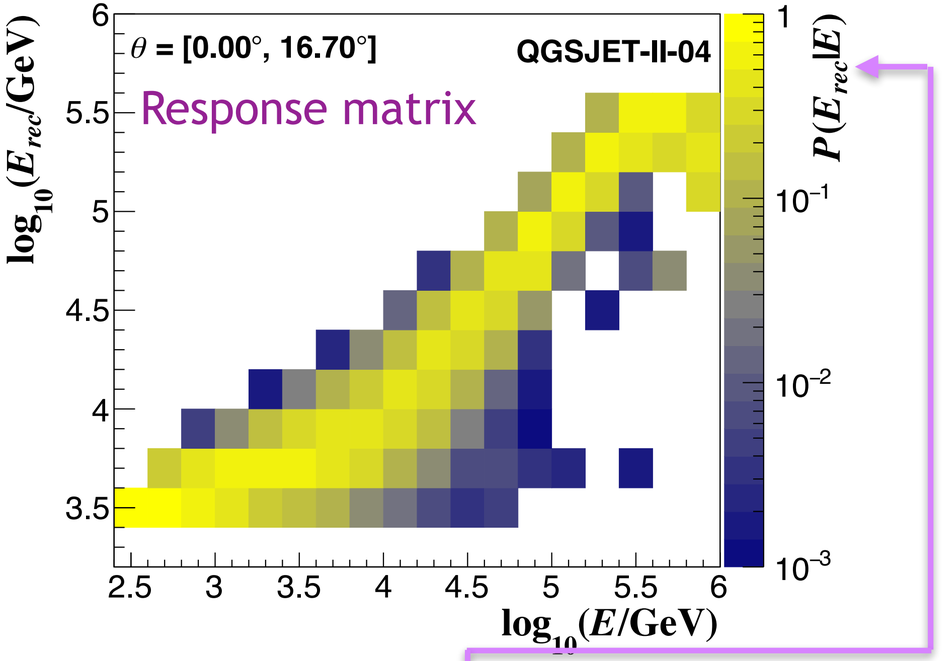

$$N^{Raw}(E_{rec,\,j}) = \sum_i P(E_{rec,\,j} \mid E_i)\, N^{Unf}(E_i)$$

- Solve for $N^{Unf}(E_i)$ using Bayesian unfolding

  [G. D' Agostini, DESY 94-099]

- Stopping criterium: Minimum of weighted mean squared error

[G. Cowan, Stat. Data analysis, Oxford Press. 1998]

$$\mathrm{WMSE} = \frac{1}{N_{points}} \sum_{i}^{N_{points}} \frac{stat_i^2 + sys_i^2}{n_i}$$

HAWC H+He Energy Spectrum

H+He

[HAWC Collab., PRD 105 (2022)]

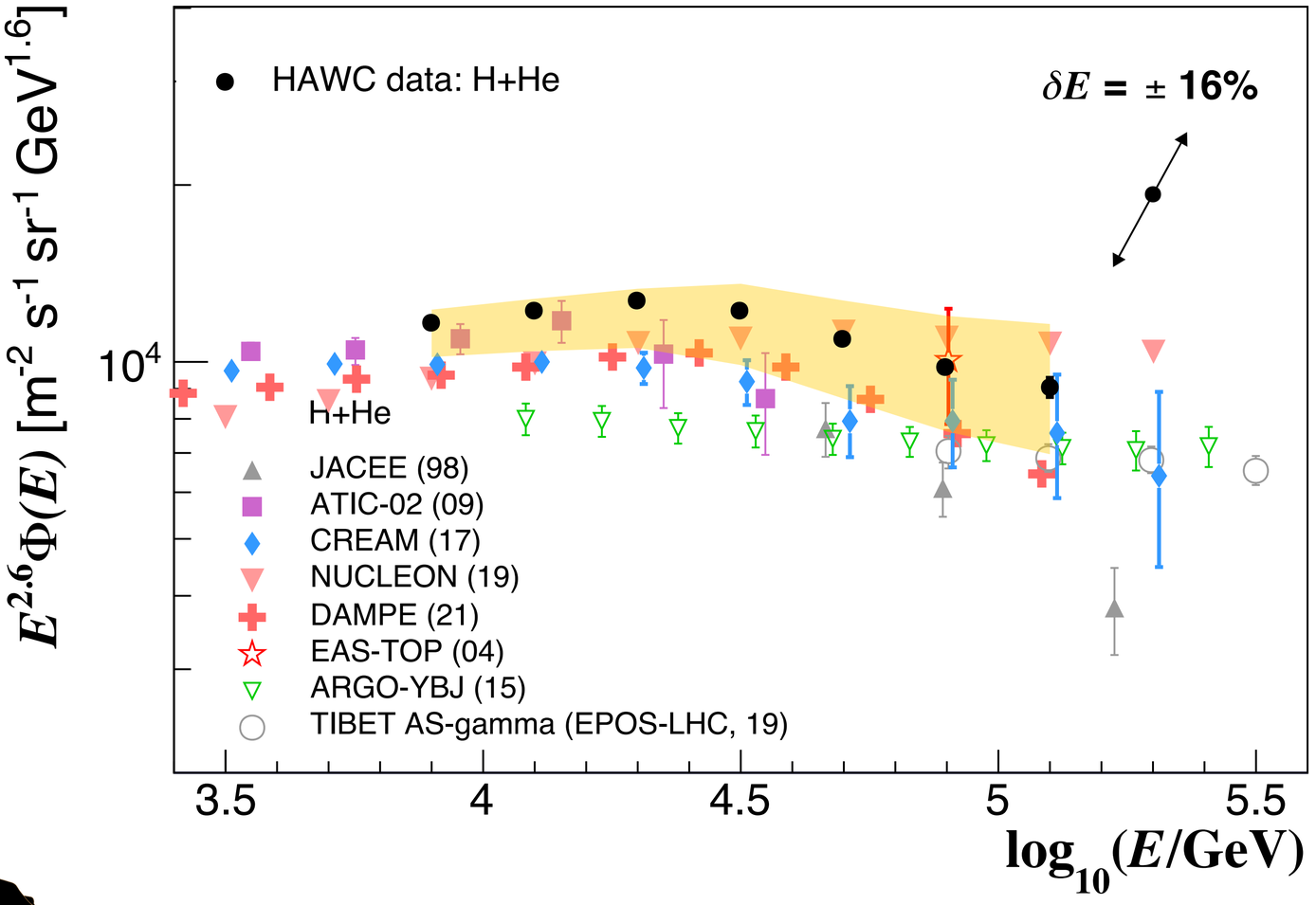

- **HAWC** data confirm previous hints from ATIC-2, CREAM I-III and NUCLEON about the existence of a break in the spectrum of the light component of cosmic rays in the 10^4 - 10^5 GeV range.
- **HAWC** result is strengthened by recent DAMPE data.
- **HAWC** data is in agreement with ATIC-2 close to 10^4 GeV.

HAWC H+He Energy Spectrum

Fit of spectrum

H+He

[HAWC Collab., PRD 105 (2022)]

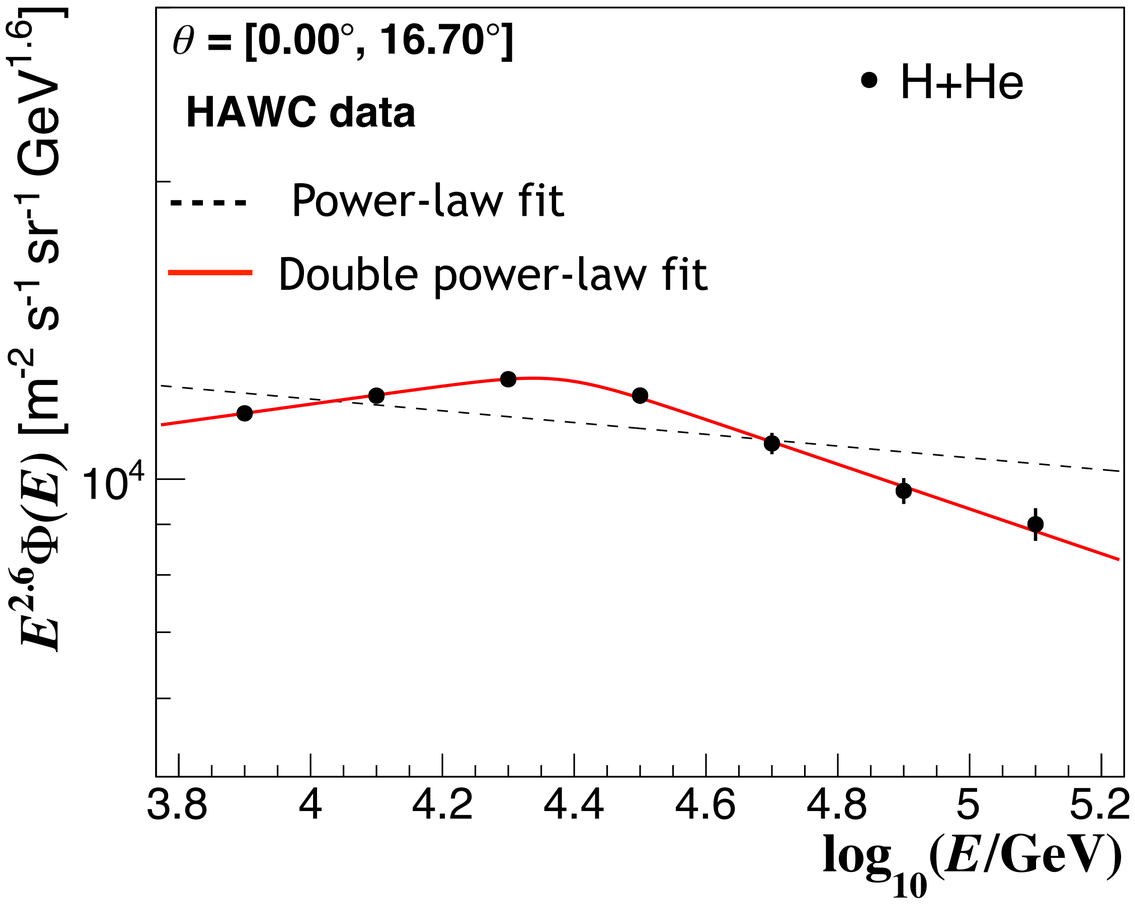

- **Test Statistics:**

  TS = - $\Delta\chi^2$ = 177.25

  p-value = 2 x 10^{-5}

-> 4.1σ deviation from scenario with single power-law.

- Results for the double power-law fit:

  γ_1 = -2.51 ± 0.02

  γ_2 = -2.83 ± 0.02

  $\Delta\gamma$ = -0.32 ± 0.03

  $\log_{10}(E_0/\mathrm{GeV})$ = 4.38 ± 0.06

  - **$E_0 = 24.0^{+3.6}_{-3.1}$ TeV**

All-particle cosmic ray energy spectrum

- All-particle spectrum feature: wider and shifted to higher energies possibly from increasing influence of Z > 2 close to 100 TeV.
- The observed softening in the TeV range of p+He could explain the softening of the all-particle spectrum, with heavy elements playing a greater role as energies approach 100 TeV.
- HAWC and GRAPES-3 measurements suggest possible hardening in the intensities of H and He above 100TeV.

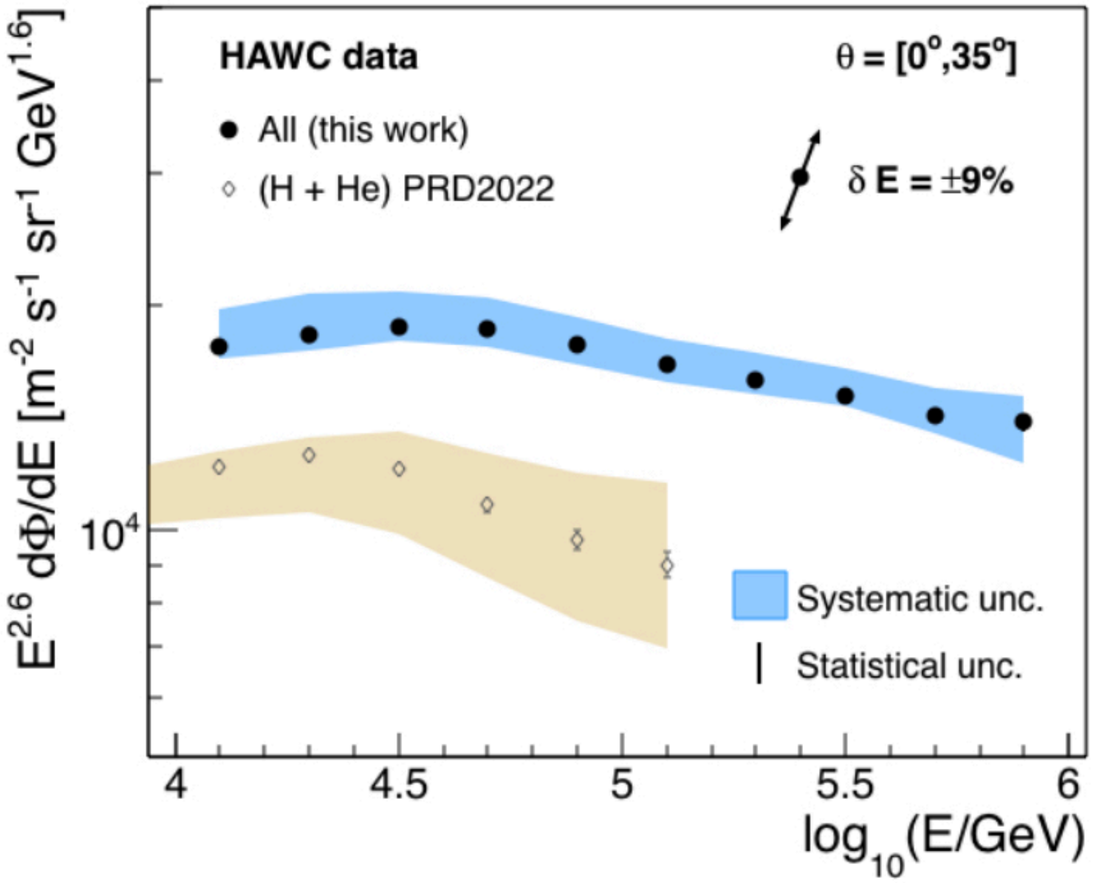

Updated all-particle spectrum in the range 10^{13} eV - 10^{15} eV, where CRs can be studied with direct and indirect experiments. Comparison to H+He spectrum as measured with HAWC [11] (open diamonds). The error bands represent the total systematic uncertainties, and the vertical error bars, statistical uncertainties.

HAWC p, He, Z>=3

HAWC measurements of the energy spectra of cosmic ray protons, helium and heavy nuclei in the TeV range
Arteaga, J.C. PoS(ICRC2021)374

- Unfold **shower age vs $\log_{10}$(E)** data to find the **elemental spectra for H, He and heavy nuclei** (Z > 2).

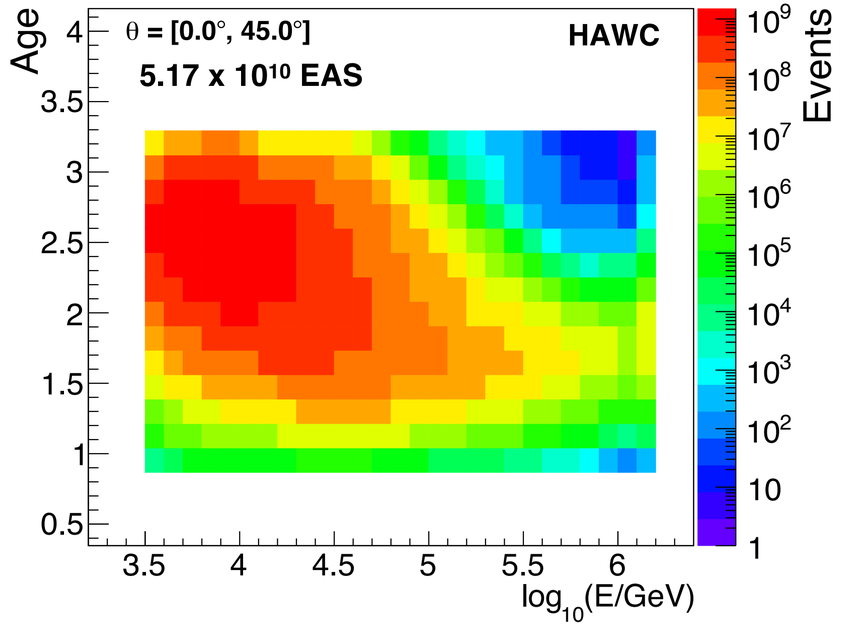

$$n(s, \log_{10} E) = T_{\text{eff}}\, \Delta\Omega \sum_{j=1} \sum_{E_T} P_j(s, \log_{10} E | \log_{10} E_T)\, A_{\text{eff},j}(E_T)\, \Phi_j(E_T)\, \Delta E_T$$

$n(s, \log_{10} E)$: # events per (s, $\log_{10} E$) bin.

$P_j(s, \log_{10} E | \log_{10} E_T)$: response matrix for EAS from mass group j (reconstruction and fluctuations).

A_{eff} : effective area = $A_{\text{thrown}}\, \varepsilon_{\text{eff}}$.

$\Phi_j(E_T)$: spectrum for mass group j.

HAWC data

- January/01/16 - June/03/19
- T_{eff} = 3.21 years
- $\Theta < 45^{O}$
- Successfully reconstructed
- $f_{\text{hit}} \geq 0.2$

- Hit PMT's within radius of 40 m > 40
- s = [1, 3.2]
- $\log_{10}$ (E/GeV) = [3.5, 6.2]

Apply Gold's unfolding algorithm

[R.Gold, Report ANL-6984, 1964]

[KASCADE Collab., App 24 (2005) 1]

Bins:
Δ $\log_{10}$ (E/GeV) = 0.1
Δ s = 0.17

HAWC p, He, Z>=3

HAWC measurements of the energy spectra of cosmic ray protons, helium and heavy nuclei in the TeV range
Arteaga, J.C. PoS(ICRC2021)374

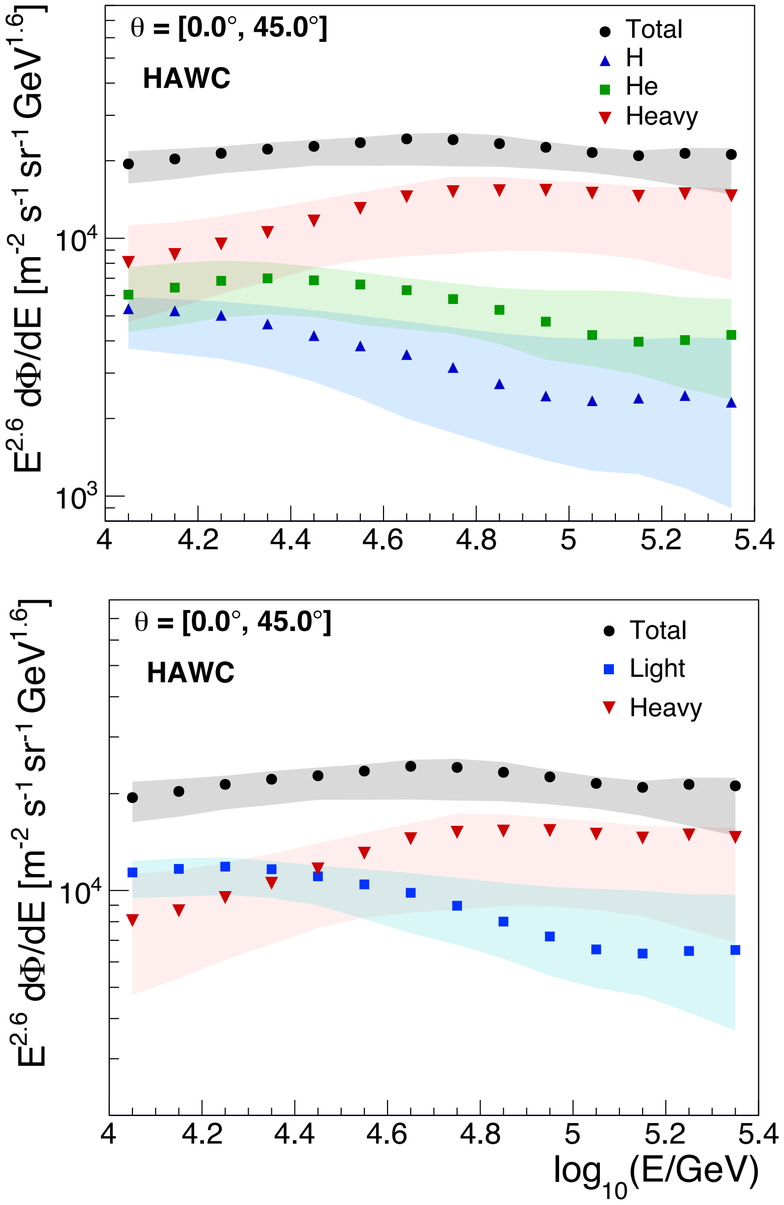

- The elemental spectra do not follow a power-law function.

  HAWC data show fine structure (> 5σ) between 10 TeV and 251 TeV:

  $\Phi H(E)/\Phi He(E) < 1$ for E = [10 TeV, 100 TeV].

- Composition becomes heavier from 10 TeV to 100 TeV.
- Bump in the the all-particle spectrum at ~ 46 TeV reported by HAWC (2017) due to superposition of individual softening in spectra of light and heavy mass groups. [HAWC Collab., PRD 96 (2017) 122001]
- Knee-like feature at ~ 32 TeV in spectra of H+He observed by HAWC comes from individual cuts in spectra for H and He. [HAWC Collab., PoS(ICRC2019) 176]

$$\Phi(E) = \Phi_0 E^{\gamma_1} \left[1 + \left(\frac{E}{E_0}\right)^{\varepsilon_0}\right]^{(\gamma_2-\gamma_1)/\varepsilon_0} \left[1 + \left(\frac{E}{E_1}\right)^{\varepsilon_1}\right]^{(\gamma_3-\gamma_2)/\varepsilon_1}$$

	E_0(TeV)	E_1(TeV)	γ_1	γ_2
H	14.1 +2.2/-0.4	103 +1/-4	-2.6 +0.2/-0.5	-3.1 ± 0.3
He	25.3 +1.1/-0.8	152 +11/-9	-2.2 +0.1/-0.3	-3.1 +0.4/-0.1
Z > 2	51 ± 1	—	-2.1 ± 0.3	-2.6 +0.04/-0.2

$E_{0,He}/E_{0,H} = 1.8\ ^{+0.3}_{-0.1}$

HAWC p, He, Z>=3

HAWC measurements of the energy spectra of cosmic ray protons, helium and heavy nuclei in the TeV range
Arteaga, J.C. PoS(ICRC2021)374

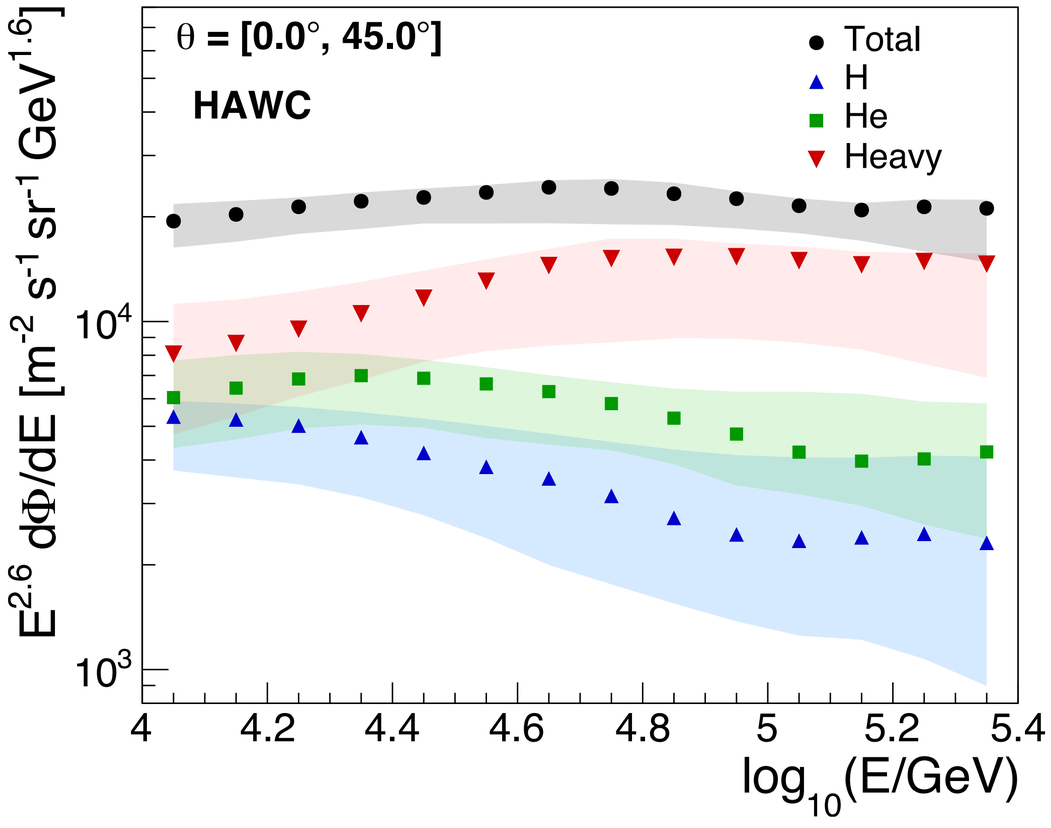

- **Statistical errors** < 0.05%.

- **Systematic errors** < 78%

  - Statistics of the MC data set + Effective area (< 7%).
  - Uncertainties in parameters of the PMTs (< 55%).
  - Hadronic interaction model: EPOS-LHC (< 30%).
  - Unfolding procedure: bias, seed, reduced cross entropy technique (< 14%) .
  - Bias in shower age (< 20%).
  - Cosmic ray composition model: GSF, poligonato, JACEE, ATIC-02 (< 19%).

HAWC p, He, Z>=3

HAWC measurements of the energy spectra of cosmic ray protons, helium and heavy nuclei in the TeV range
Arteaga, J.C. PoS(ICRC2021)374

H and He spectra: Comparison with other experiments

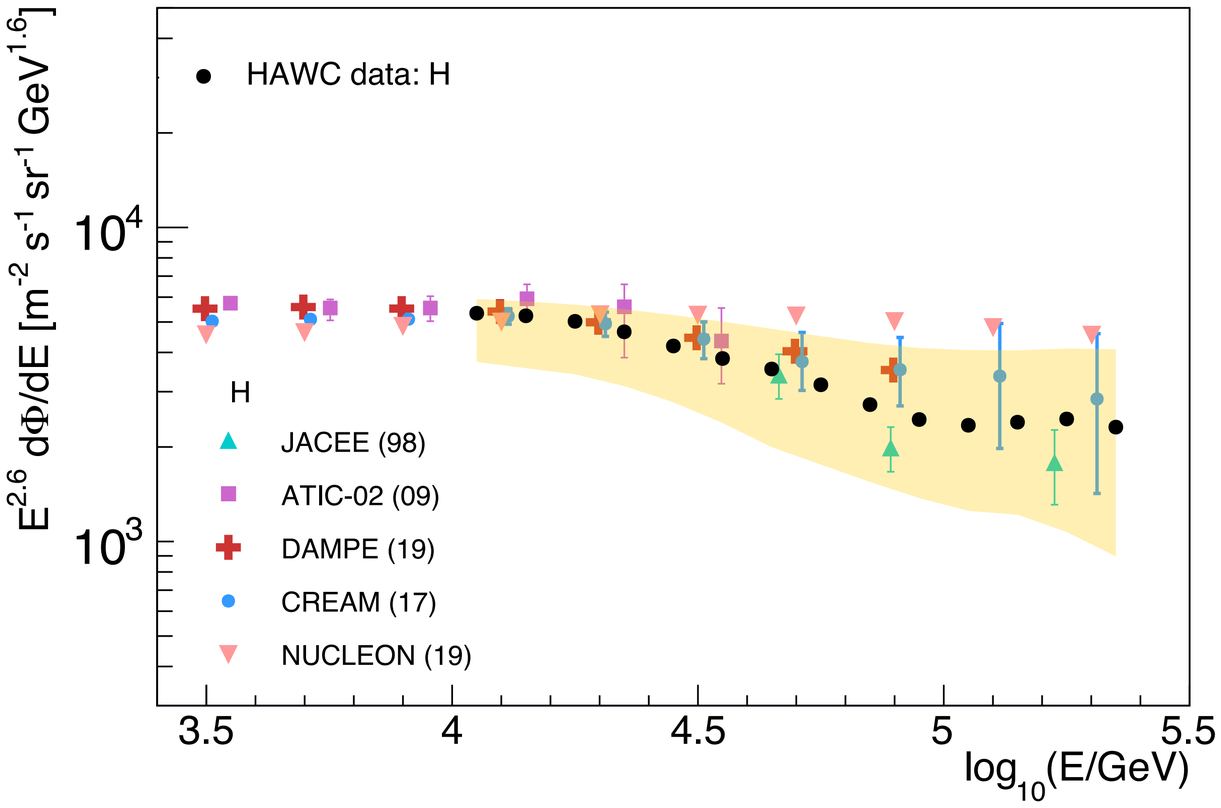

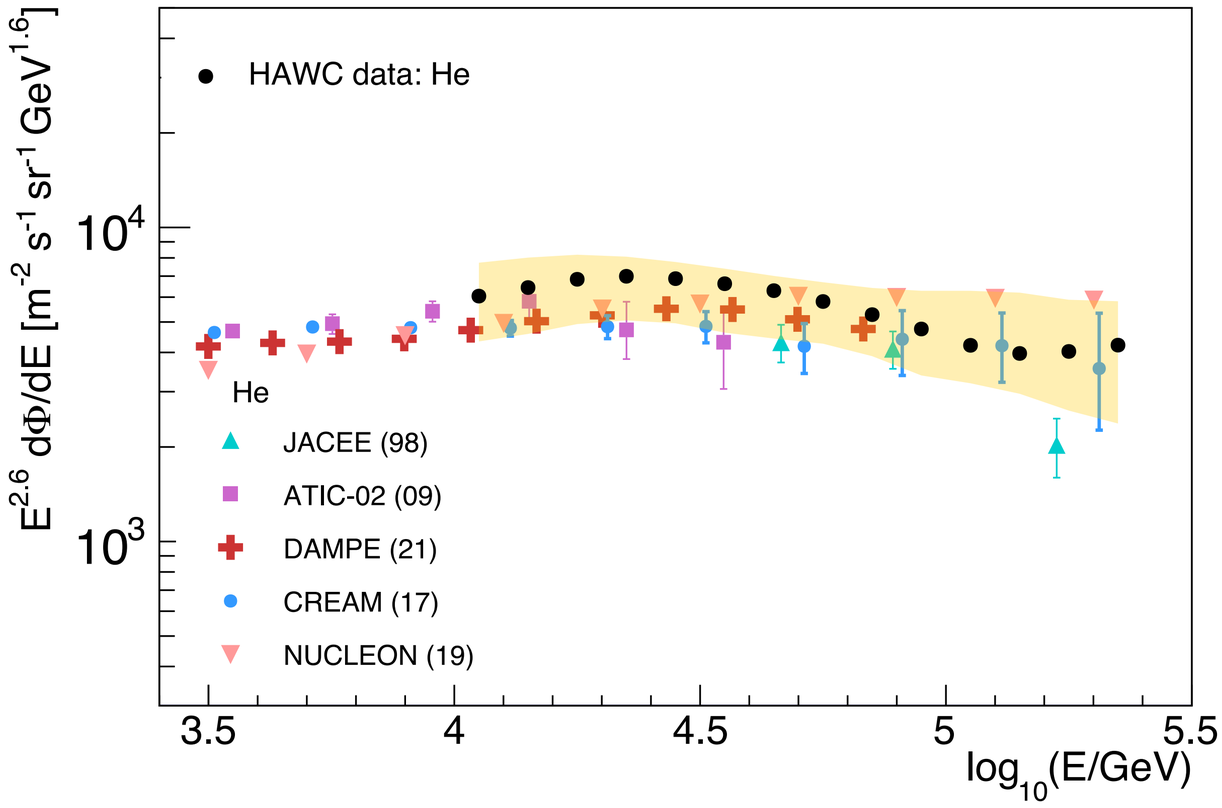

- Good agreement of **HAWC** with direct data from **DAMPE**, **ATIC-02** and **CREAM I-III** within systematic errors.
- **HAWC** confirms softenings at tens of TeV observed by **DAMPE**, first hinted by **ATIC-02**, **CREAM** and **NUCLEON**.

HAWC Composition

HAWC measurements of the energy spectra of cosmic ray protons, helium and heavy nuclei in the TeV range
Arteaga, J.C. PoS(ICRC2021)374

Light (H + He) and Heavy (Z > 2) spectra: Comparison with other experiments

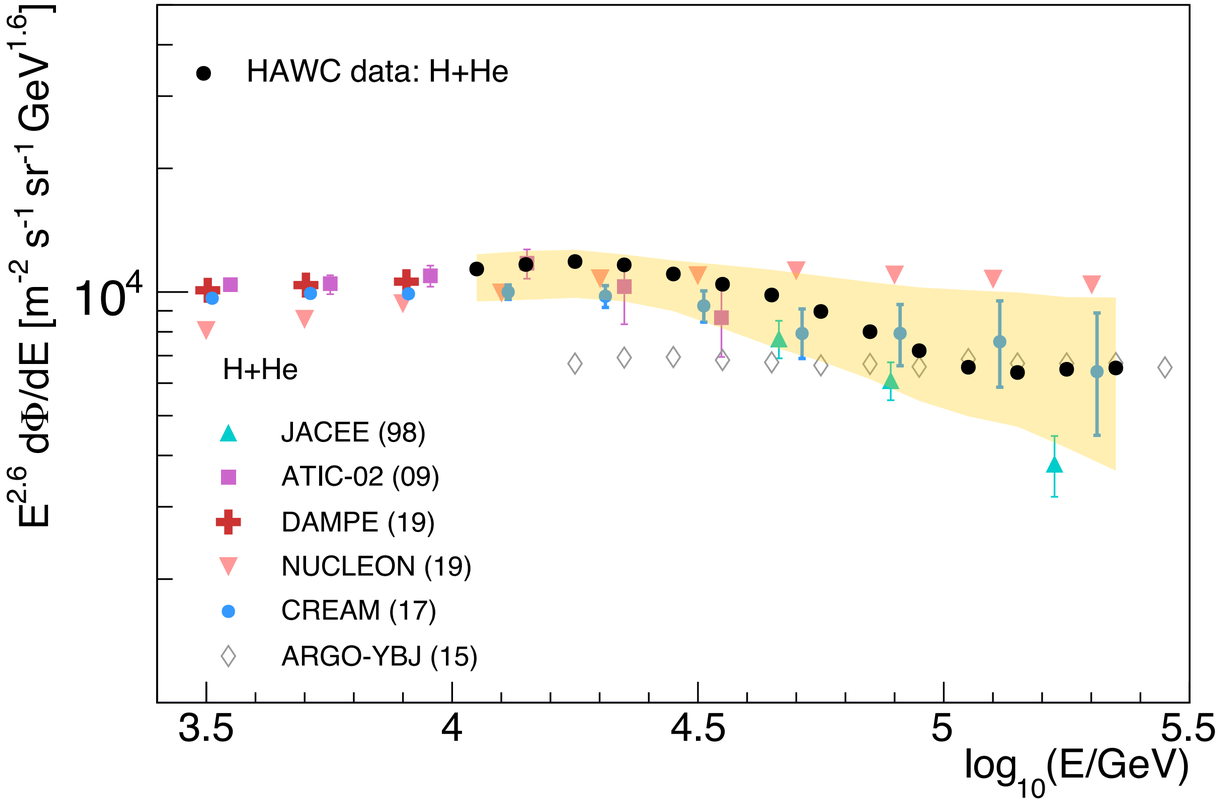

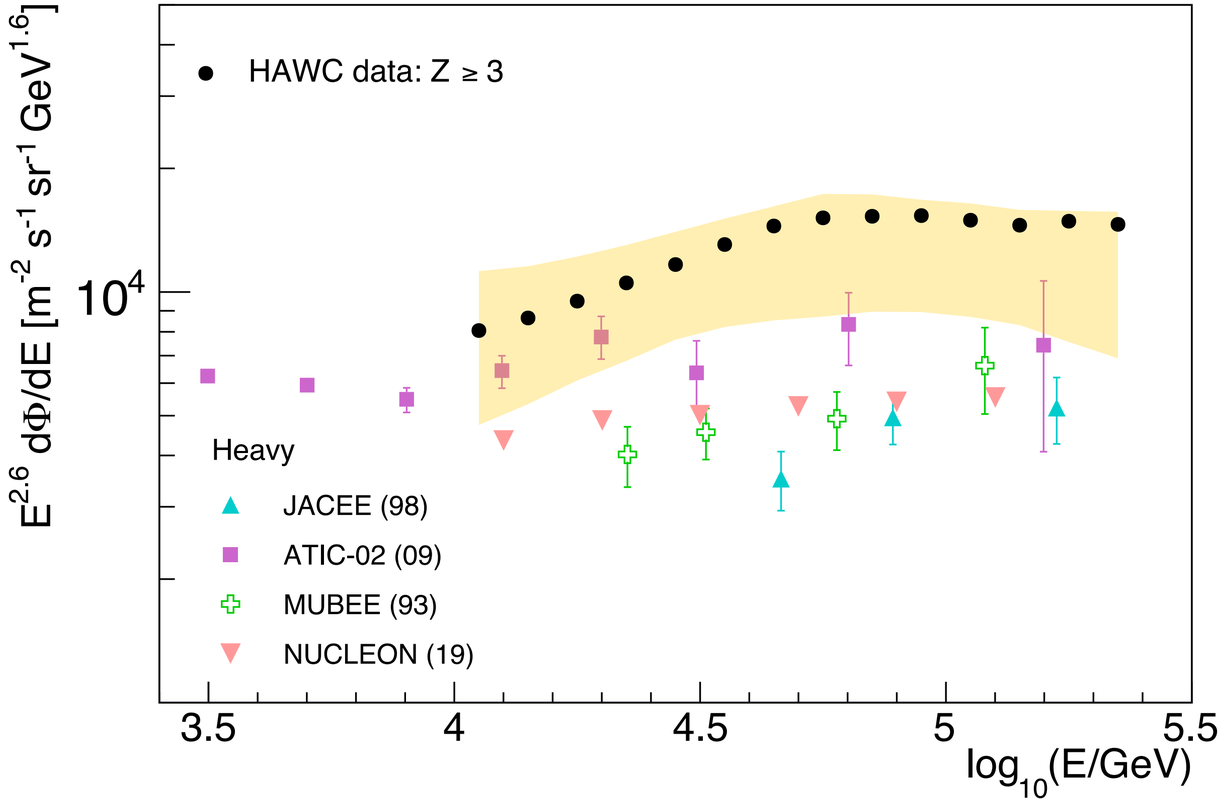

- Good agreement of **HAWC** with **ATIC-02, CREAM** and **JACEE** within systematic errors.
- **ARGO-YBJ** disagrees with **HAWC** data for E < 50 TeV.

- Agreement of **HAWC** with **ATIC-02** within systematic errors.
- **HAWC** data is above **NUCLEON**, **MUBEE** and **JACEE** observations.

Arrival Direction (Anisotropy)

Method for measuring CR anisotropy

1 Build a binned data map using the equatorial coordinates of the events

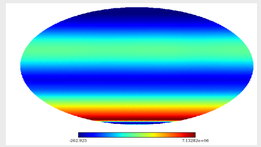

2 Construct a “reference” map by integrating acceptance over 24 hours.

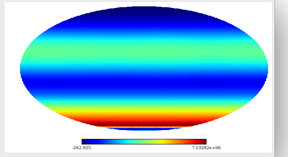

Time-scrambling: $(\theta, \phi, t) \rightarrow (\alpha, \delta)$

$(\theta, \phi, t') \rightarrow (\alpha', \delta')$

Direct integration: $\langle N(\alpha, \delta) \rangle = \int dt \int d\Omega A(ha, \delta) \cdot R(t) \cdot \epsilon(ha, \alpha, t)$

3 Correlate pixels to increase sensitivity to different angular scales

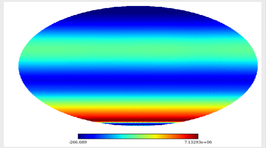

Relative Intensity

$$\delta I(\alpha, \delta)_i = \frac{N(\alpha, \delta)_i - \langle N \rangle(\alpha, \delta)_i}{\langle N \rangle(\alpha, \delta)_i}$$

4 Calculate relative differences between data and reference with significance.

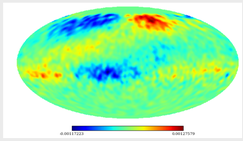

$$s_i = \sqrt{2}\left\{ N_i \log\left[\frac{1+\alpha}{\alpha}\left(\frac{N_i}{N_i + N_o}\right)\right] + N_o \log\left[(1+\alpha)\left(\frac{N_o}{N_i + N_o}\right)\right]\right\}^{1/2}$$

5 Calculate statistical significance for each pixel

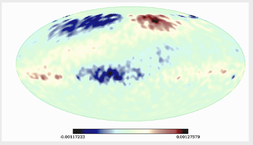

Iterative maximum likelihood method

Ahlers, BenZvi, Desiati, Díaz-Vélez, Fiorino, Westerhoff (arXiv:1601.07877)

The likelihood of observing n cosmic rays is given by the product of Poisson probabilities

$$\mathcal{L}(n|I,\mathcal{N},\mathcal{A}) = \prod_{\tau i} \frac{(\mu_{\tau i})^{n_{\tau i}} e^{-\mu_{\tau i}}}{n_{\tau i}!}$$

Maximize the likelihood ratio via null hypothesis in N, A y I

$$\lambda = \frac{\mathcal{L}(n|I,\mathcal{N},\mathcal{A})}{\mathcal{L}(n|I^{(0)},\mathcal{N}^{(0)},\mathcal{A}^{(0)})}$$

maximum values ($I^\star$,$N^\star$,$A^\star$) must follow

$$I^\star_{\mathfrak{a}} = \sum_\tau n_{\tau\mathfrak{a}} \Big/ \sum_\kappa \mathcal{A}^\star_{\kappa\mathfrak{a}} \mathcal{N}^\star_\kappa ,$$
$$\mathcal{N}^\star_\tau = \sum_i n_{\tau i} \Big/ \sum_j \mathcal{A}^\star_j I^\star_{\tau j} ,$$
$$\mathcal{A}^\star_i = \sum_\tau n_{\tau i} \Big/ \sum_\kappa \mathcal{N}^\star_\kappa I^\star_{\kappa i} ,$$

which can be solved iteratively.

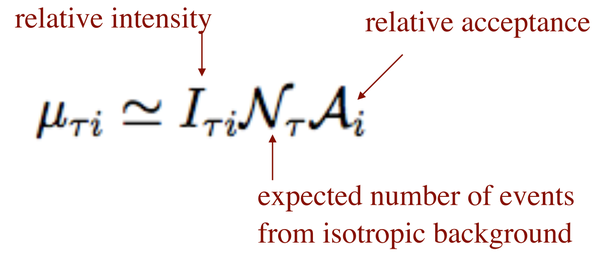

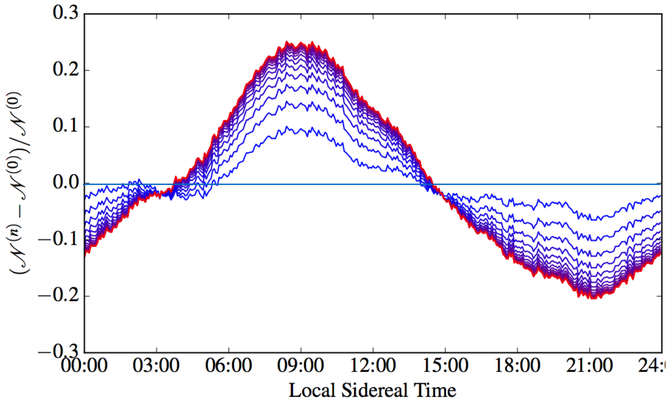

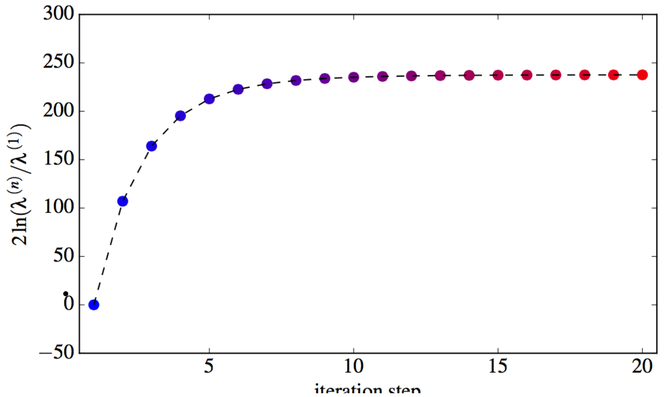

CR Anisotropy vs. Energy (2-years)

- 2-years of HAWC CR data
- 8 energy bins
- Energies from 1.4 TeV to 70 TeV.

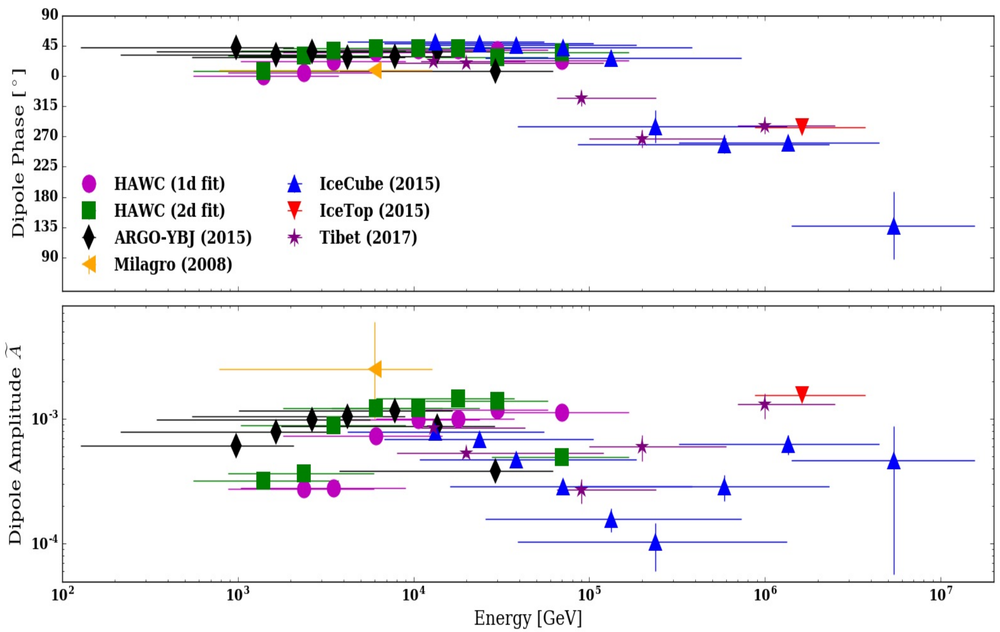

The Astrophysical Journal, 865:57 (15pp), 2018 September 20 https://doi.org/10.3847/1538-4357/aad90c

Observation of Anisotropy of TeV Cosmic Rays with Two Years of HAWC

A. U. Abeysekara[1], R. Alfaro[2], C. Alvarez[3], J. D. Álvarez[4], R. Arceo[3], J. C. Arteaga-Velázquez[4], D. Avila Rojas[2],

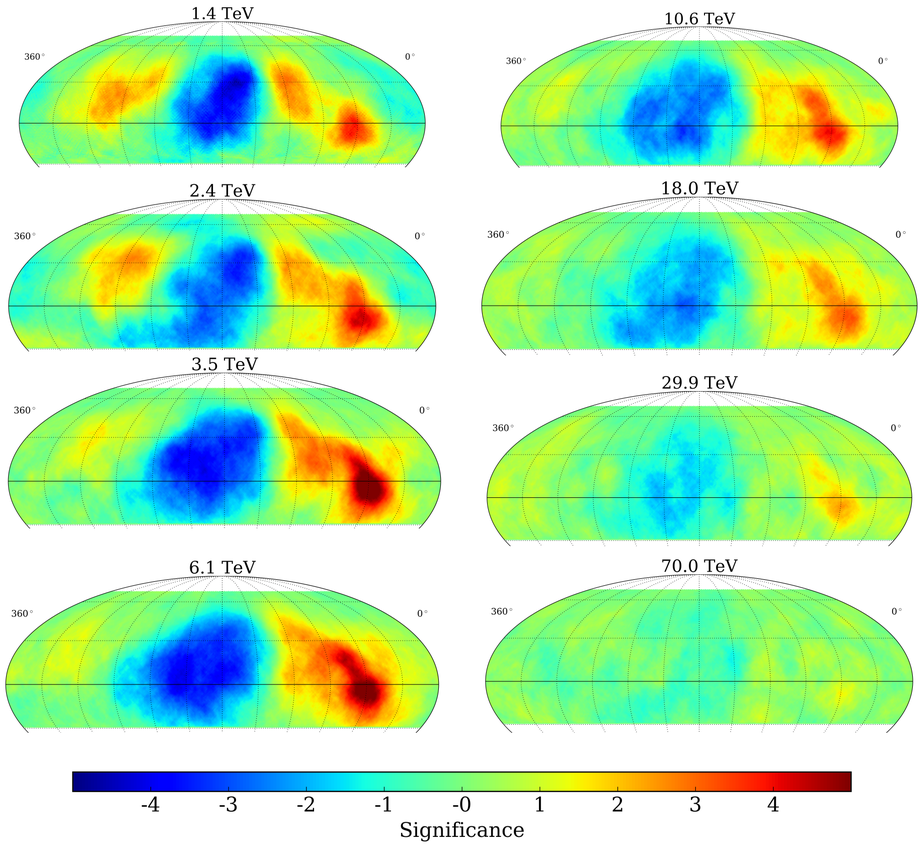

All-Sky at 10 TeV

All-Sky Measurement of the Anisotropy of Cosmic Rays at 10 TeV and Mapping of the Local Interstellar Magnetic Field
HAWC Collaboration: A.U. Abeysekara et al., and IceCube Collaboration, M.G. Aartsen et al., ApJ**871**(2019), 096.

Large Scale

Relative Intensity

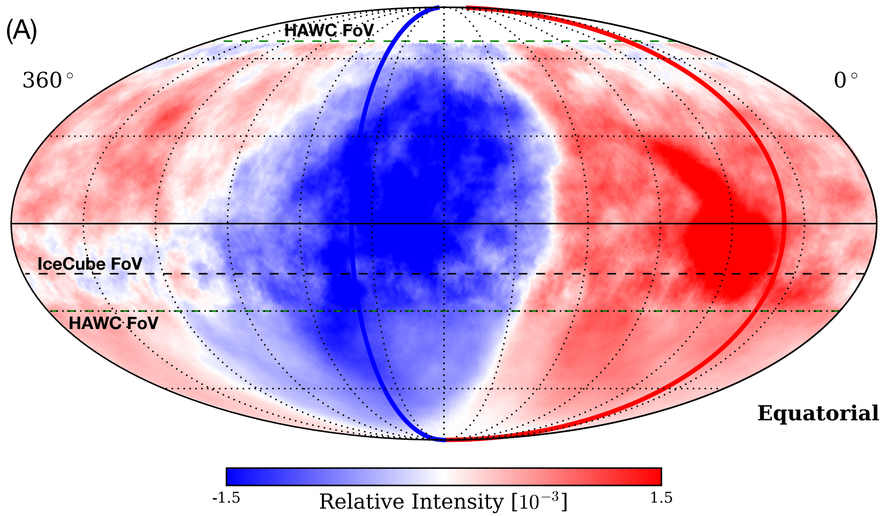

Significance Map

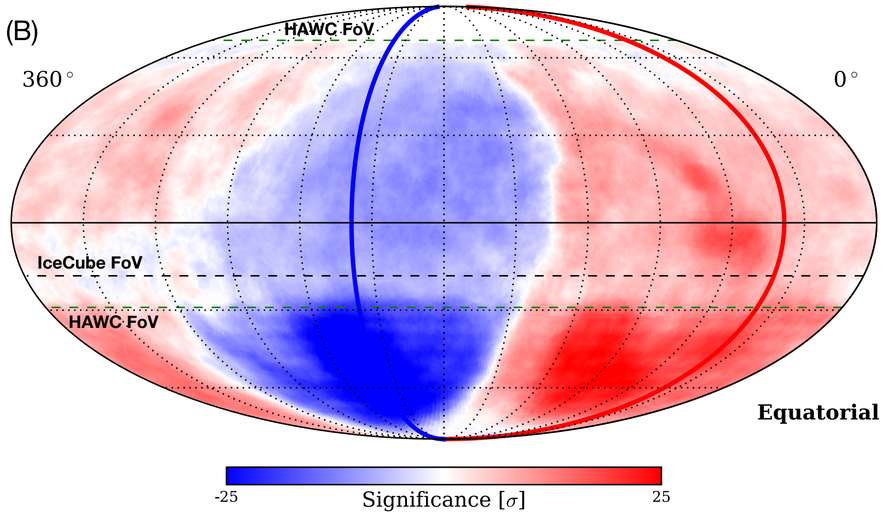

All-Sky at 10 TeV

All-Sky Measurement of the Anisotropy of Cosmic Rays at 10 TeV and Mapping of the Local Interstellar Magnetic Field
HAWC Collaboration: A.U. Abeysekara et al., and IceCube Collaboration, M.G. Aartsen et al., ApJ**871**(2019), 096.

Large Scale

Small Scale ($\ell > 3$)

Relative Intensity

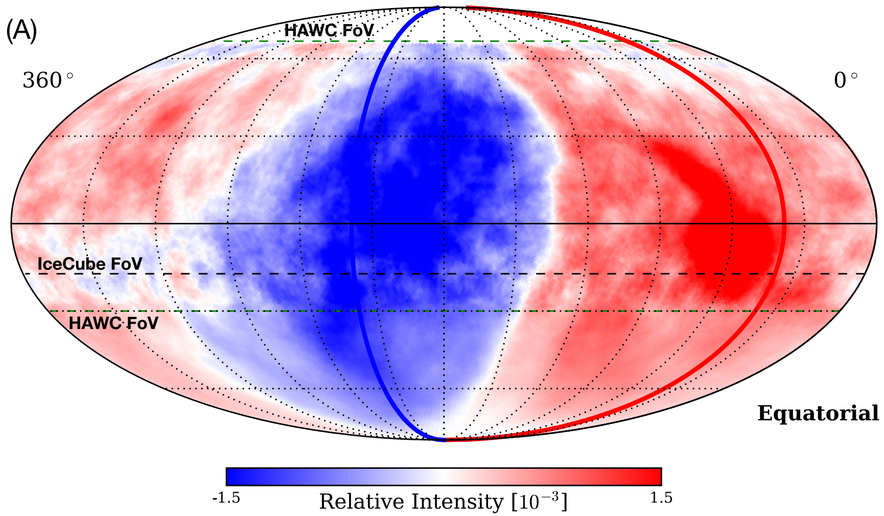

Significance Map

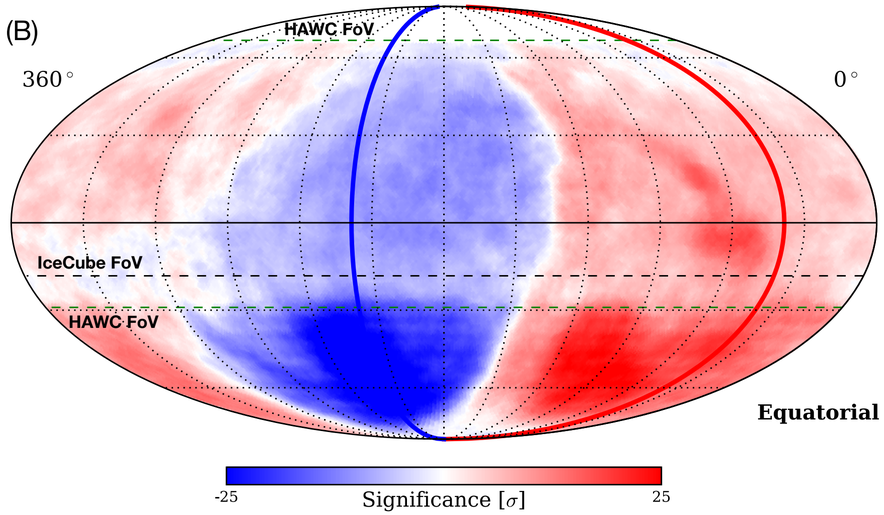

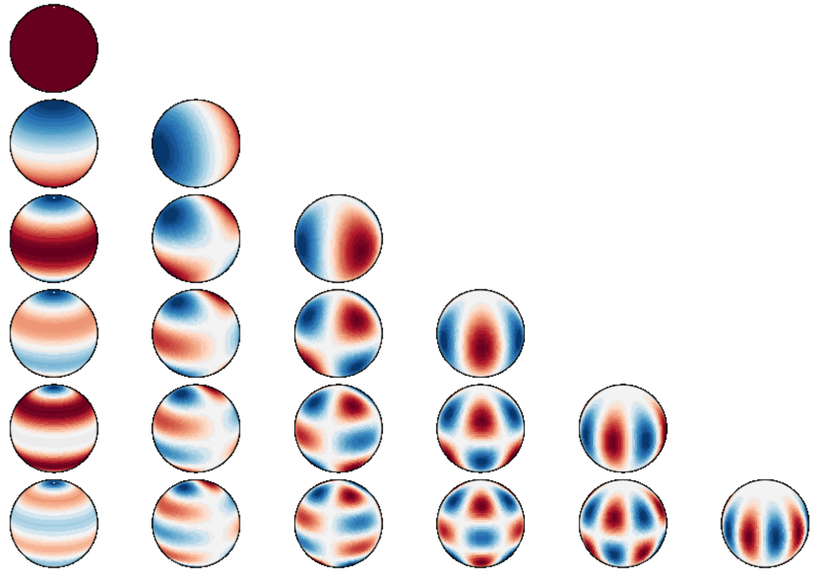

All-Sky at 10 TeV

All-Sky Measurement of the Anisotropy of Cosmic Rays at 10 TeV and Mapping of the Local Interstellar Magnetic Field
HAWC Collaboration: A.U. Abeysekara et al., and IceCube Collaboration, M.G. Aartsen et al., ApJ**871**(2019), 096.

Large Scale

Small Scale ($\ell > 3$)

Relative Intensity

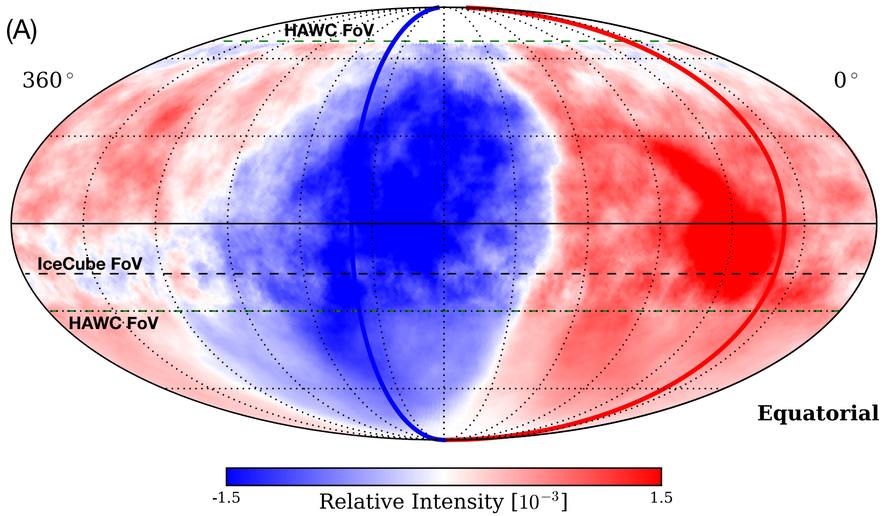

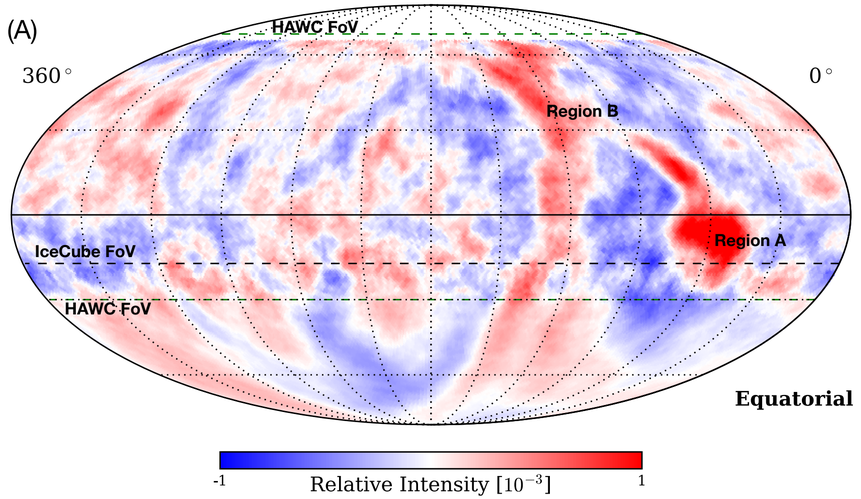

Significance Map

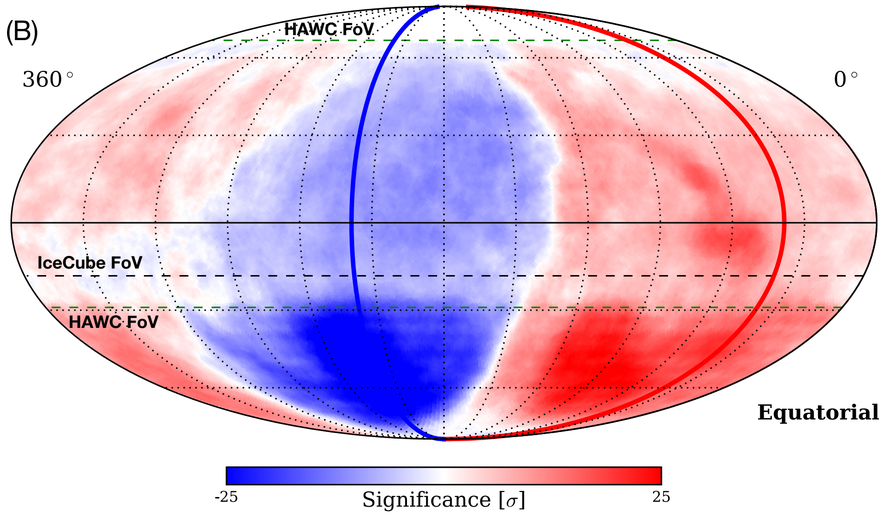

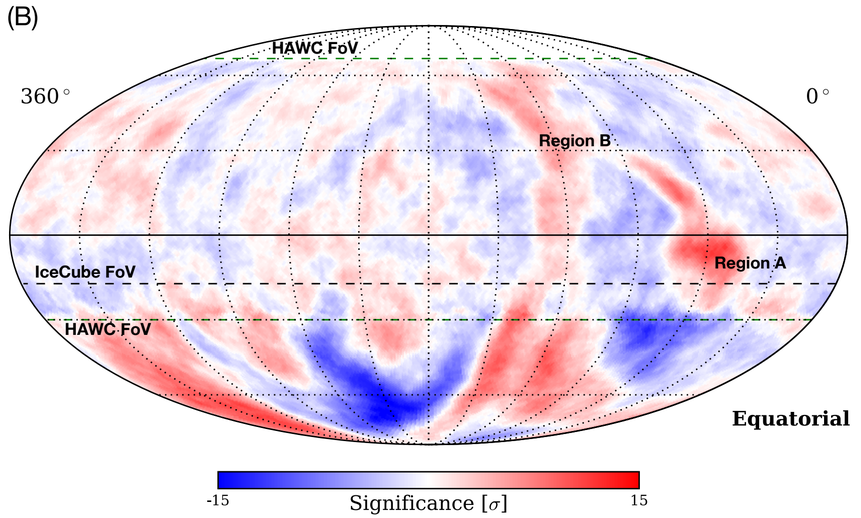

HAWC

IceCube
SOUTH POLE NEUTRINO OBSERVATORY

Angular Power Spectrum

All-Sky Measurement of the Anisotropy of Cosmic Rays at 10 TeV and Mapping of the Local Interstellar Magnetic Field

HAWC Collaboration: A.U. Abeysekara et al., and IceCube Collaboration, M.G. Aartsen et al., ApJ**871**(2019), 096.

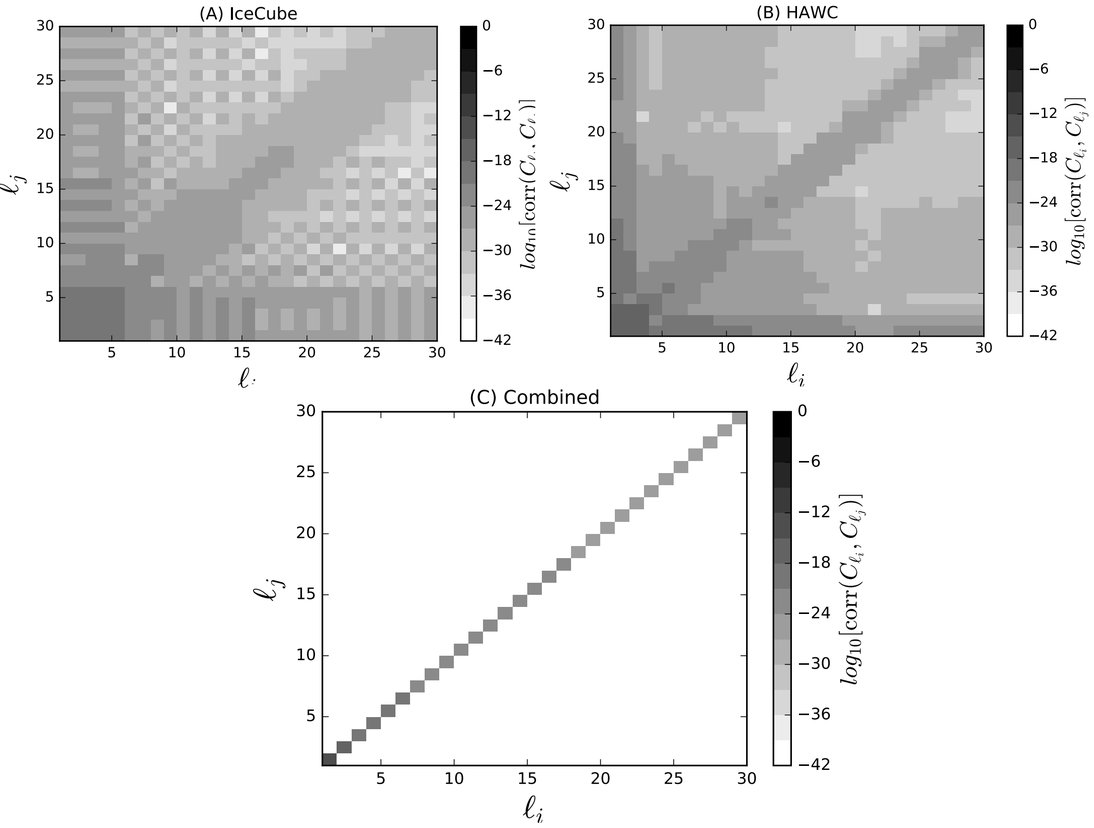

Correlation matrix for C_ℓ modes with partial sky coverage from individual experiments (A, B) and for the combined field of view (C).

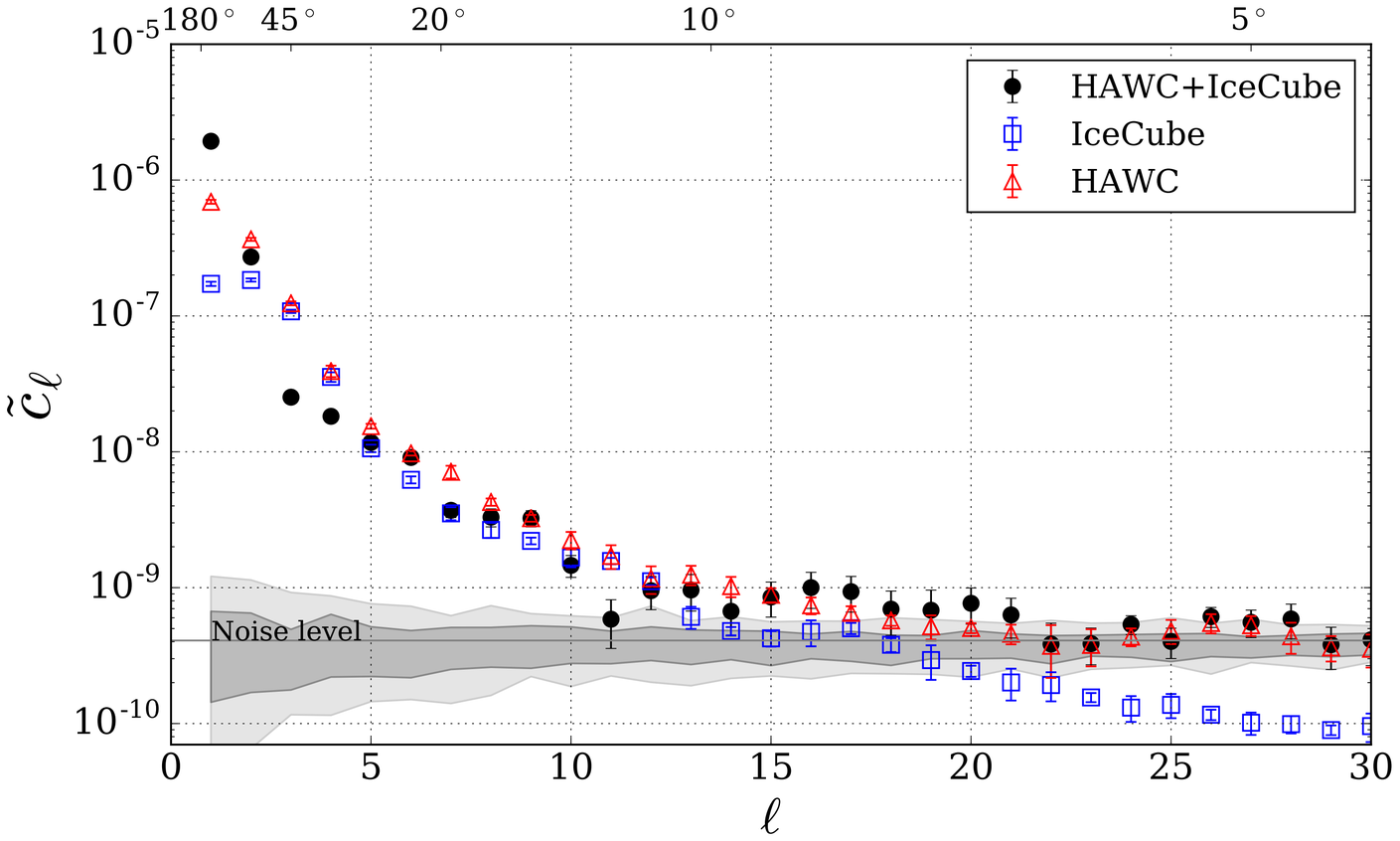

Angular power spectrum of the cosmic ray anisotropy at 10 TeV. The IceCube data set alone has a lower noise level and is sensitive to higher ℓ components. The dark and light gray bands represent the power spectra for isotropic sky maps at the 68% and 95% confidence levels, respectively.

All-Sky Measurement of the Anisotropy of Cosmic Rays at 10 TeV and Mapping of the Local Interstellar Magnetic Field

HAWC Collaboration: A.U. Abeysekara et al., and IceCube Collaboration, M.G. Aartsen et al., ApJ**871**(2019), 096.

The horizontal components of the dipole obtained using the values from the spherical harmonic $a_{\ell m}$ coefficients

$$\delta I(\boldsymbol{u}_i) = \sum_{\ell=1}^{\infty} \sum_{m=-\ell}^{\ell} a_{\ell m} Y_{\ell m}(\boldsymbol{u}_i)$$

is obtained from

$$\boldsymbol{\delta} \equiv (\delta_{0h}, \delta_{6h}, \delta_N) = \sqrt{\frac{3}{2\pi}}(-\Re(a_{11}), \Im(a_{11}), a_{10})$$

are $\boldsymbol{\delta}_{0h} = 9.16 \times 10^{-4}$ and
$\boldsymbol{\delta}_{6h} = 7.25 \times 10^{-4}$ ($\pm 0.04 \times 10^{-4}$),
respectively, with respect to the 0*h* and 6*h* R.A. axes.

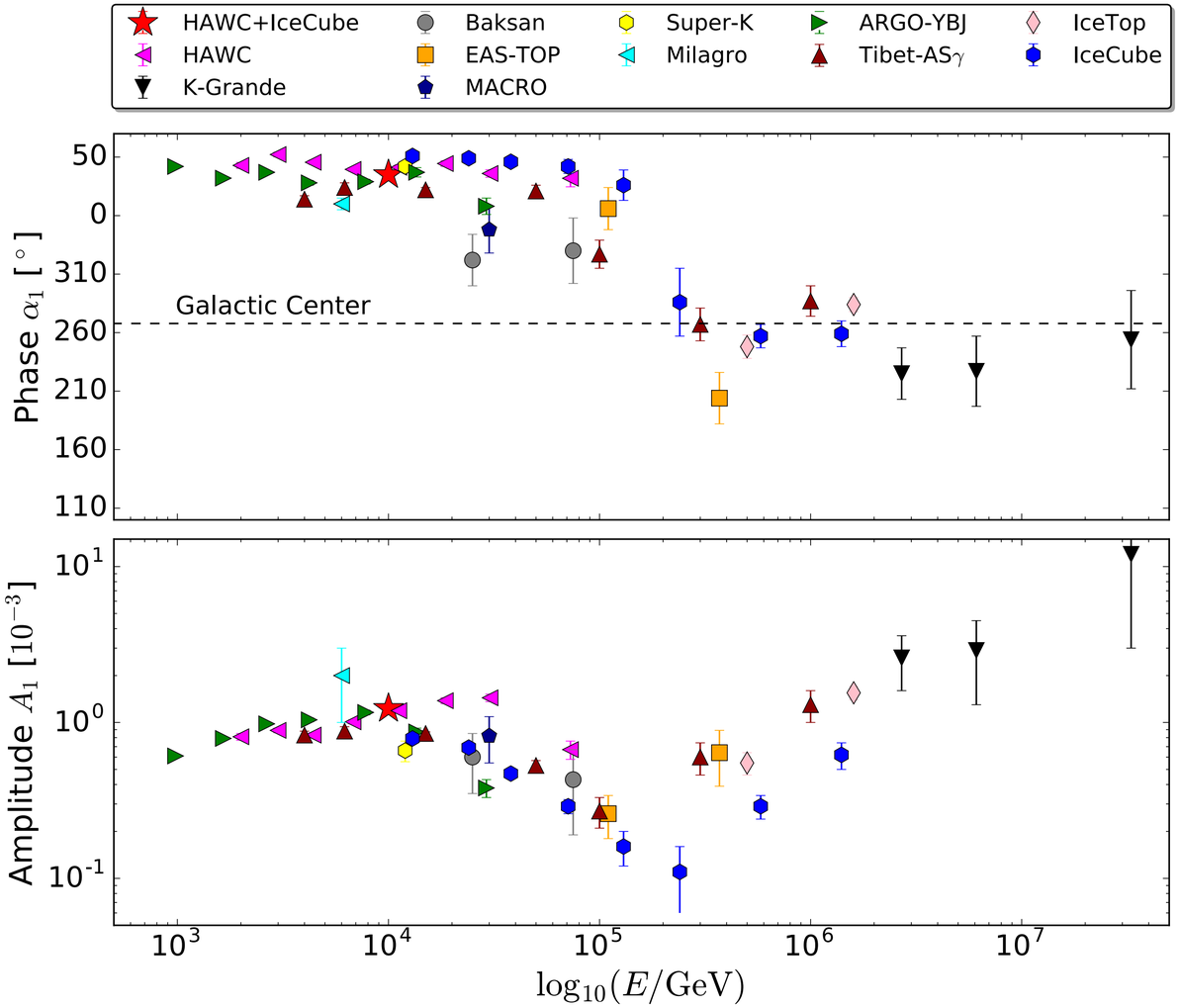

The measured dipole amplitude and phase are shown along with previously published results from other experiments in the TeV–PeV primary particle energy range. The systematic uncertainty in the amplitude and phase of the dipole are expected to be and $\delta a_1 \sim 26$, respectively

ICECUBE SOUTH POLE NEUTRINO OBSERVATORY

HAWC

Cosmic Ray Anisotropy, the Heliosphere, and the LIMF

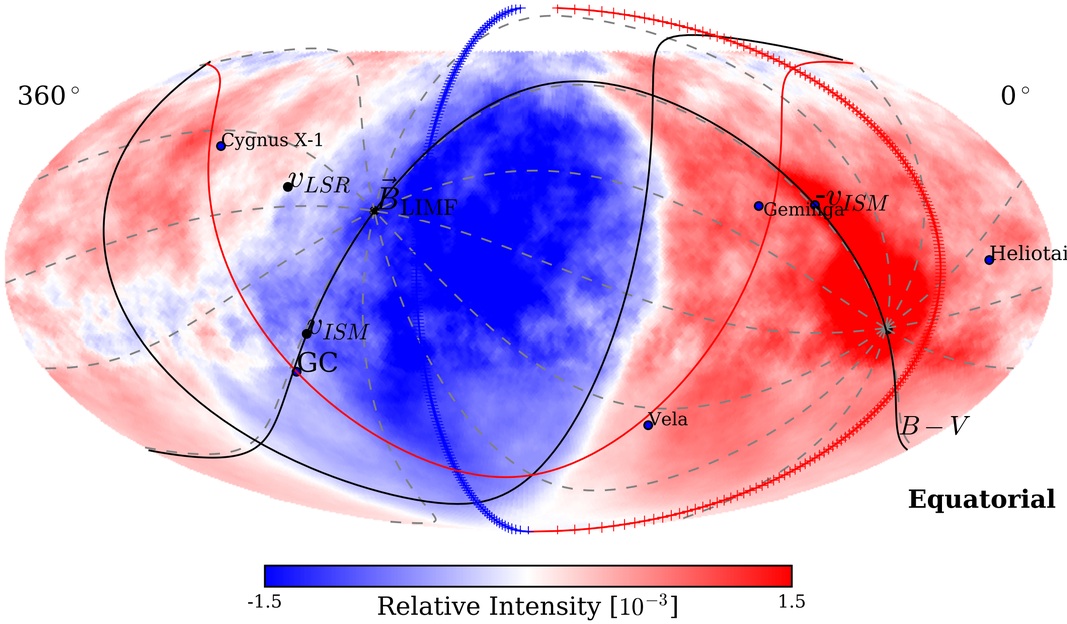

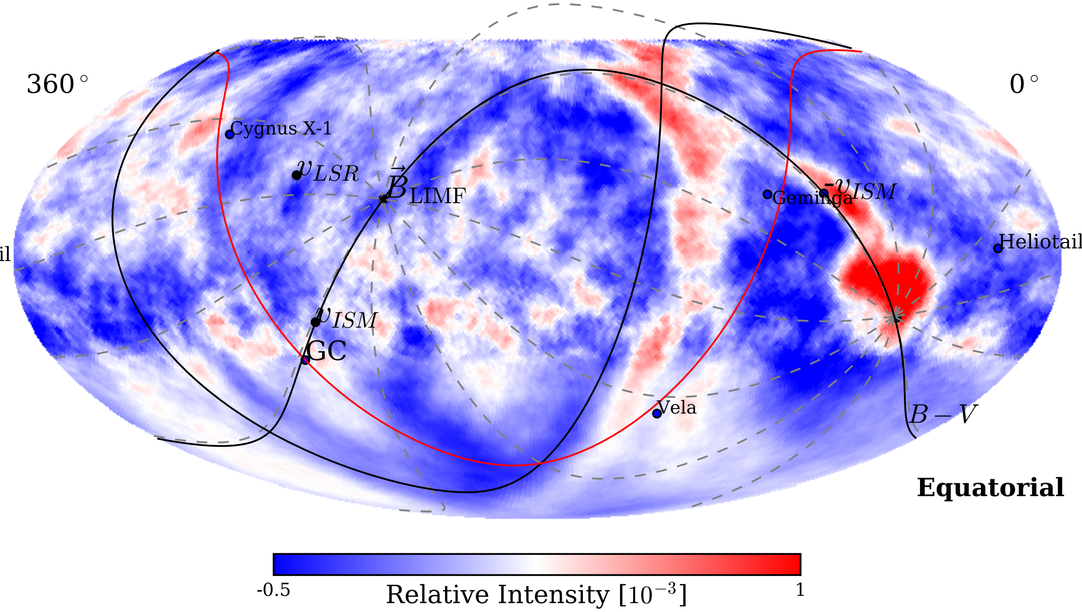

Table 4
Magnetic Field Alignment

Source	R.A. [°]	Decl. [°]	$\Delta\psi$ [°]	δ_N [10^{-4}]
Funsten et al. (2013)	229.7 ± 1.9	23.3 ± 2.5	9.0	−5.03
Frisch et al. (2015)	237.9 ± 16	22.2 ± 16	12.2	−4.77
Zirnstein et al. (2016)	234.4 ± 0.7	16.3 ± 0.6	6.5	−3.42
Boundary Fit	229.2 ± 3.5	11.4 ± 3.0	···	−2.36
Dipole/Quadrupole	218.4 ± 0.3 (±2.6)	20.7 ± 0.3 (±2.6)	···	−4.41

Note. The last two rows correspond to measurements of the large-scale anisotropy from this study. The R.A. measurement in the last row is obtained from the dipole vector, and the decl. is obtained from the $\ell = 2$ quadrupole component. The second to last column corresponds to the angular distance $\Delta\psi$ between the boundary fit and the various LIMF estimates. The last column gives the corresponding vertical dipole component under the assumption that the dipole is oriented toward the given decl. Error in parentheses for dipole and quadruple correspond to systematic uncertainties.

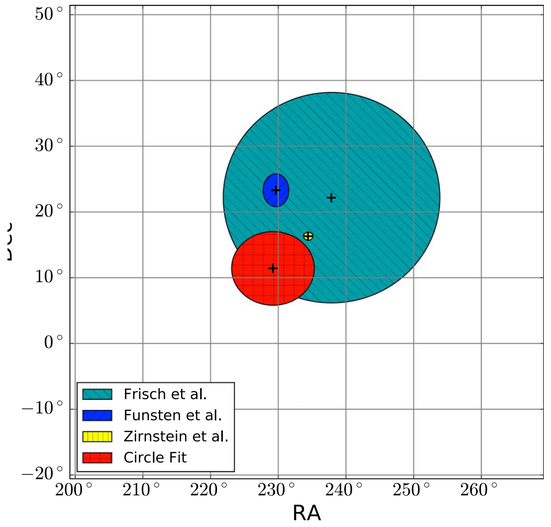

HAWC CRA (7-years)

Relative Intensity

```
bin0: E_med=4.46 (-2.01, +9.95)
bin1: E_med=10.5 (-4.15, +27.1)
bin2: E_med=47.6 (-20.2, +91.8)
bin3: E_med=126 (-56.8, +307)
```

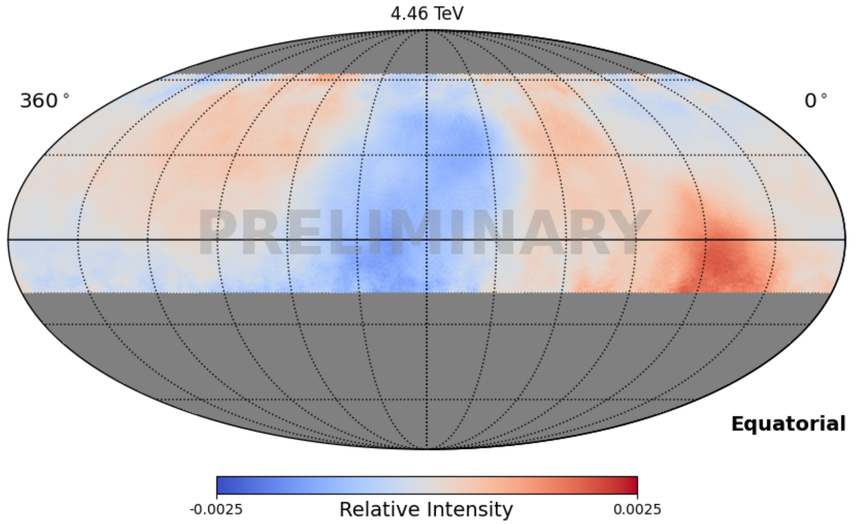

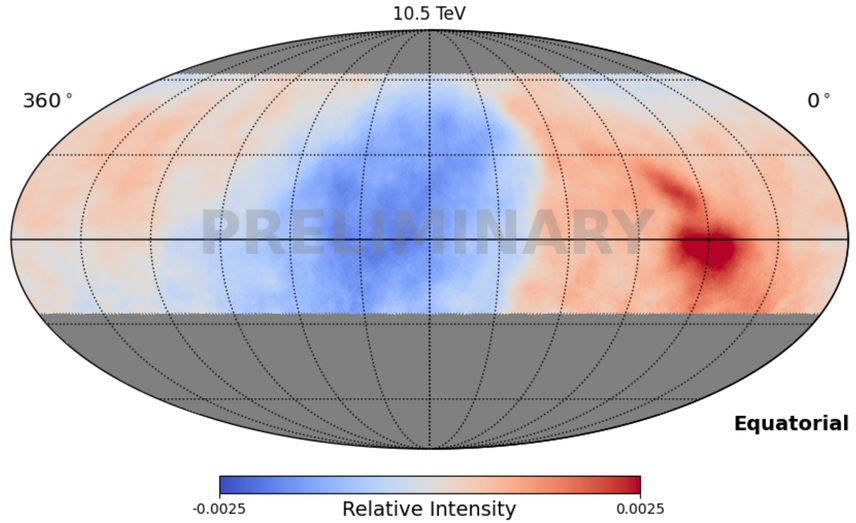

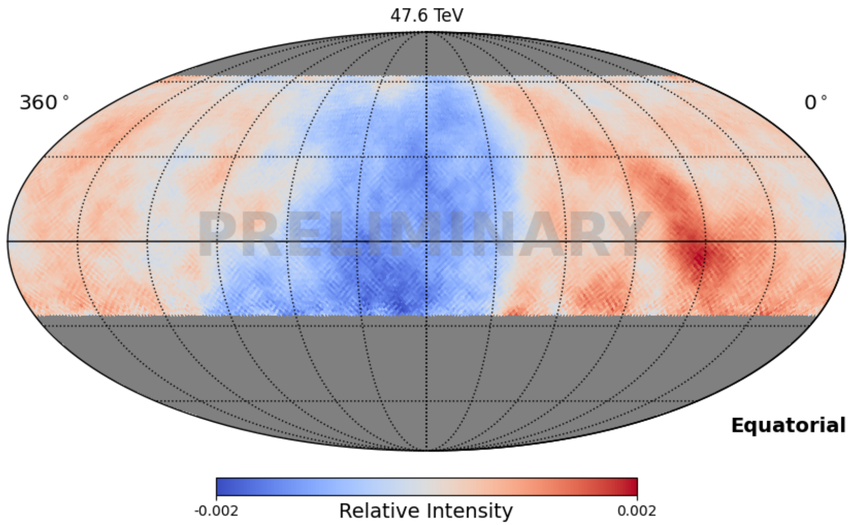

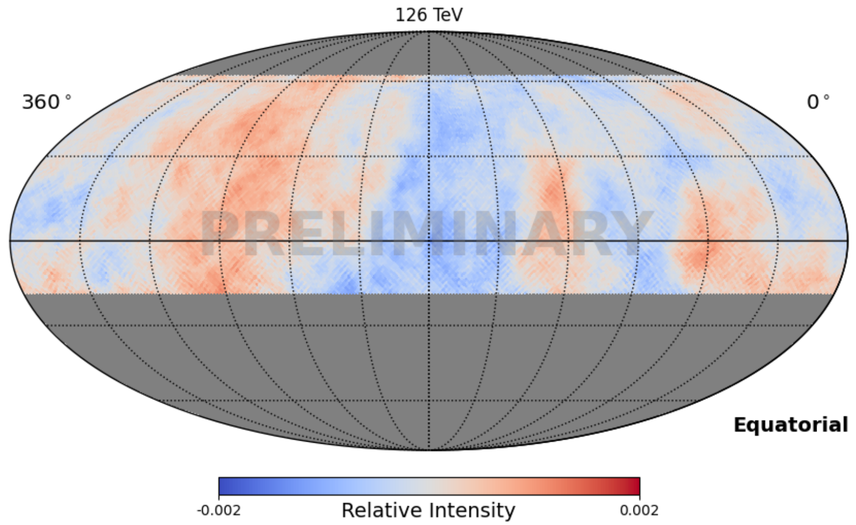

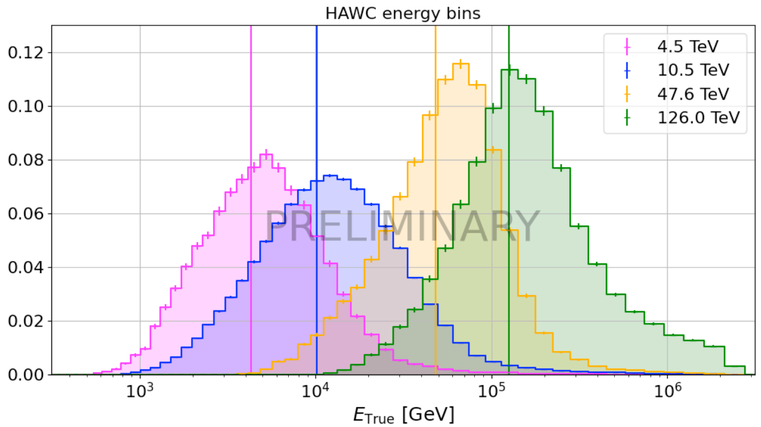

HAWC CRA (7-years)

Li-Ma Significance

```
bin0: E_med=4.46 (-2.01, +9.95)
bin1: E_med=10.5 (-4.15, +27.1)
bin2: E_med=47.6 (-20.2, +91.8)
bin3: E_med=126 (-56.8, +307)
```

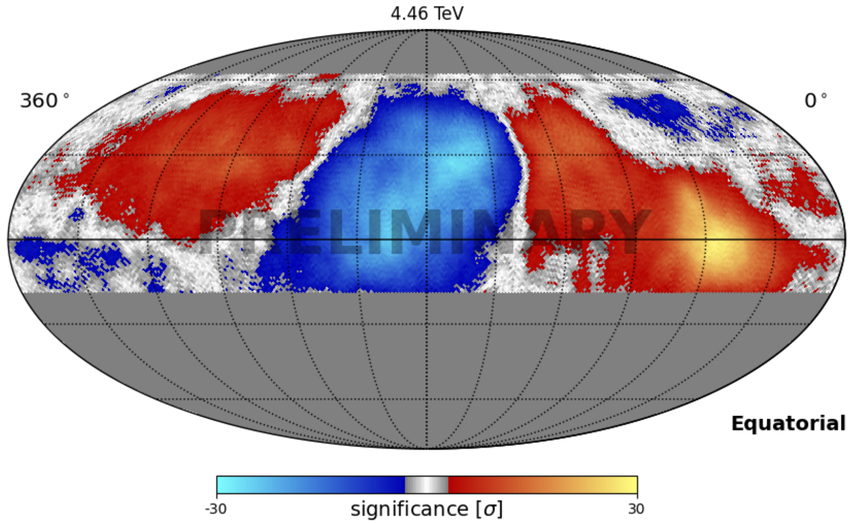

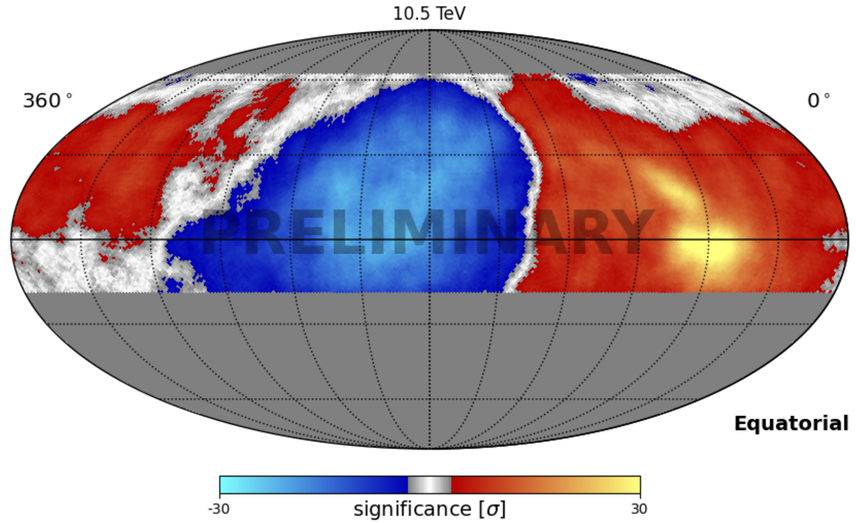

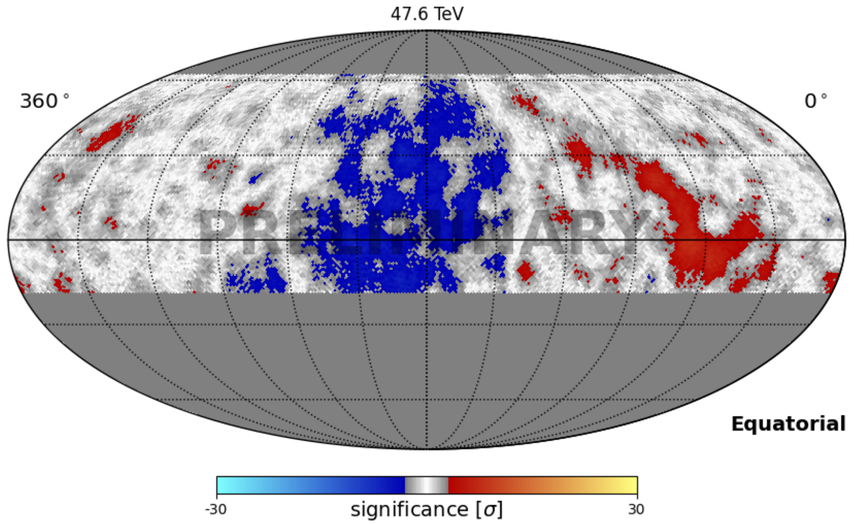

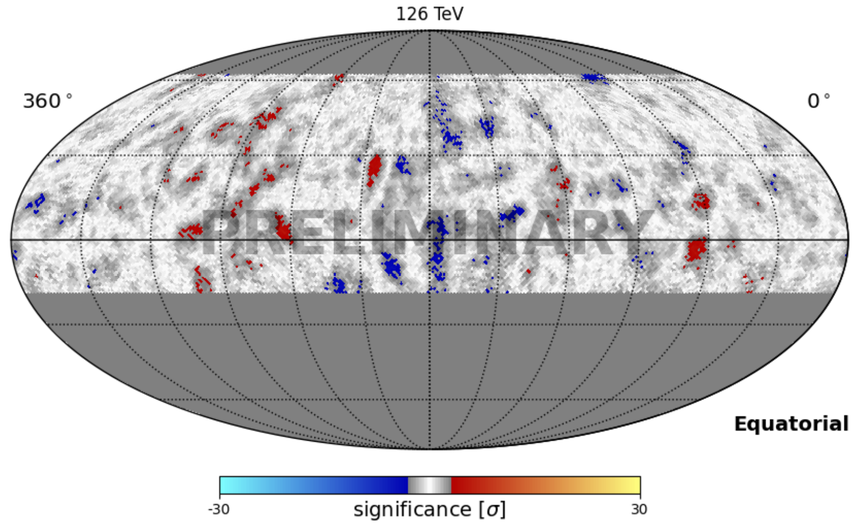

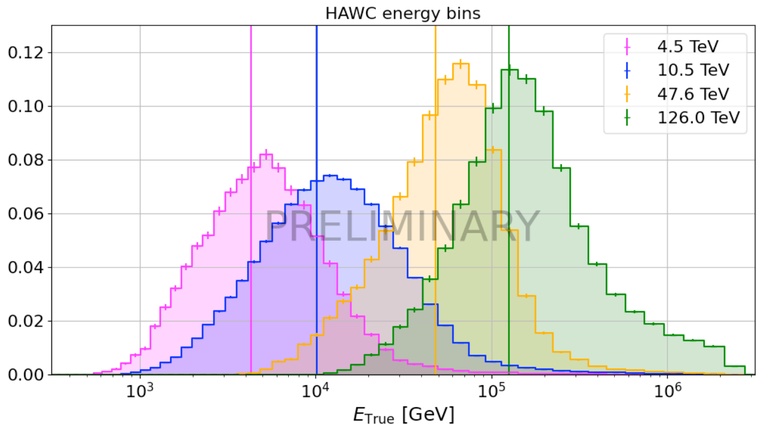

HAWC CRA (7-years) Variation Over Time

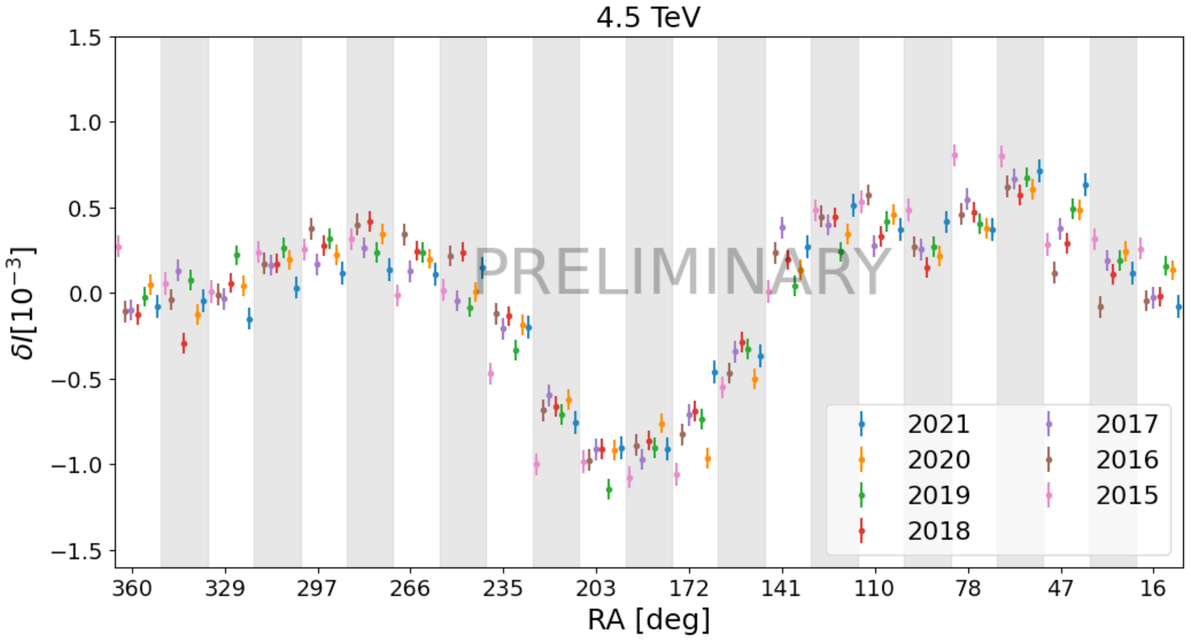

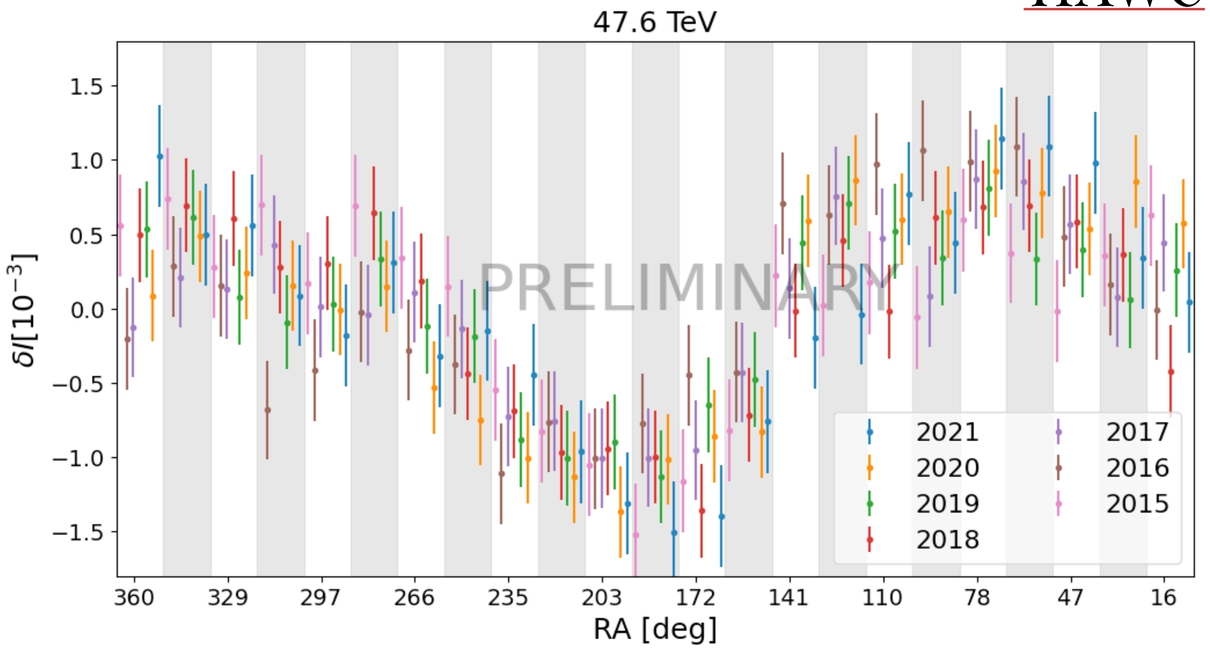

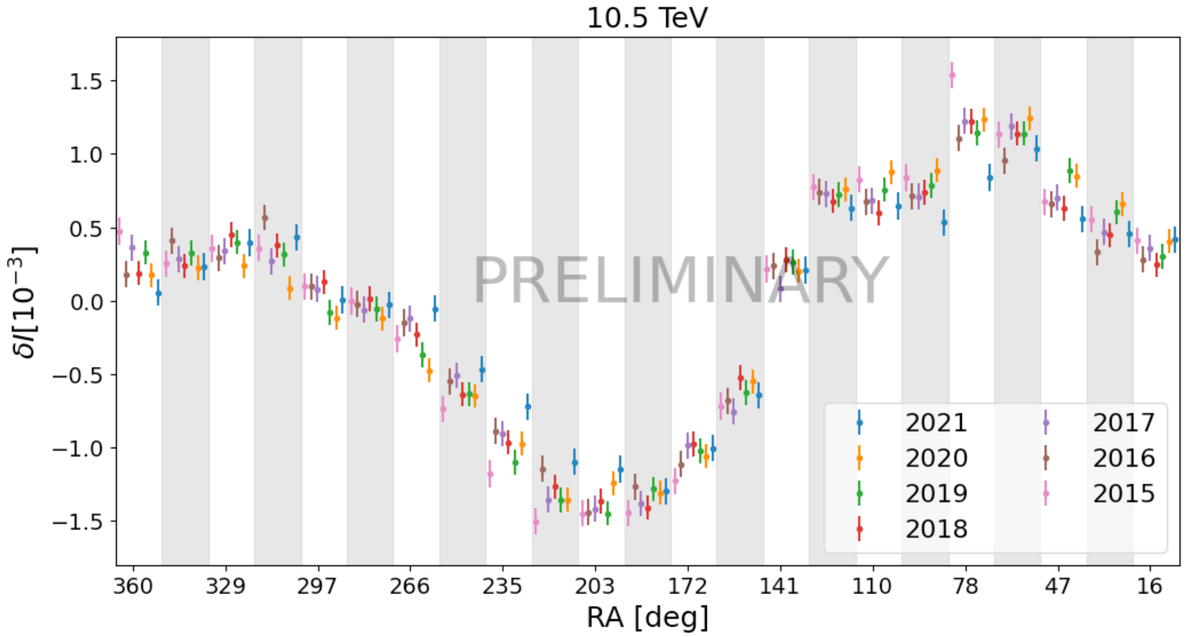

- Most year to year variations are not statistically significant.
- Systematic uncertainties not accounted for
- Gaps in data taking result in
  - modulation of dipole from interference with C-G
  - rate variations from atmospheric effects (diurnal and semi-diurnal)
- Future plans to study time-dependent effect and possible correlation with solar cycle

Antiproton limits

Constraining the $\bar{p}/p$ Ratio in TeV Cosmic Rays with Observations of the Moon Shadow by HAWC
A. U. Abeysekara *et al.* (HAWC Collaboration) Phys. Rev. D 97, 102005 – Published 16 May 2018

maximize the log-likelihood function

$$\log \mathcal{L} = -\frac{1}{2}\sum_{i}^{N}\frac{(\delta I_i - \delta I(x_i, y_i, r))^2}{\sigma_i^2}$$

where δI(x, y, r) is the superposition of two Gaussians, with ratio r = $\bar{p}/p$

$$\delta I(x,y) = F_p(x,y) + F_{\bar{p}}(x,y) = F_p(x,y) + r \cdot F_p(x,y)$$

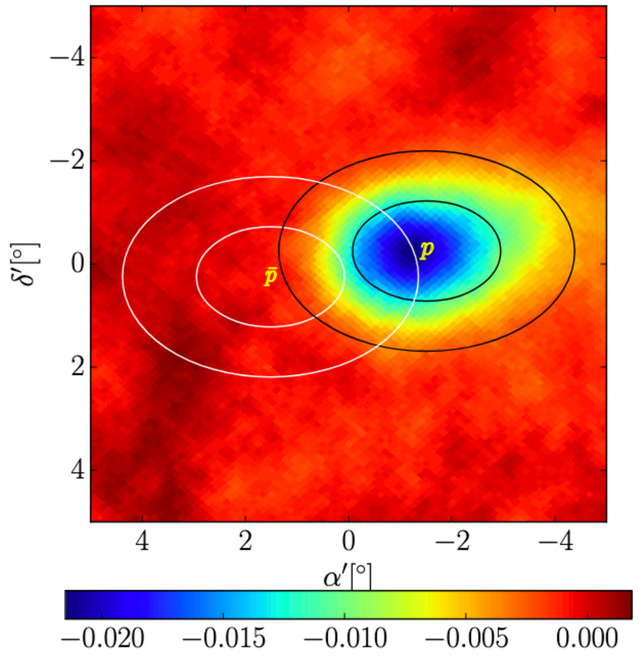

The observed proton shadow at 1.6 TeV, with 1σ and 2σ width contours of the fitted Gaussian overlaid. The white ellipses show the expected position of an antiproton shadow obtained by a 180○ rotation about the origin.

log (E/GeV)	σ_x	σ_y	$\bar{p}/p$[95(90) CL][%]
3.0	1.45 ± 0.12	0.90 ± 0.07	8.4 (6.6)
3.2	1.24 ± 0.05	0.74 ± 0.02	3.2 (2.5)
3.4	0.93 ± 0.02	0.58 ± 0.01	1.1 (0.3)
3.6	0.65 ± 0.01	0.51 ± 0.01	1.1 (0.8)
3.8	0.56 ± 0.01	0.49 ± 0.01	1.9 (1.2)
4.0	0.48 ± 0.01	0.47 ± 0.01	1.9 (1.1)

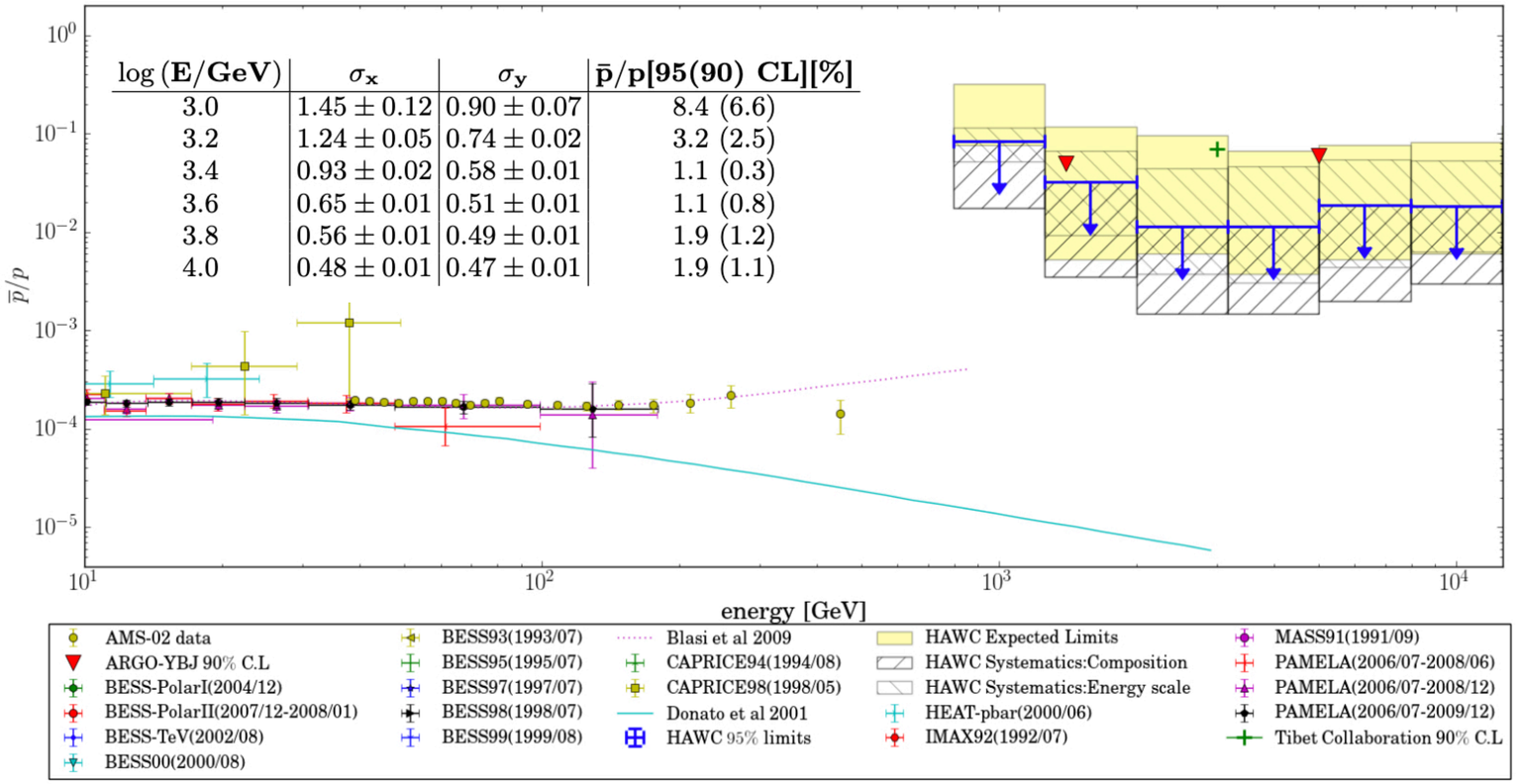

Measurements of $\bar{p}/p$ in the GeV range and upper limits at the TeV scale. The yellow and shaded bands show HAWC sensitivity and systematic uncertainties respectively. The solid line shows the expected ratio from a purely secondary production of antiprotons [47]. The dotted line postulates primary antiproton production in supernovae [21]. Note that the other upper limits published above 1 TeV by ARGO-YBJ, L3 and Tibet AS-γ are 90% intervals while the HAWC limits are at the 95% C.L.

Summary

- All-particle spectrum of cosmic rays from 10TeV to 1PeV confirms a spectral cutoff at tens of TeV, with >5σ (stat.), reduced to 2.6σ when accounting for syst. uncertainties that is in agreement with other experiments, though HAWC detects higher cosmic-ray intensities compared to ICETOP, ARGO-YBJ, and TIBET-III, likely due to different energy estimation methods. The study bridges indirect and direct observations.

- A dedicated analysis of cosmic ray composition with HAWC has allowed to measure the spectrum of H+He of cosmic rays in the energy range 6 TeV, to 158 TeV. The spectrum shows a softening at 24.0 TeV with a statistical significance of 4.1 σ. This analysis shows the potential of high-altitude water Cherenkov observatories like HAWC for composition studies of cosmic rays.

- HAWC and IceCube have measured a nearly full-sky map of cosmic ray arrival directions at 10 TeV, providing new insights into cosmic ray diffusion and magnetic turbulence in the interstellar medium. The angular power spectrum suggests two distinct mechanisms shaping the observed features, with evidence supporting alignment of cosmic ray anisotropy along the local interstellar magnetic field (LIMF).

- Using the Moon shadow as a template, the HAWC Observatory places upper limits on the antiproton-to-proton ratio ($\bar{p}/p$) up to 10 TeV. The limits, ranging from 1.1% at 2.5 and 4 TeV to 1.9% at 10 TeV, set constraints that models predicting a rise in $\bar{p}/p$ must meet.

Discussion

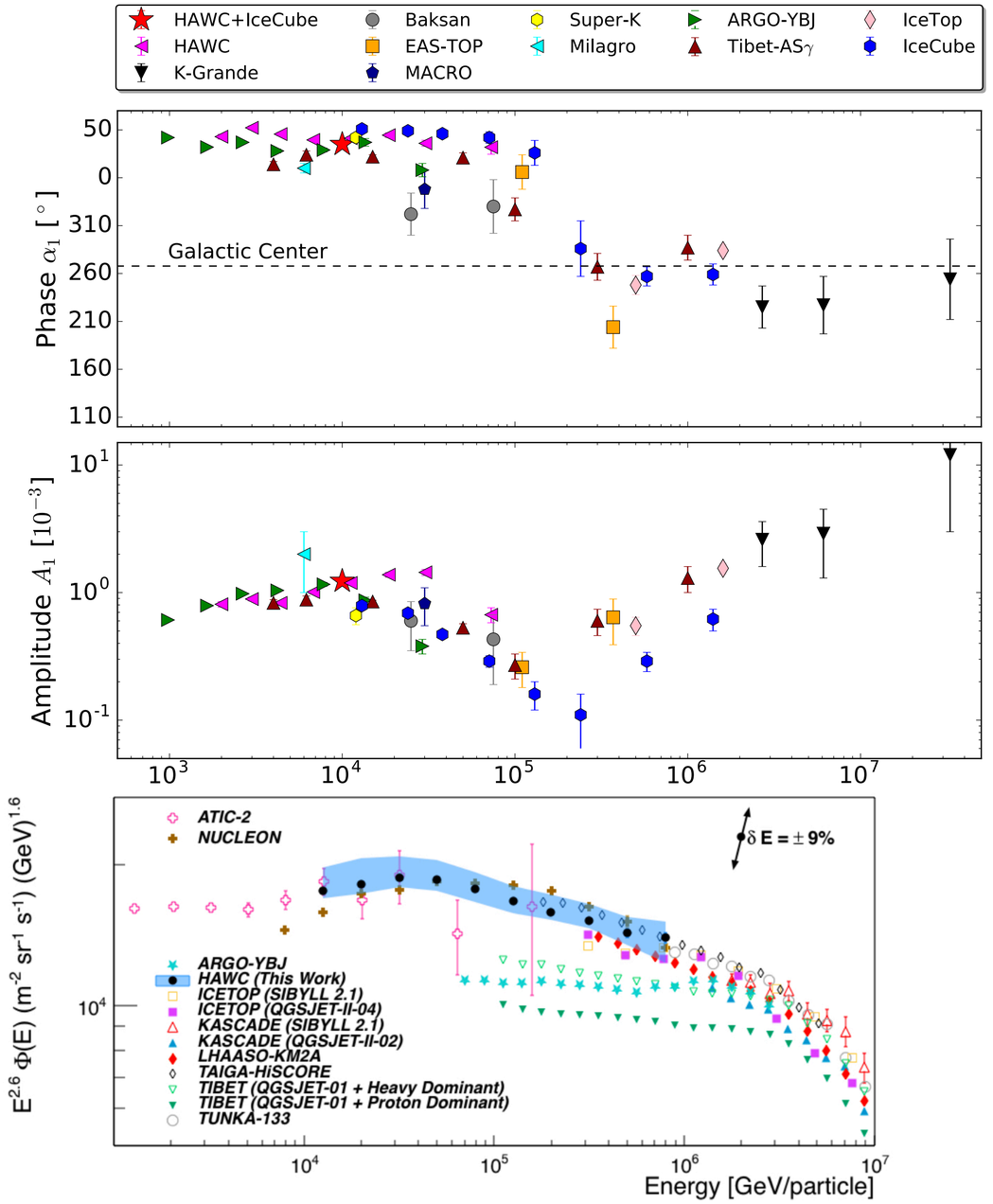

- All-particle spectrum feature: wider and shifted to higher energies possibly from increasing influence of Z > 2 close to 100 TeV, consistent with heavy element data from NUCLEON, the mean shower age from HAWC and analysis of the efficiency of the age cut.
- Decrease in Φ_{H+He}/Φ_{Tot} ratio from 10 to 158TeV suggests relative increase in contribution of heavy nuclei in the total spectrum.
- Max. confinement energy by B-fields either at source or in Galaxy: rigidity dependent cuts at ~PeV
- Contribution of three different types of sources with power-law spectra and distinct magnetic rigidity cutoffs: nova explosions: 200 GV, SNRs 50 TV (produce H and He spectra with a knee-like feature), super-bubbles 4 PV.
- The existence of a local of TeV accelerators supported on data of the phase and dipole anisotropy of galactic cosmic rays.
- Further studies needed at energy spectra of heavier nuclei in 10 TeV – 1 PeV range.

Backup

The HAWC Observatory (Outriggers)

HAWC Collaboration

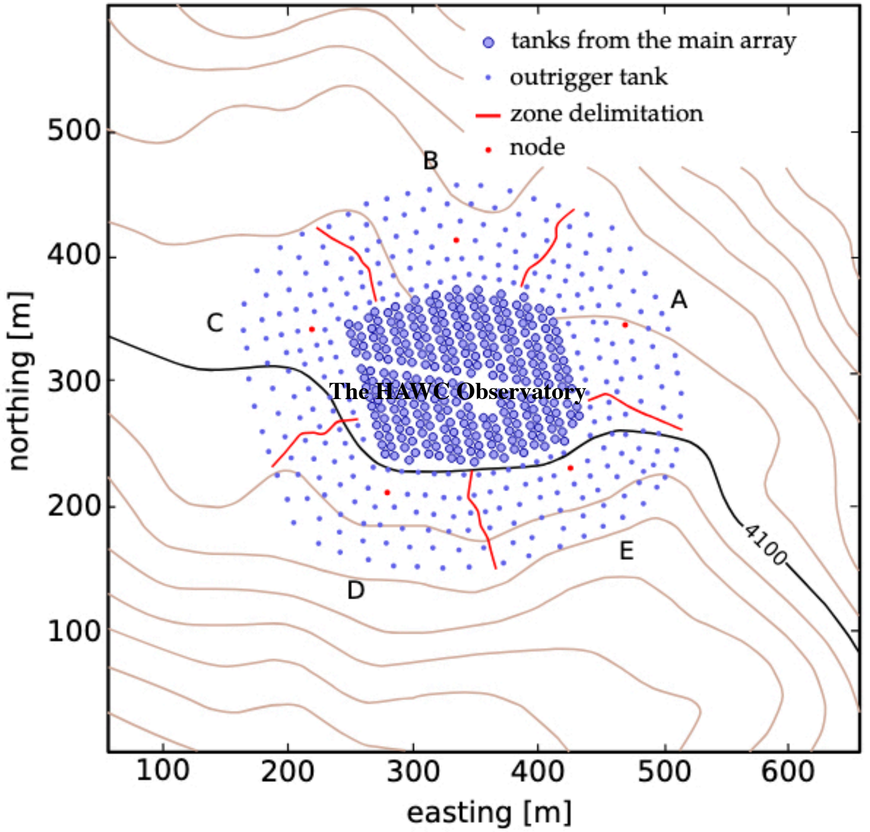

Origin of Galactic Cosmic Rays?

HAWC Collaboration: A. Albert et al. 2021, Nature Astron(2021).

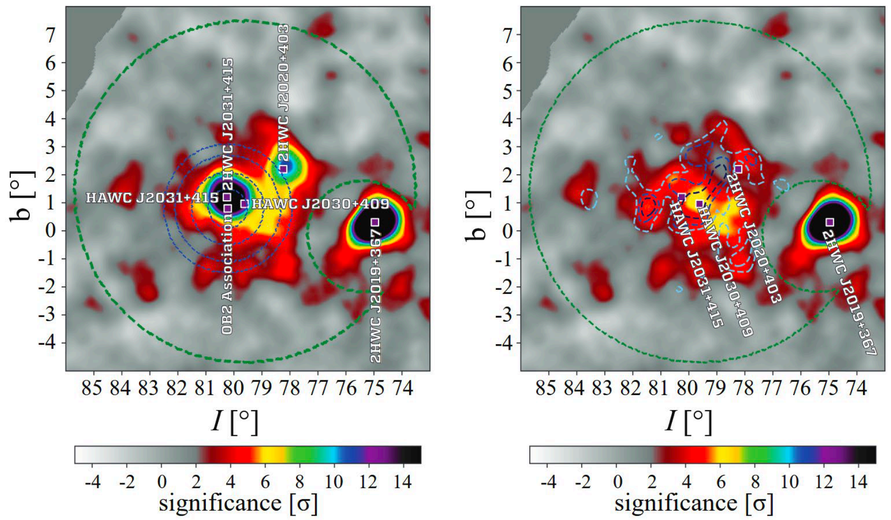

- Observations of 1-100 TeV γ rays coming from the ‘Cygnus Cocoon’
- These γ rays are likely produced by 10-1000 TeV freshly accelerated CRs originating from the enclosed star forming region Cygnus OB2
- The measured flux is likely originated by hadronic interactions.
- The spectral shape and the emission profile of the Cocoon changes from GeV to TeV energies, which reveals the transport of cosmic particles and historical activity in the superbubble.

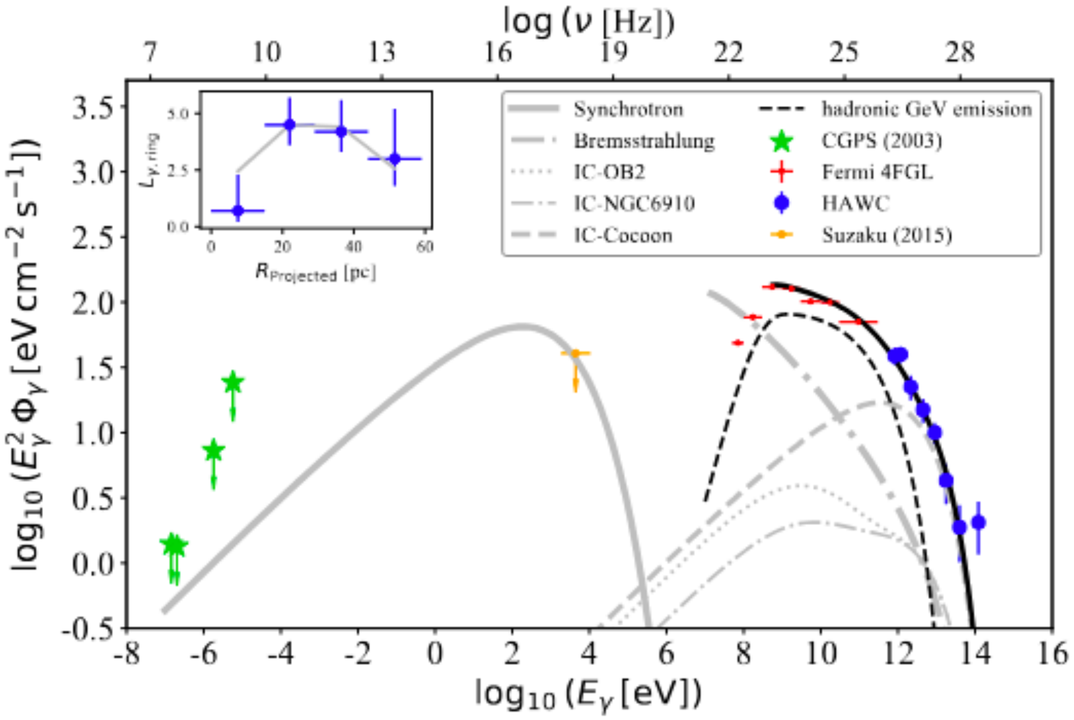

Leptonic modeling at the Cocoon region. Multi-wavelength observations of the Cygnus Cocoon constrain the Synchrotron and Bremsstrahlung radiation of relativistic electrons. The light grey curves correspond to a “minimum leptonic model”, where only γ-rays above 1 TeV are explained by electron emission. Observations between 0.1–100 GeV are explained by hadronic interaction (black dashed curve). The red points are the GeV flux points by Fermi-LAT and the blue circles are the HAWC flux points The sum of the emission above ~0.3 GeV is indicated by the black solid curve.

EAS Age and Energy Estimation

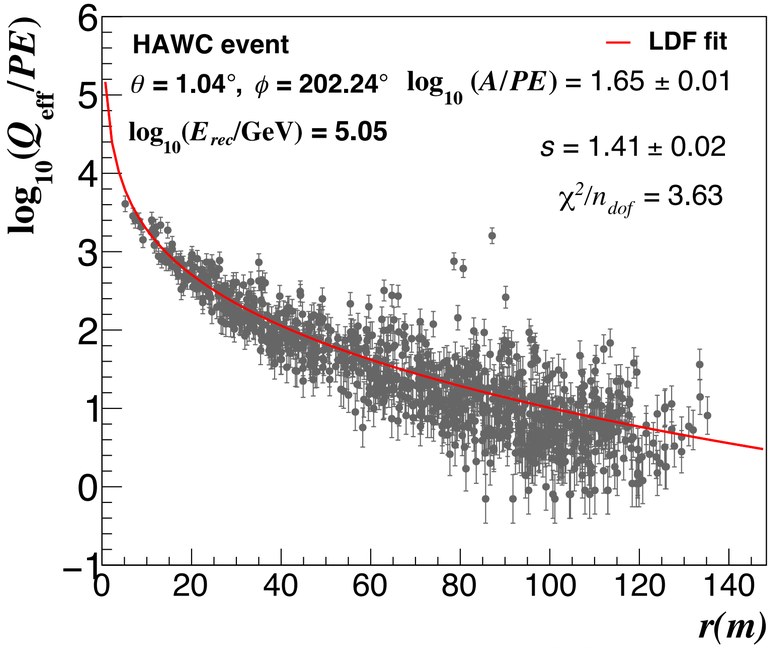

[HAWC Collab., PRD 105 (2022)]

Lateral age parameter (*s*)

- Obtained event-by-event
- Fit of Qeff(r) with a NKG-like function:

$$f_{ch}(r) = A \cdot (r/r_0)^{s-3} \cdot (1 + r/r_0)^{s-4.5}$$

with r_0 = 124.21 m.

A, ***s*** are free parameters

[HAWC Collab., APJ 881 (2017); J.A. Morales Soto et al., PoS(ICRC2019 359 (2019)]

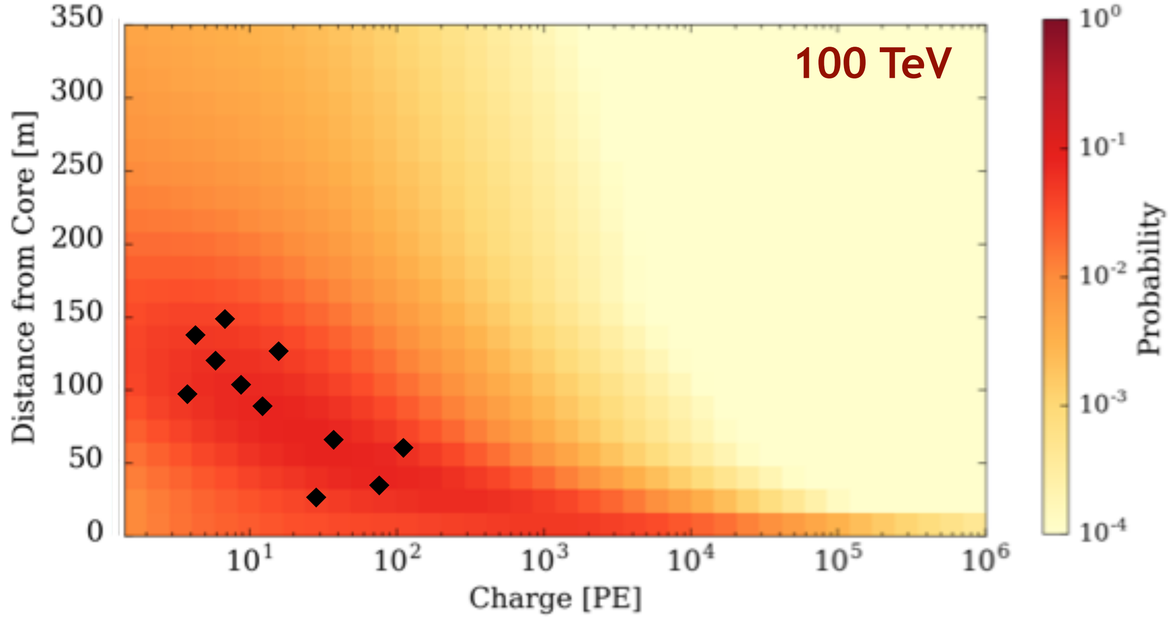

EAS primary energy:

- Produce LDF tables of MC protons**:**
  Binning in r, Qeff, θ and E
- Maximum likelihood to find table that best fits the Qeff(r) distribution of the event, from which **E** is obtained.

[HAWC Collab., PRD 96 (2017); Z. Hampel-Arias' PhD thesis, 2017]

Select a sample enriched with light nuclei

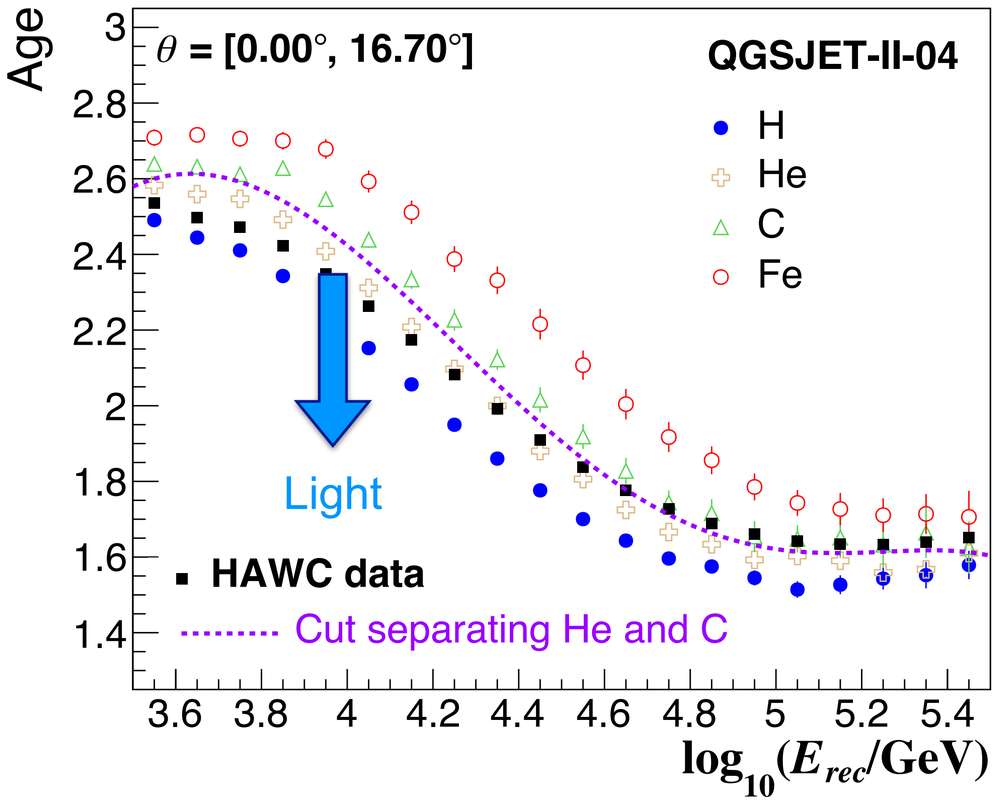

- Age parameter is sensitive to composition
- Select a subsample using a cut on the age
  - Subsample must have a large relative abundance of H and He.

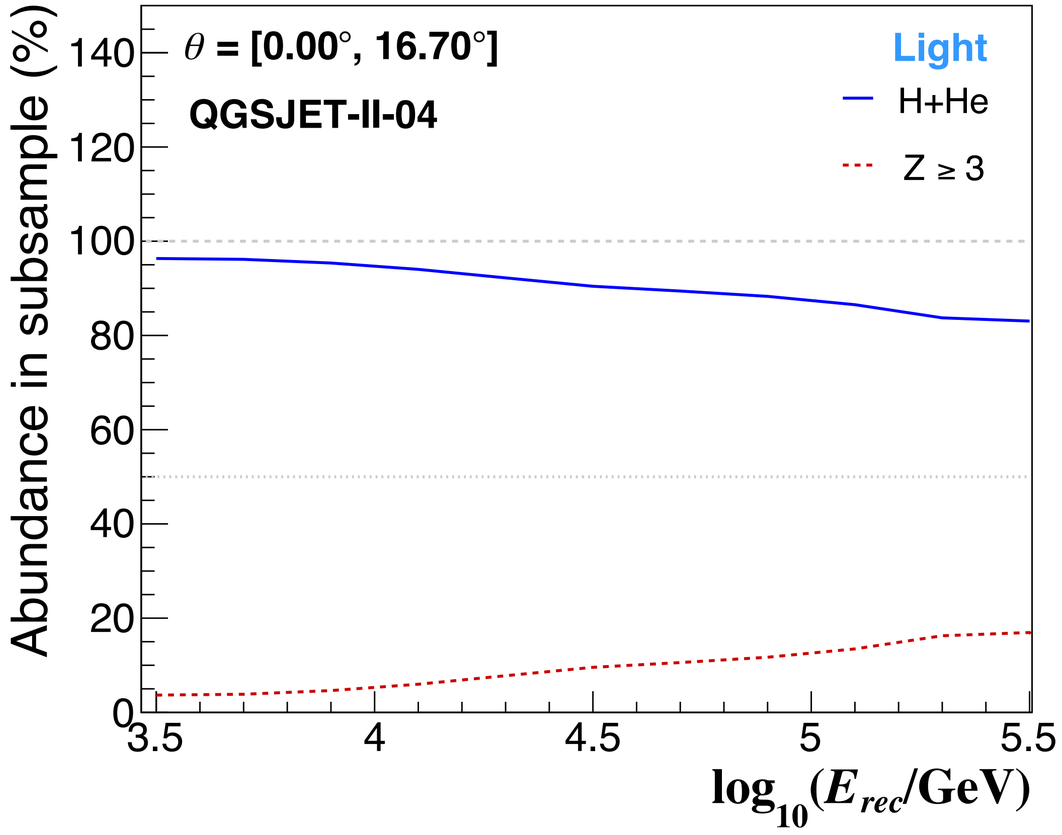

- Content of H + He in subsample
  - More than 82% of H and He in subsample

Data Selection

Selection cuts

- Important to reduce systematic effects on results:
  - θ < 16.7°
  - Successful core and arrival direction reconstruction
  - Activate at least 40 PMTs within 40 m from core
  - Fraction hit (# of hit PMT's/# available channels) ≥ 0.2
  - $\log_{10}$(E/GeV) = [3.5, 5.5]

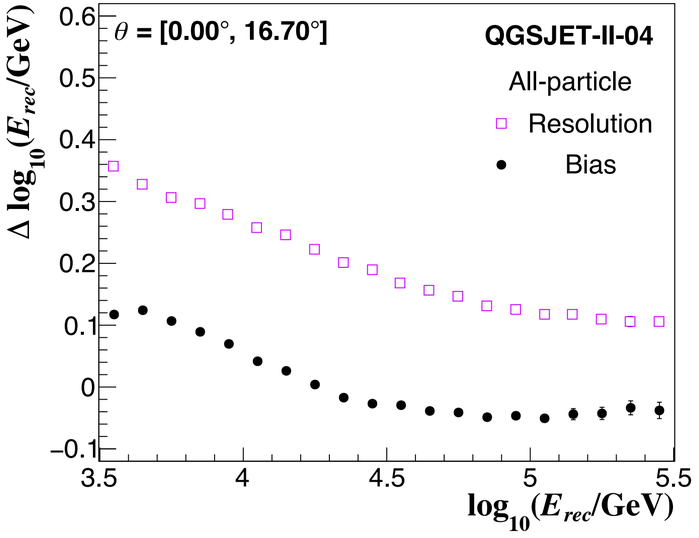

- Resolution:

E ≥ 10 TeV:

Δcore	≤ 15 m
$\lvert\Delta\log_{10}(E/GeV)\rvert$	≤ 0.26
ΔΨ	≤ 0.55°

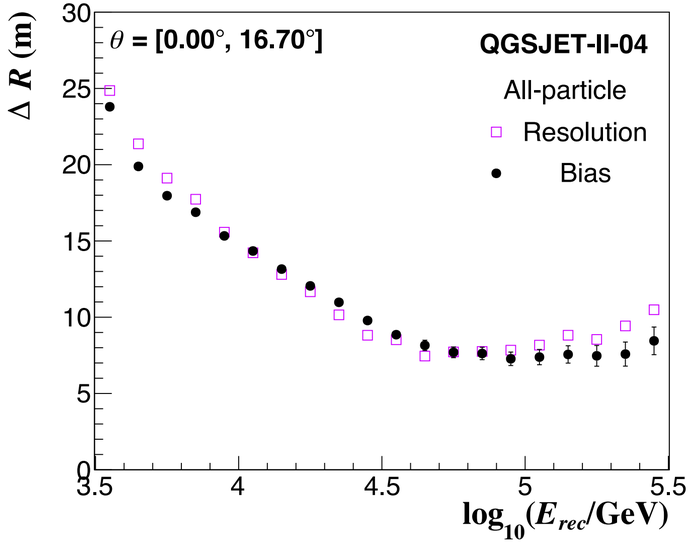

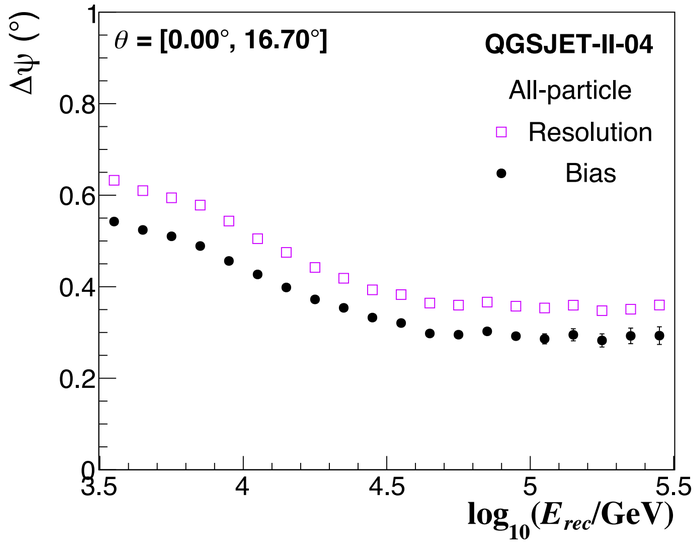

Obtain effective area from MC simulations

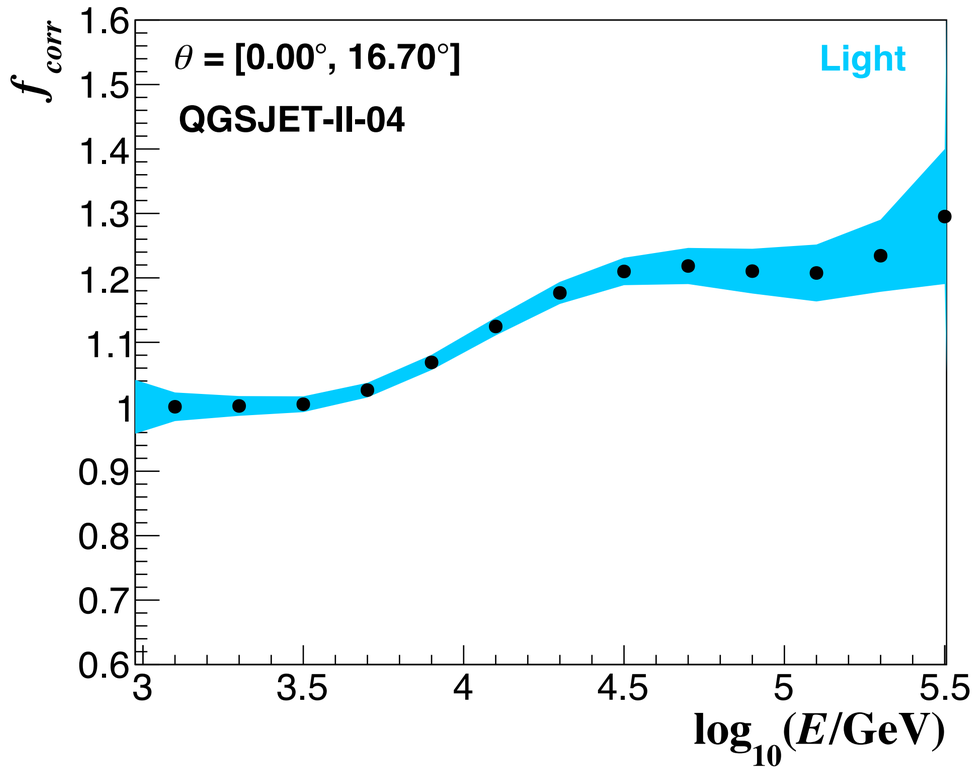

- Correction factor due to contamination of heavy events

$$f_{corr} = (N_{light} / N_{light}^{H+He})$$

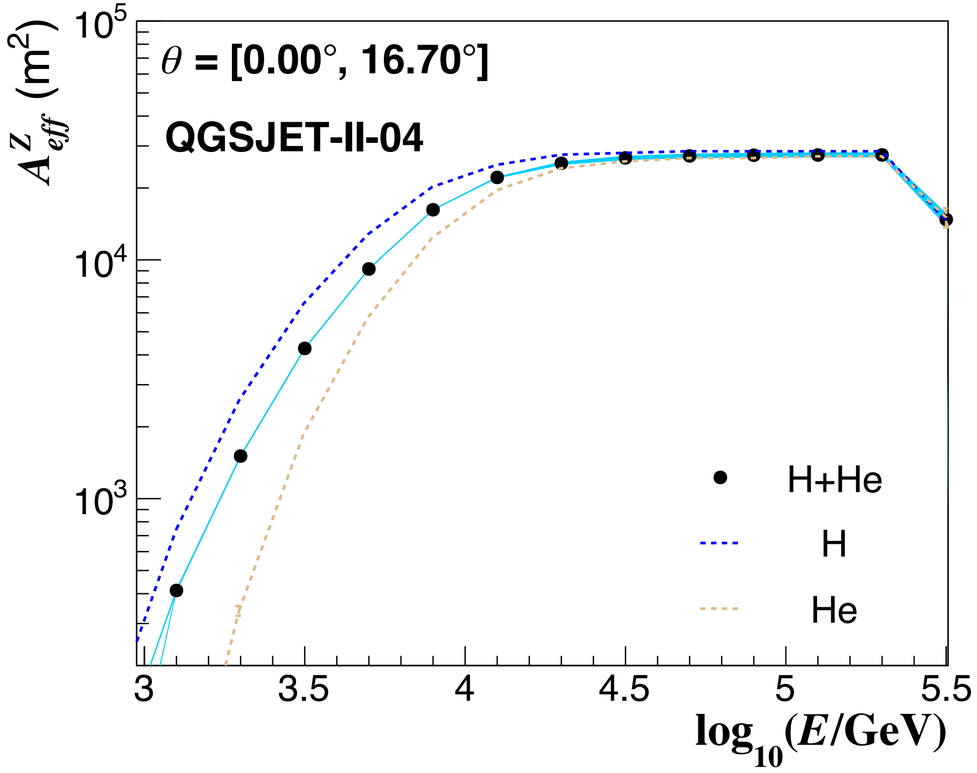

- Effective area of H+He in subsample

$$A_{eff}^{H+He}(E_i) = A_{thrown}\, \varepsilon^{H+He}(E_i)\, \frac{\cos\theta_{max} + \cos\theta_{min}}{2}$$

HAWC H+He Energy Spectrum

Get energy spectrum from N^{Unf} and effective area

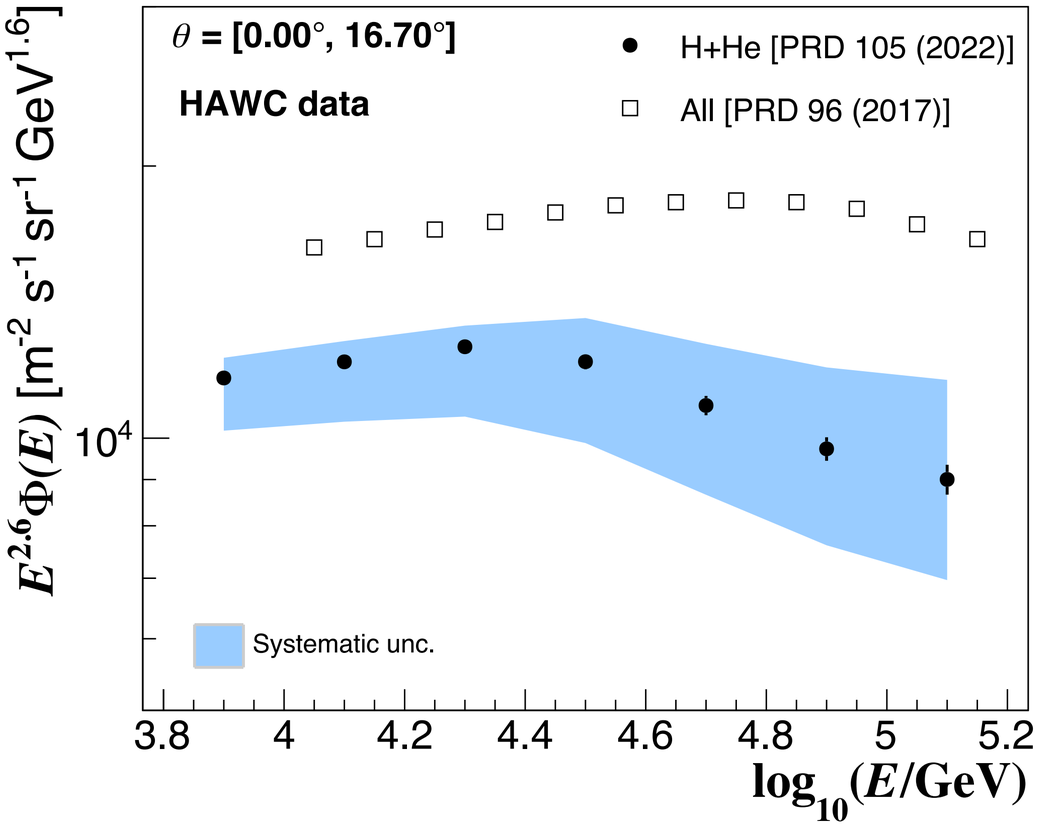

- Energy spectrum was calculated as:

$$\Phi = N^{Unf}(E)/[\Delta E^{T} \cdot \Delta t_{eff} \cdot \Delta\Omega \cdot f_{corr}(E) \cdot A_{eff}^{H+He}(E)]$$

Statistical and systematic uncertainties

H+He

$\log_{10}$(E/GeV) = 4.5 (32 TeV)

	Relative error Φ (%)
Statistical	**+/- 1.92**
Exp. Data	+/- 0.01
Response matrix	+/- 1.92
Systematic	**+11.77/-18.71**
Composition	+0.86/-17.25
Aeff	+1.85/-2.04
Cut at He or C	+2.87/-0.75
Gold unfolding	+1.23
Seed unfolding	-1.42
Smoothing unfold.	+3.73/-1.32
PMT efficiency	+5.00
PMT threshold	+2.33/-1.53
PMT charge	+1.83
PMT late light	+8.77/-0.14
Hadronic model	-6.47
Total	**+11.93/-18.81**

H+He Energy Spectrum

Statistical and systematic uncertainties

H+He

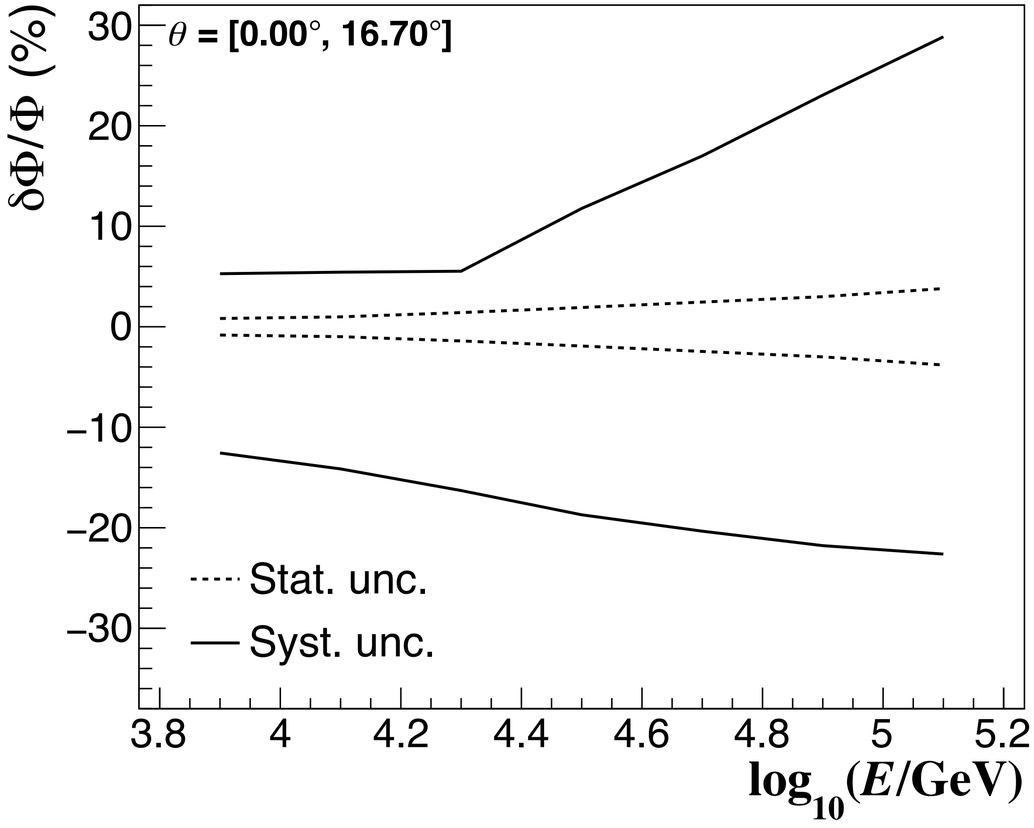

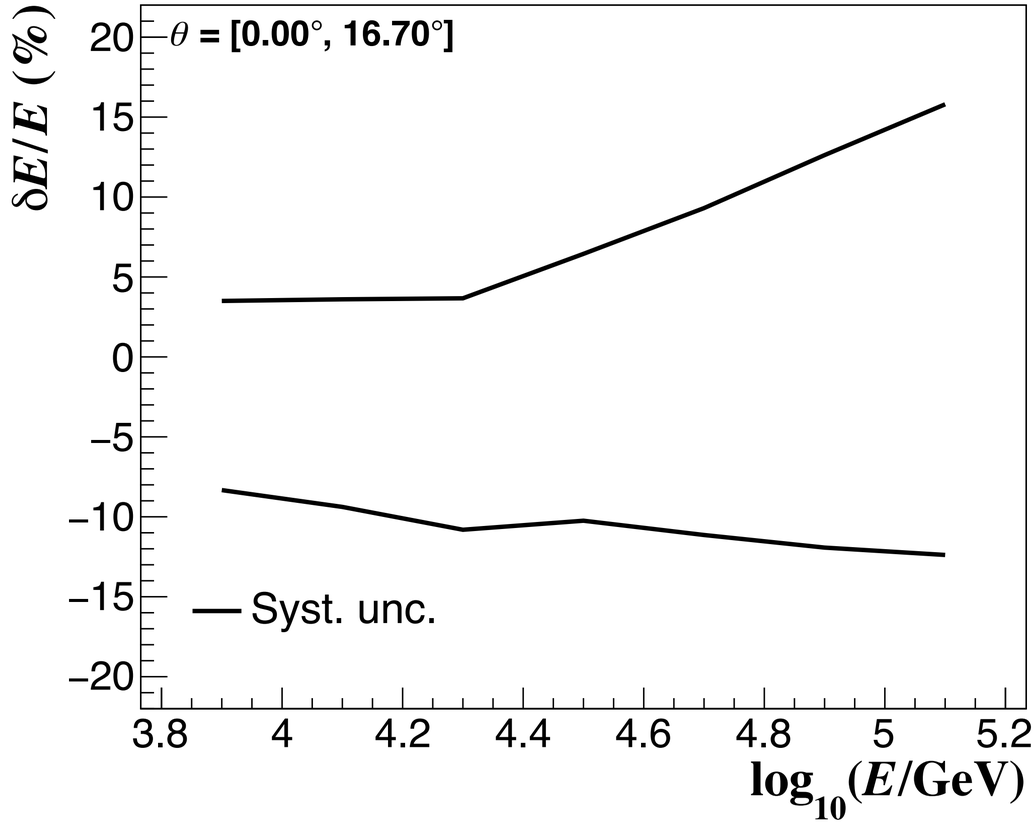

H+He Energy Spectrum

According to MC simulations with our nominal composition model, the fraction of light nuclei in the subsample selected with the shower age cut varies from roughly 97% at Erec = 3.2 × 103 TeV down to 82% at 3.2 × 105 TeV.

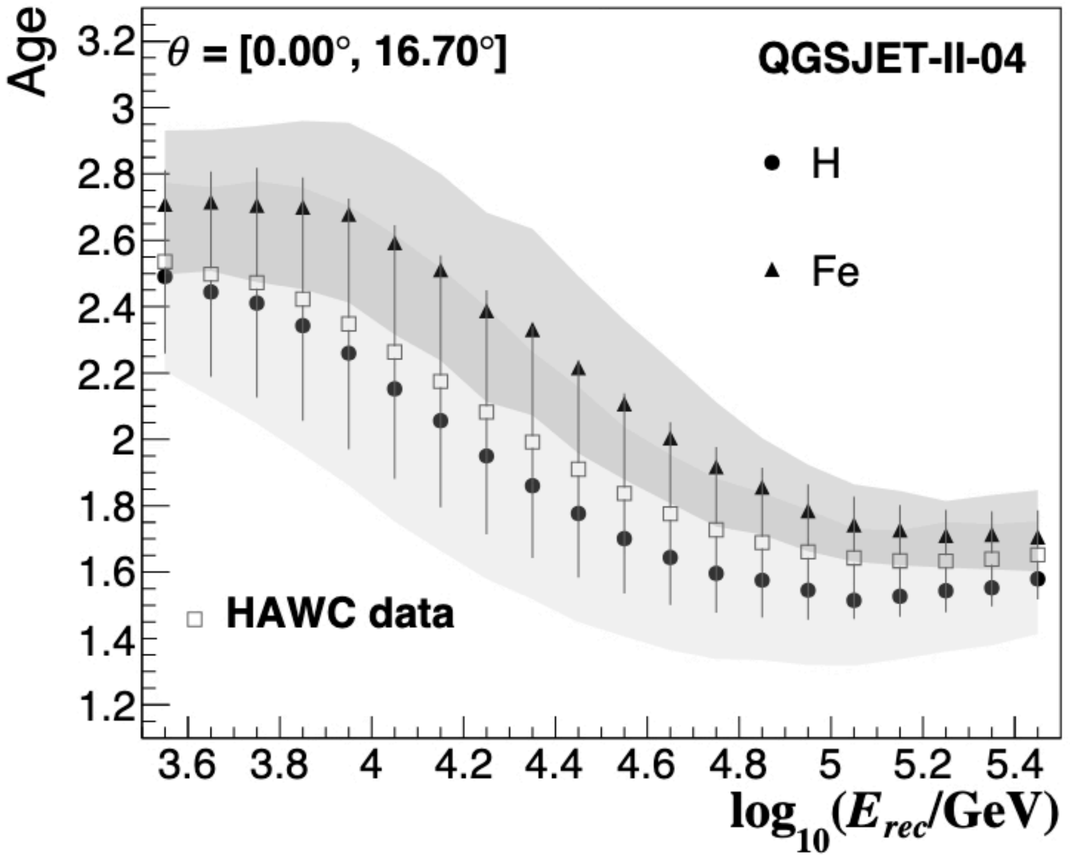

H+He Energy Spectrum

Fit of spectrum

H+He

1. Use following functions:

—> Single power law:

$$d\Phi(E)/dE = \Phi_0 \, E^{\gamma 1}$$

—> Broken power law:

$$d\Phi(E)/dE = \Phi_0 \, E^{\gamma 1}[\, 1 + (E/E_0)^{\varepsilon} \,]^{(\gamma 2 - \gamma 1)/\varepsilon}$$

2. Minimize χ^2 with MINUIT and take into account correlation between points:

$$\chi^2 = \sum_{i,j} [\Phi_i^{data} - \Phi^{fit}(E_i)] \, [V_{stat}^{Tot}]^{-1}_{ij} \, [\Phi_j^{data} - \Phi^{fit}(E_j)]$$

[C. Patrignani et al. (PDG), Chin. Phys. C, 40 (2016) and (2017) update]

Gold's Unfolding

Use **matrix formalism**:

$$N_{\mathrm{data}} = P N_{\mathrm{unfold}}$$

Introduce statistical errors using new response matrix

$$P' = (CP)^T (CP),$$

and new unfolded vector

$$N'_{\mathrm{data}} = (CP)^T C N_{\mathrm{data}}$$

where

$$C_{ij} = \delta_{ij}/\sigma_i; (\sigma_i = 1/\sqrt{n_i})$$

N_{unfold} is found **iteratively** using the set of equations:

$$N^{k+1}_{\mathrm{unfold},i} = \frac{N^k_{\mathrm{unfold},i} N'_{\mathrm{data},i}}{\sum_j P'_{ij} N^k_{\mathrm{unfold},j}}$$

Priors given by nominal composition model.

Smoothing intermediate spectra with ROOT-CERN libraries (353HQ-twice algorithm).

Stopping criterium: Minimum of Weighted Mean Square

Error:

$$\mathrm{WMSE} = \frac{1}{m} \sum_j^m \frac{\sigma^2_{\mathrm{stat},j} + \delta^2_{\mathrm{bias},j}}{N_{\mathrm{unfold},j}}$$

[R.Gold, Report ANL-6984, 1964]
[KASCADE Collab., App 24 (2005) 1]

HAWC Composition

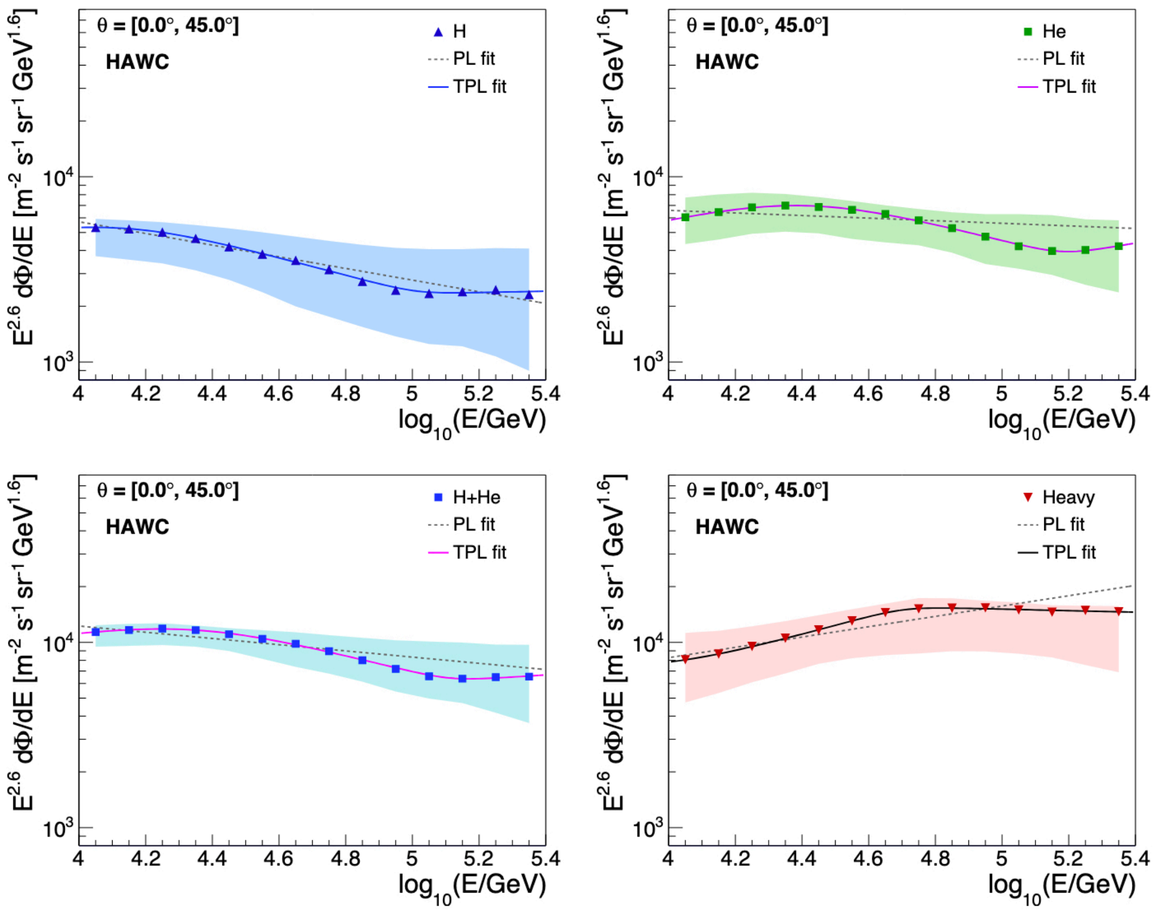

Fits to the unfolded energy spectra. PL represents the fit with a single power law and TPL.
Results checked with the reduced cross-entropy unfolding method

J.C Arteaga, PoS(ICRC2021)374

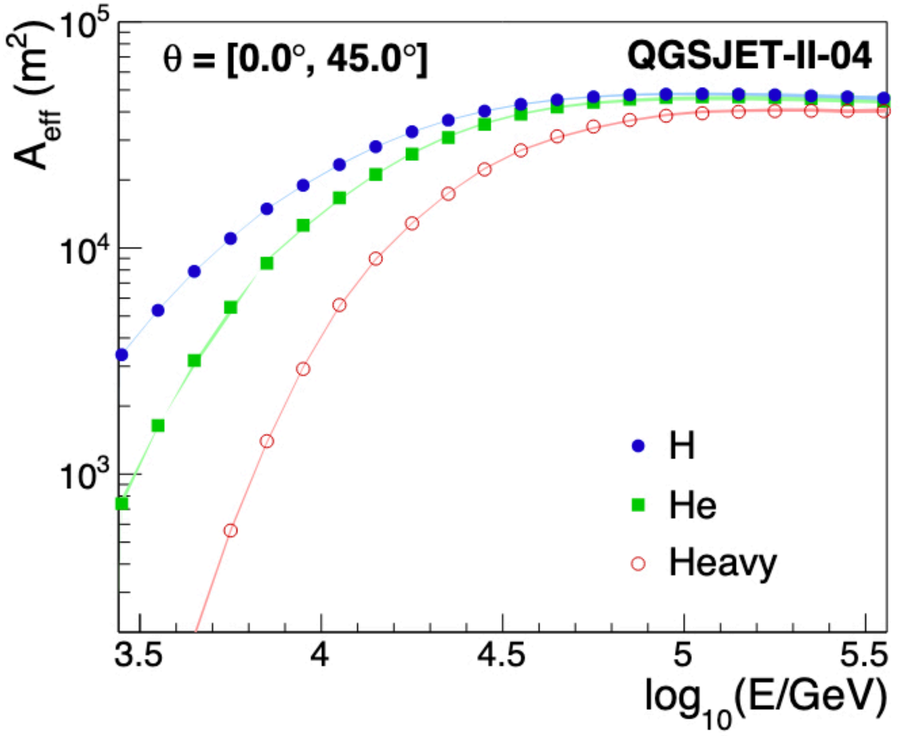

HAWC's effective area for different mass groups obtained with MC simulations.

HAWC Composition

- Results show that the spectra of these mass groups have fine structures, in particular, individual softenings, whose energy positions increase with the primary mass.
- Observation of softening in the spectra of H and He at ~ 14 TeV and ~25TeV respectively.
- Confirms recent detections by DAMPE of similar features in p and He spectra.
- Agreement between both techniques confirms potential of high-altitude EAS for studying TeV cosmic rays.
- Additional feature in spectrum of the heavy CR component in TeV region and indications in HAWC data of possible hardening in the intensities of H and He near 100TeV in agreement with GRAPES-3.

J.C Arteaga, PoS(ICRC2021)374

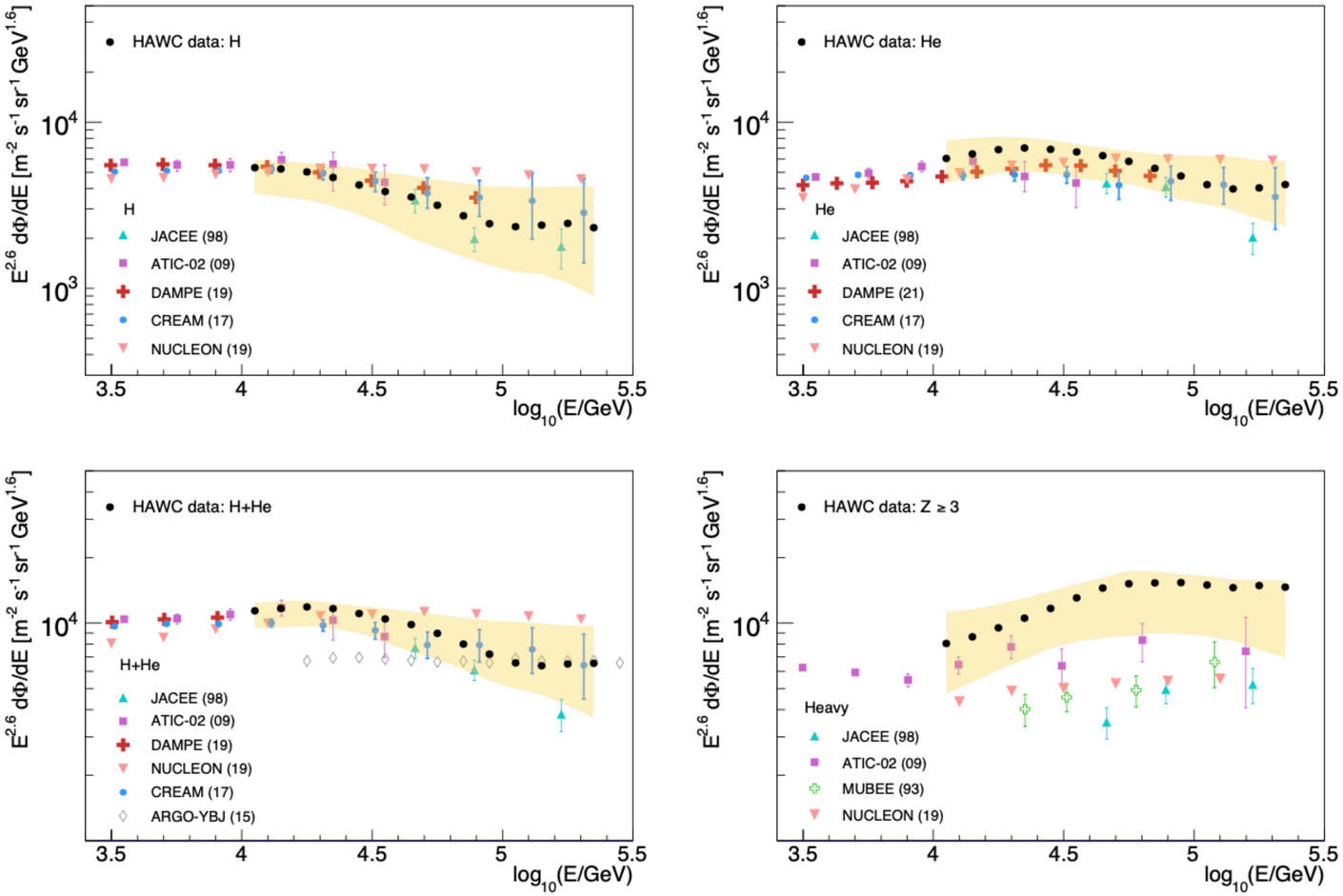

Atmospheric pressure correction

Atmospheric tides:

- Lunar gravitational tides.
- Thermally driven tides: heating associated with solar radiation. Dynamics determined by both the Coriolis force and gravity. (X. Zhang, et a. J. Geoph. Res.: Space Physics (2010))

$$\Delta\{\ln R\} = \beta \Delta P$$

$$\beta = -0.009 \pm 0.001\,\mathrm{hPa}^{-1}$$

$$w_i = e^{-\beta(p(t_i)-p_0)}$$

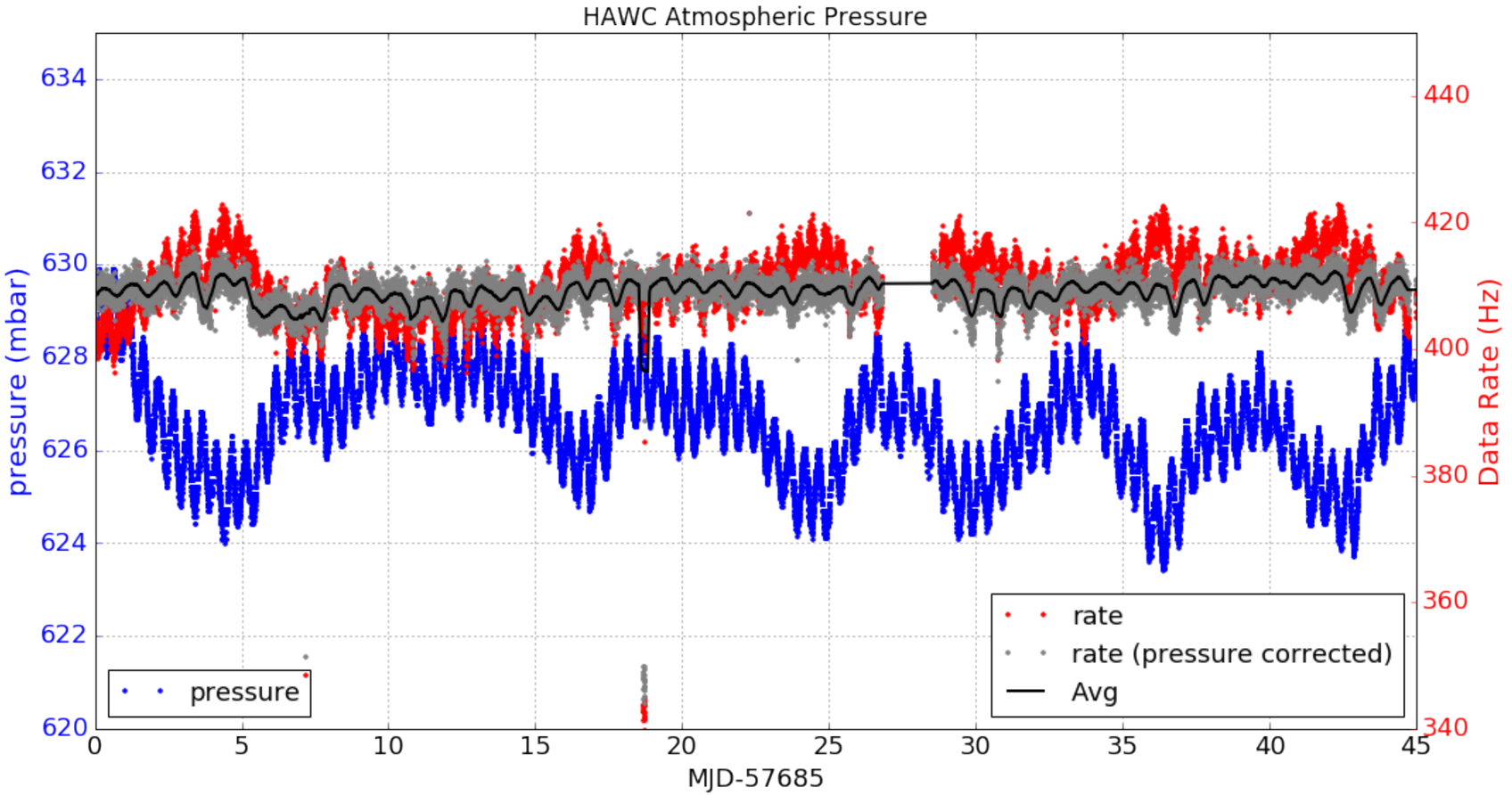

Correcting for Solar Dipole Modulation

$$\delta_\odot = \frac{v(t)}{c}\left[\gamma(E)+2\right]\cos\xi$$